AL FARABI KAZAKH NATIONAL UNIVERSITY

UDC 66.0:546

KHAN NATALYA VLADIMIROVNA

Preparation and application of micro-/nano-structures based on sulfur and silver halides

6D072000 – Chemical technology of inorganic substances

Dissertation submitted in fulfilment of the requirements for the degree of
Doctor of Philosophy (Ph.D.)

Scientific supervisors:
Doctor of chemical sciences, Professor
Burkitbayev Mukhambetkali Myrzabayevich

Doctor of chemical sciences,
Urakaev Farit Khisamutdinovich
Sobolev Institute of Geology and Mineralogy
SB RAS, Russia

Ph.D., Matej Baláž
Institute of Geotechnics SAS, Slovakia

The Republic of Kazakhstan
Almaty, 2023

CONTENT

NORMATIVE REFERENCES

In this thesis references to the following standards are used:

GOST 6.38-90 Unified system of documentation. The system of organizational and administrative documentation. Requirements for documents.

GOST 7.1-84 System of standards on information, librarianship and publishing. Bibliographic description of the document. General requirements and rules.

GOST 7.1-2003 System of standards on information, librarianship and publishing. Bibliographic record. Abbreviations of words in Russian. General requirements and rules.

GOST 7.9-95 System of standards on information, librarianship and publishing. Summary and abstract. General requirements.

GOST 8.417-81 State system for ensuring the uniformity of measurements. Units of physical quantities.

GOST 7.32-2001 System of standards on information, librarianship and publishing. The research report. Structure and rules of presentation.

LIST OF ABBREVIATIONS

AgX (X=Cl, Br, I) – silver chloride/bromide/iodide

BET – Brunauer-Emmett-Teller surface area analysis

CTAB – thrimethylammonium bromide

CTAC – thrimethylammonium chloride

CTAI – thrimethylammonium iodide

CR – congo red

DMF – dimethylformamide

DMSO – dimethylsolfoxide

DSC - Differential Scanning Calorimetry

EDS – energy dispersive X-ray spectroscopy

GO – graphene oxide

HRTEM – high resolution transmission electron microscopy

KAc – potassium acetate

MB – methylene blue

MBC – minimal bactericidal concentration

MeOH – methanol

MO – methyl orange

MFC – minimal fungicidal concentration

NH_4X – ammonia chloride/bromide/iodide

NMP – N-methyl-2-pyrrolidone

O/W – oil-in-water

S/AgX (X=Cl, Br, I) – multicomponent materials based on sulfur and silver chloride/bromide/iodide

PAN – polyacrylonitrile

PANI – polyaniline

PVT – poly(1-vinyl-1,2,4-triazole)

PVA – polyvinyl alcohol

RhB – rhodamine B

SEM – scanning electron microscopy

S-ZVI – sulfur-zero-valent iron

rGO – reduced graphene oxide

TGA – thermogravimethric analysis

W/O – water-in-oil

XPS – X-ray photoelectron spectroscopy

XRD – X-ray diffraction

INTRODUCTION

General description of the work

The thesis is devoted to the production of micro-/nano-structures containing sulfur and silver halides and their testing as photocatalysts and antimicrobial agents. Micro-/nano-structures were obtained using the following percentages of components: 90:10 wt. % (S90:AgX (X=Cl, Br, I) 10) and 70:30 wt.% (S70:AgX30). The materials were obtained via solvothermal synthesis using two methods of sulfur deposition. The physicochemical properties of the obtained micro-/nano-structures were studied and the most effective composition capable of maintaining photocatalytic activity and exhibiting antimicrobial properties was determined.

The relevance of the work

Currently, one of the global issues are environmental and energy problems. To solve them, modern science is trying to find new materials that will have the versatility and potential to treat these problems somehow. More and more research is being devoted to finding new methods for obtaining various materials based on semiconductors and doping or combining them with other materials to improve their functional properties.

In particular, silver halides are widely used semiconductors for photocatalysis and electrochemistry, since these materials have strong optical adsorption, good photoelectric properties, and are sources of elemental silver, the formation of which can lead to improved properties. However, due to the limited (albeit high) absorption of visible light, low oxidation or reduction ability, and high cost, the use of silver halides is limited[1]. The application of non-metallic dopants can solve these problems [2]. The use of α-sulfur can make it possible to achieve suitable photostability and band edges for photocatalytic processes [3; 4]. In addition, sulfur is one of the most common elements with a low cost, having a large number of allotropic modifications (second after carbon) and having a number of unique properties – hydrophobic, antibacterial, etc. [5].

Another important environmental problem that poses a threat to the global ecosystem are pathogenic microorganisms [6]. Despite the presence of antibiotics and antifungal drugs, the number of harmful microorganisms is growing, along with their ability to adapt to the effects of drugs. Therefore, the development of new materials that would be efficient against various types of bacterial strains is extremely relevant. It is known that sulfur and silver halides are able to prevent the reproduction of pathogenic microorganisms, and their combination in one multicomponent material can give a synergistic effect. The above-mentioned point to the need to obtain a material that would be sufficiently effective for both photocatalytic processes and

biomedical applications, and at the same time would be safe for the environment and economically profitable.

Purpose of the work is the preparation of the sulfur and silver halides micro-/nano-structures and the investigation of their physico-chemical properties, photocatalytic activity, antimicrobial and antifungal properties.

The tasks of the thesis:

- preparation of the sulfur and silver halides micro-/nano-structures;
- characterization of the prepared sulfur and silver halides micro-/nano-structures with help of physico-chemical methods of analysis;
- investigation of the photacatalytic activity, antibacterial and antifungal properties of the prepared sulfur and silver halides micro-/nano-structures;
- identification of micro-/nano-structures with the highest photocatalytic and/or antibacterial and antifungal activity;
- development of the principal scheme for producing of the sulfur and silver halides micro-/nano-structures and the calculation of material balance of the process.

The object of the study are sulfur and silver halides micro-/nano-structures.

The subject of the study are the physico-chemical, photocatalytic, antibacterial and antifungal properties of the prepared sulfur and silver halides micro-/nano-structures.

The scientific novelty of the thesis

In this work, sulfur and silver halides based micro-/nano-structures in DMSO medium were obtained for the first time using solvothermal synthesis. For the first time, two methods of sulfur deposition from a DMSO medium were proposed: spontaneous deposition at room temperature and precipitation by diluting a DMSO solution with water. A hypothesis was put forward according to which, the dilution of the studied systems of micro-/nano-structures in DMSO with water affects the morphology and size of sulfur grains. The DMSO-water system, due to the properties of DMSO as a surfactant forming micelles that envelop sulfur particles and to some extent prevent its agglomeration, due to the hydrophobic properties of sulfur.

For the first time, the obtained sulfur and silver halides based micro-/nano-structures were tested as photocatalysts, antibacterial and antifungal agents. The 70 wt. % of sulfur and 30 wt. % of silver halides percentage ratio was found to be the optimal composition between the two components of the studied micro-/nano-structures. This percentage ratio makes it possible to exhibit both solid antimicrobial properties and maintain high photocatalytic activity of micro-/nano-structures. Composition 70 wt. % of sulfur and 30 wt. % of silver bromide was determined to be the most effective for micro-/nano-structure, which is capable of displaying the highest degree of photocatalytic and biological activity.

Theoretical significance. The results of the thesis expanded the known knowledge in the field of material science, solvothermal synthesis of materials based on sulfur or silver halides and their application in photocatalysis and microbiology.

Practical significance. The developed micro-/nano-structures have prospects as potential candidates for universal application both for conducting photocatalytic processes and for combating harmful microorganisms.

The main provision for the defense:

1) The synthesis of sulfur and silver halides micro-/nano-structures effectively takes place in a DMSO medium at 120 ° C and, due to the high positive dependence of the solubility of sulfur in DMSO on temperature, excess sulfur precipitates when the reaction mixture is cooled to room temperature, while a highly supersaturated sulfur solution is formed over the precipitate, and it dilution leads to the formation of a heterogeneous system consisting of sulfur microparticles coated with grains of silver halides of smaller sizes.

2) The application of the method of sulfur precipitation by cooling the reaction mixture for 12 hours to room temperature during the synthesis of micro/nano-structures leads to the formation of irregularly shaped sulfur particles with a size of 20 to 50 μm, and the application of the method of sulfur precipitation from a supersaturated solution by diluting the reaction mixture with water gives irregularly shaped sulfur particles with a size of 10 to 25 μm.

3) Micro-/nano-structures with the 70 wt. % of sulfur and 30 wt. % of silver bromide composition represented by the greatest photodegradation ability of the Orange II organic dye ($C_{16}H_{11}N_2NaO_4S$), decomposing about 90 % of the dye molecules when exposed to visible light ($\lambda \approx$ 380-760 nm, I = 15 mW/cm^2) for 3 hours.

4) Micro-/nano-structures with 70 wt.% of sulfur and 30 wt. % of silver chloride/bromide composition have the greatest ability to suppress pathogenic microorganisms such as *S.aureus* ATCC 6538-P, *C.albicans* ATCC 10231, *E.coli* ATCC 8739, *P.aeruginosa* ATCC 9027, *E.Amylovora*, *S.aureus* ATCC BAA-39, *E.coli* ATCC BAA-196.

The personal contribution of the author of the study consists in the analysis of available literature data on the topic of the thesis, performing experiments on the synthesis of sulfur and silver halides micro-/nano-structures, photocatalytic, antibacterial and antifungal properties study of the obtained micro-/nano-structures.

Contribution to scientific publications writing: investigation, validation, data curation, methodology, writing – original draft, review, editing.

Approbation of work

The results of the thesis were reported and discussed at international scientific conferences, such as the XVII International Conference "Resource-reproducing, low-waste and environmental

technologies of subsoil development", Kazakhstan, Aktau, - 2018; "Nanomaterials and Technologies - VIII", International Level, Russia, Buryat State University named after Dorzhi Banzarov, - 2019; "X International Beremzhanov Congress on Chemistry and Chemical Technology", Kazakhstan, Almaty, - 2019.

Publications

The main results on the topic of the thesis are presented in 9 publications, including:

- one article in an international journal with a non-zero impact factor (IF=7.392, Q1) according to the Web of Science database;

- one article in an international journal included in the Scopus database;

- three articles in scientific journals recommended by the Committee for Quality Assurance in the Field of education and Science of the Ministry of Education and Science of the Republic of Kazakhstan;

- one patent on utility model of Republic of Kazakhstan;

- three abstracts at international conferences.

Relation of the thesis with research and government programs

The dissertation was carried out within the framework of program-targeted funding of the Ministry of Education and Science of the Republic of Kazakhstan (BR05234566), a scientific project of the Ministry of Education and Science of the Republic of Kazakhstan (AP08855868). Also, certain research results were obtained thanks to the Institute of Geotechnics of SAS (Košice, Slovakia) and IGM SB RAS named after V.S. Sobolev (Novosibirsk, Russia).

Volume and the structure of the thesis

The thesis is consisting of introduction, four sections, conclusions and a list of references. The work is presented on 110 pages, contains 43 figures, 15 tables, and 304 bibliographical references.

1 LITERATURE REVIEW

1.1 Synthesis of silver halides based multicomponent materials

Multicomponent materials based on silver halides are of great interest to science and technology [7]. Multicomponent materials mean generalization of all existing systems such as composites, nanocomposites, nanostructures, heterostructures, micro/nano powders and others. The synthesis methodology plays a vital role in fabrication of such materials [8]. There are many methods for obtaining multicomponent materials based on silver halides; however, it is possible to distinguish five most common approaches: deposition-precipitation [8–14], ultrasound [12; 15–28], hydrothermal [15, 22–24], solvothermal [32–38] and mechanochemical [39–47] methods.

1.1.1 Deposition-precipitation synthesis

One of the most popular methods is deposition-precipitation, which commonly used for emplacement of metal, metal oxides, metal sulfides or metal hydroxides onto support materials (carriers) [9]. Usually in this approach the deposition of active particles onto carriers in suspension is used [9]. For the reaching of the precipitation there are three most commonly used methods: pH increase, reduction and ligand removal [8]. In the case of silver halides there are should be the source of Ag^+ and X^- (X = Cl, Br, I) ions and other materials (kaolin, cellulose, graphitic carbon nitride g-C_3N_4, titanium oxide TiO_2 and others [8–22]), that can serve as carriers. There are numerous of research works devoted to the production of nanoparticles, nanocomposites, composites, heterostructures etc.[8–22]. In this method $AgNO_3$ serves as source of Ag^+ ions [8–17]. For obtaining of the X^- ions the most commonly used reagents are NaX or KX [10–14], and rarely cetyl thrimethylammonium chloride, bromide or iodide (CTAC, CTAB, CTAI) [15–17; 20; 21]. In addition, an alkali media can be used for limitation the number of nucleation sites for AgX and it homogenous distribution.

The advantages of the method are simplicity and the fact that precipitation requires less supersaturation than the formation of a new phase directly from the liquid [30]. Moreover, supersaturation can be controlled at a constant moderate level, by gradually adding a precipitating agent [30]. However, the method also has a number of disadvantages, which include the need for careful control of the rate and order of adding substances, and also the rate stirring and pH of the system must be controlled [30].

1.1.2 Ultrasound-assisted synthesis

The ultrasonic method is one of the recent synthesis methods that was discovered by scientists [23]. Sonochemistry originates in extreme transient conditions caused by ultrasound, which creates unique hot spots that can reach temperatures above 5000 K, pressures over 1000 atmospheres and heating and cooling rates over 1010 K s^{-1} [24]. This method makes it possible to

obtain various systems and materials. One of such systems is samples based on Ag and AgX [25–28]. In this method various techniques are used. For example, it can be simple one-step ultrasound process without additional thermal or reducing treatment, in which the solution of $AgNO_3$ serves as source of Ag^+ and as Cl^- source the solution of NaCl or KCl is used (the solution can be prepared in water or organic solvents). Also can be used additional substances as shape-directing agent [25] or pH-control-agent [27]. Sometimes for formation of multicomponent materials the introduction of commercial AgX and subsequent sonication with other components is used [28].

Like other methods, ultrasound has advantages and disadvantages. In comparison with traditional energy sources, ultrasonic irradiation provides special reaction conditions, such as a short duration of sufficiently high temperatures and pressures in liquids that cannot be obtained by other methods [32]. However, more and more studies indicate that this method is conditioned by the expansion of the range of problems, the presence of inefficient energy dissipation as well as low yield [23].

1.1.3 Hydrothermal synthesis

The hydrothermal synthesis method is a process of obtaining various substances (materials) using hydrolysis reactions at high temperatures [23]. The method is considered hydrothermal if water is used as a solvent [33]. The basis of the method lies in the process of crystallization from a solution, namely the formation of crystal nuclei and their subsequent growth. [23; 33]. Usually, this method is accompanied by the use of the special equipment as autoclaves [34; 48]. Hydrothermal method is one of the common methods for production of materials based on AgX [34–38; 48–53]. Here, $AgNO_3$ is used as source of Ag^+ [34–38; 48–53] and X^- can be obtained from the different precursors: 1) metal halides ($FeCl_3$, NaCl, $SnCl_2$ [34–38]); 2) hydrochloric acid (HCl) [49–52]; 3) CTAC, CTAB, CTAI [48; 53]. The method is also represented by advantages and disadvantages. The main advantages are that it is possible to obtain substances that are unstable closer to the melting point and that it possible to synthesize large crystals of high quality. As for disadvantages, it is necessary to have expensive equipment and constant monitoring of temperature and pH is necessary [23].

1.1.4 Solvothermal synthesis

Solvothermal method of synthesis is close to hydrothermal and was discovered in the 19th century. In the 20th century, this method gained popularity again thanks to nanotechnology [33]. If instead of water other solvents are used, then the process is considered solvothermal [33; 54]. Another feature of this method is using of different vessels in which the temperature of the solvents can reach their critical point [62]. Today, this method of synthesis is not limited only to autoclaves, as also various reactors or thermostats are used, which can ensure the maintenance of certain reaction conditions [55–58]. Solvothermal method is widely used for obtaining of multicomponent

systems based on AgX [18; 59–68]. Usually, in this method $AgNO_3$ serves as source of Ag^+ [6; 18; 60–63; 66–72]. Less often, for these purposes, silver acetate (CH_3COOAg) [69] or methylene dichloride (CH_2Cl_2) can be used [72]. As for X^- ions sources, KX or NaX are used more often [6; 18; 61–70; 72; 73], and also in some cases, a halogen gas atmosphere [59; 61], CTAB [67; 69] or $FeCl_3$ [65] (in case of obtaining iron containing system) and $TiCl_4$ (in the case of obtaining TiO_2 containing systems) are used to produce AgX systems. This method is represented by the same advantages and disadvantages as hydrothermal. The pros of the method is ability to obtain unstable materials, obtaining of the crystals of high quality and the diversity of available solvents [57; 58]. As for cons, they include the high cost of equipment, the complexity of designing installations, as well as the limited stability of organic solvents [57; 58].

1.1.5 Mechanochemical synthesis

Mechanochemical method of synthesis is a process based on mechanical forces, including deformation and fracturing [74; 75]. This method is used special equipment such as high-energy. The flowing of the chemical reactions is caused by influence of mechanical energy, supplied by milling of the materials [75]. Mechanochemistry is diversified; with help of this method catalytic and complex reactions can be conducted and polymers, simple and multicomponent systems or nanocomposites can be prepared [74–77]. Also multicomponent materials based on AgX can be obtained by mechanochemical method [39; 41–47; 78]. Different techniques of producing AgX can be applied, namely milling of solid reagents like $AgNO_3$ and NH_4Cl (NaBr) in the presence of diluent for obtaining of the AgX nanoparticles [39; 41; 78] and subsequent photoreduction for formation of Ag^0 and final AgCl/Ag nanocomposite [42]; milling of the solid AgX with liquid polymer (this technique is also called polymer assisted grinding [43]) [44]. According to [39; 41; 78], using of the diluent allows to get smaller particles of AgX. The main advantages of the mechanochemical synthesis are simple and available equipment, the high yield of product, method can avoid the formation of side products or decomposition of reactants [43]. In addition, for the implementation of mechanosynthesis, the use of solvents, extermelly high temperatures and organic precursors is not required. As for disadvantages, it is long time reactions, difficulty in selecting reaction modes and lack of knowledge in this field [43].

1.2 Synthesis of sulfur based multicomponent materials

Different systems based on sulfur are highly prospective materials, which can be used in various fields [79–89]. There are numerous synthesis methods and in this chapter will be given the most used approaches and techniques. Pronciples selected in the previous paragraph, the methods were mentioned. If the method is repeated, then its principle and description will be omitted in this section.

1.2.1 Microemulsion based synthesis

Microemulsion method of synthesis one of the most applicable methods for producing sulfur nanoparticles [79–83] This method is attractive due to its ability to produce monodisperse nanoparticles [79] and regulate its growth [82]. There are two types of microemulsions that differ from each other in the ratio of the constituent components as well as the hydrophilic-lipophilic balance [79; 80; 82; 83]. The first type of microemulsion is called water-in-oil (W/O) or reverse microemulsions – when the hydrophilic parts of the surfactant molecules are adsorbed on the surface of the water, while the hydrophobic parts of the molecule are directed to the oil [79; 80; 82; 83]. The second type is oil-in-water (O/W) microemulsions – when the lipophilic parts of the surfactant molecules are collected on the surface of the oil, while the hydrophilic parts of the molecules are in the water side [79; 80]. The first method is more popular for the production of sulfur nanoparticles and sulfur containing multicomponent systems [79–89]. In this method the source of oil phase is necessary, usually it is cyclohexane [79; 81–86] and other substances like octane, paraffin etc. [87–89]. There should also be the surfactant and co-surfactant (e.g. SPAN 80, TWEEN 80, CTAB, 1-butanol) [79; 81–89]. Hydrogen sulfide (H_2S) and polysulfides (Na_2S_x, CaS_x, $(NH_4)_2S_x$) are usually used as a source of sulfur [79–89]. The advantages of this method include simplicity of the experiment as design, exclusion of extreme reaction conditions and the ability to control the growth and size of particles [23; 79]. As for disadvantages it requires a large amount of surfactants, necessity of temperature and pH maintenance, and the use of substances with high melting point that are represented by limited solubility [23].

1.2.2 Electrochemical synthesis

Electrochemical method of synthesis is method in which the flowing of the process possible due to the passing of the electric current between cathode and anode (there are can be more than two electrodes) in an electrolyte [90]. Electrochemical synthesis takes place at the interface of the electrolyte, which also serves as electrode [90]. The method is attractive because an electrochemical reaction can produce products that cannot be formed as a result of a chemical reaction [79; 90]. Usually, in this method the deposition of the product occurs on the surface of the electrode in form of film or coating [90]. Sulfur containing multicomponent materials can also be obtained by electrochemical method [79; 91–97]. The processes of the electrolysis and electrolytic cell are mostly used [91–93]. These approaches are based on using of the graphite electrode, which performs the function of the counter electrode and on the solution of the electrolytes, which also plays role of the source of sulfur [79; 91–97]. As for other electrochemical approaches of obtaining sulfur containing materials, electrochemical exfoliation [90], electrochemical oxidizing/reduction [90; 95; 96] and electrochemical convention [97] can be highlited.

As for the advantages of the method, the process does not require high temperatures, and its kinetics and thermodynamics can be controlled by changing the cell potential [90]. The disadvantages is that electrochemical synthesis gives disordered products at the output, together with amorphous impurities [90].

1.2.3 Mechanochemical synthesis

Mechanochemical method of synthesis is also widely used for of obtaining the sulfur based materials (composites, nanocomposites, systems etc.). As previously mentioned, high-energy mills are used in this method. The source of sulfur is usually elemental sulfur [98–101]. There is a technique that uses a combination of two methods. First, one or more components of a complex system are obtained, and only then under certain conditions milling is carried out in mills. For example, [102], carbon nanotubes are obtained by oxidizing them with acidic conditions, and after that the elemental sulfur is subjected to mechanical impact together with the nanotubes to obtain the final product. In [98], to obtain a sulfur-zero-valent iron (S-ZVI), ZVI is first obtained from reduced iron and sodium persulfate, and after obtaining ZVI, it is milled with sulfur. However, the most commonly used approach in mechanosynthesis is the mixing of raw materials with each other [99–101]. There may be its own peculiarities and conditions, as for example in [99; 100], where a diluent and a catalyst are used to obtain sulfur particles, but the mixing of the components is preformed in one step. In [101], under special stoichiometric conditions and taking into account the chemistry of the initial substances, milling is carried out on a large scale. In addition, mechanosynthesis can be carried out both in an inert environment, for example, in argon [98; 101], and under ambient conditions [98–100].

1.2.4 Hydrothermal synthesis

Sulfur containing multicomponent materials are commonly obtained by hydrothermal method. In this method as sulfur source different substances can serve, but more popular technique is using of elemental sulfur and dissolving it in in water [103–106], small amounts of carbon disulfide (CS_2) [107], or DMSO with participation of water in the process [108]. Here using nonwater solvents is necessary for full passing of sulfur into solution, because it can not to be dissolved in water [107–109]. Thiourea ($CS(NH_2)_2$) also can serve as precursor of sulfur [110; 111], which is usually dissolved in water. There is also a reaction (1) by which it is possible to obtain sulfur: when sodium thiosulfate ($Na_2S_2O_3$) and hydrochloric acid (HCl) react, sulfur precipitates [112]. In addition, there are rare cases of using other sources of sulfur to produce composites, nanocomposites, systems, heterostructures, etc., like methionine [113] or L-cycteine [114].

$$Na_2S_2O_3 + 2HCl \rightarrow 2NaCl + H_2O + SO_2\uparrow + S\downarrow \quad (1)$$

1.2.5 Solvothermal synthesis

The solvothermal synthesis is one of the most applicable methods for producing sulfur nanoparticles [82]. Most often, elemental sulfur serves as a precursor for the production of sulfur and DMSO, N-methyl-2-pyrrolidone (NMP), isopropanol, CS_2 are used as solvents [82]. When obtaining multicomponent systems, the process may become more complicated, but the pronciple remains the same. Here, the most common solvent for sulfur is CS_2 [82; 115; 116]. However, other solvents are also used, and also doping is applied. For example, in [117], to obtain sulfur-doped bismuth oxychloride (BiOCl), sulfur is uniformly dispersed in this substance at high temperature in an autoclave. Acetone can also be used as a solvent to produce a sulfur doped composite [118]. Also thioacetamide (CH_3SNH_2) can be used as a source of sulfur [85]. In addition, for the same aims $Na_2S_2O_3$, can be used, which is affected by HCl, where the reaction (1) also takes place [85]. After that, to obtain multicomponent system, a solvothermal approach is used to mix all the components of a complex system [85].

General information about the advantages and disadvantages of the synthesis methods mentioned above is given in Table 1.

Table 1 – Advantages and disadvantages of the methods of synthesis, that are used for producing of the multicomponent materials based on AgX and sulfur [8-117].

Synthesis	Advantages	Disadvantages
1	2	3
Deposition-precipitation	Simplicity; Precipitation requires less supersaturation.	Necessity of constant control of the process (rate and order of the adding of reactants, rate of stirring, pH).
Ultrasound-assisted	The method gives specific conditions that other methods cannot give.	Presence of inefficient energy; Low yield.
Hydrothermal	Possibility to obtain substances that are unstable closer to the melting point; Possibility to synthesize large crystals of high quality.	Expensive equipment; Necessity of constant control of temperature and pH.

Continuation of Table 1

1	2	3
Solvothermal	Ability to obtain unstable materials; Obtaining of the crystals of high quality; The diversity of solvents.	The high cost of equipment; The complexity of designing installations; Limited stability of organic solvents.
Mechanochemical	Simple and available equipment; The high yield of product; Avoiding of the formation of side products; Avoiding of the decomposition of reactants.	Contamination; Difficulty in selecting reaction modes; Lack of knowledge in this field.
Microemulsion	Simplicity of the experiment design; Exclusion of extreme reaction conditions, Ability to control the growth and size of particles.	Requires a large amount of surfactants; Necessity of temperature and pH maintenance; Substances with high melting point are represented by limited solubility.
Electrochemical	The process does not require high temperatures; Kinetics and thermodynamics of the process can be controlled by changing the cell potential.	Gives disordered products with amorphous impurities at the output.

1.3 A brief introduction to DMSO and its application

1.3.1 A brief introduction to DMSO

DMSO was firstly obtained back in 1867 by the scientist Alexander Zaytsev [119; 120]. DMSO can be obtained by extracting it from lignin or a binding substance of trees, and by the dimethyl sulfide oxidation reaction [121]. This substance has been used for a long time for various purposes, due to its special properties [119–124]. The structure of DMSO is shown in Figure 1, where a sulfur atom (yellow color) is surrounded by one oxygen atom (red color) and two carbon atoms (grey color), from which three hydrogen atoms (white color) are located in three directions.

DMSO is an odorless, tasteless and colorless liquid, with high polarity, low toxicity, that exhibits an aprotic nature [119; 121–123]. However, there are studies which report that this substance has a straw-yellow color and a characteristic smell resembling garlic; this type of reagent is usually referred to as technical, and the presence of odor and color is explained by the presence of dimethyl sulfide [123]. DMSO is very often used in thermal processes, since it has a fairly high boiling point (189 °C) [119; 120]. It can also serve as a source of carbon, sulfur and oxygen in chemical reactions [119]. Another feature of this material is that it is capable of dissolving both polar and non-polar substances, which, in turn, indicates the possibility of using this compound in many synthesis processes [119–123]. In addition, DMSO is a fairly cheap material, which indicates the availability of its application [119].

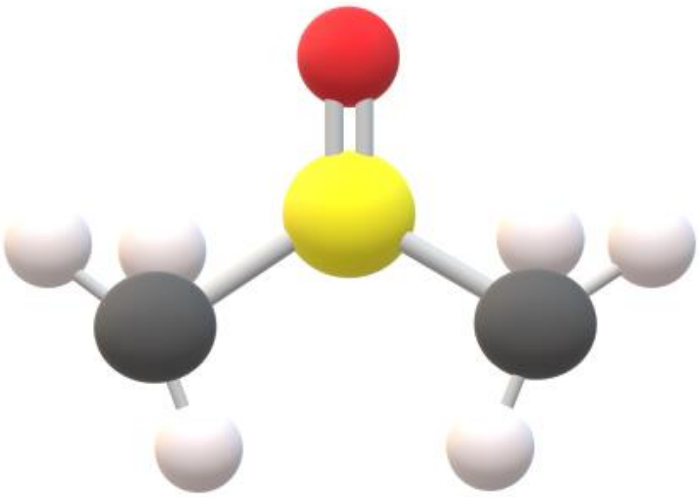

Figure 1 – The structure of DMSO molecule

1.3.2 Application of the DMSO in different fields of science and technology

DMSO is widely used in medicine and in other areas close to it. For instance, in drug production DMSO is used due to its high penetration ability [124], because it can pass through placenta, blood-brain barrier and even bladder wall [120]. There are studies that are devoted to the investigation of the effect of DMSO on the ability to inhibit a group of cell lines [125; 126]. These studies have shown that an increase in the concentration of DMSO in acceptable doses leads to positive results for particular biological cell line. According to [127; 128], DMSO promotes faster healing of surgical sutures and it is also used in skin care, scar treatment and pain relief. It is used as the vehicle control-of-choice in *in-vitro* and *in-vivo* studies [123]. This organic solvent is actively used in microbiology; as it helps to measure microbial activity [129–131]. For a more

comprehensive introduction to the use of DMSO in medicine and related fields, it is possible to refer to Figure 2, where the data are schematically presented.

Other field of application of the DMSO is agriculture. Usually, it is used for preparation of solutions and serves as additional tool [132–135]. In [132], DMSO was used as extractor for extraction of the chlorophyll from lentil leaves. It performance was compared with acetone and ethyl alcohol. Results revealed that DMSO is better extractor of chlorophyll. In addition, DMSO is used for treating vegetables, e.g. in work [133], carrot was treated with it. As a result, DMSO treated samples were larger in length and weight than the control samples. However, there is a study that considers the negative effect of DMSO [134]. The hydrogel, which was obtained by using a water solution with the addition of DMSO showed an adverse effect. Thus, the state of the soil changed after the use of such hydrogels, as there was a modification of polysaccharides in the soil. In work [135], fruit trees were treated with a low-concentration DMSO solution with various additives, cultivated, and then fruit extracts were obtained, which were examined for toxicity to microorganisms. DMSO has high prospects for use in agriculture due to its cheapness and accessibility.

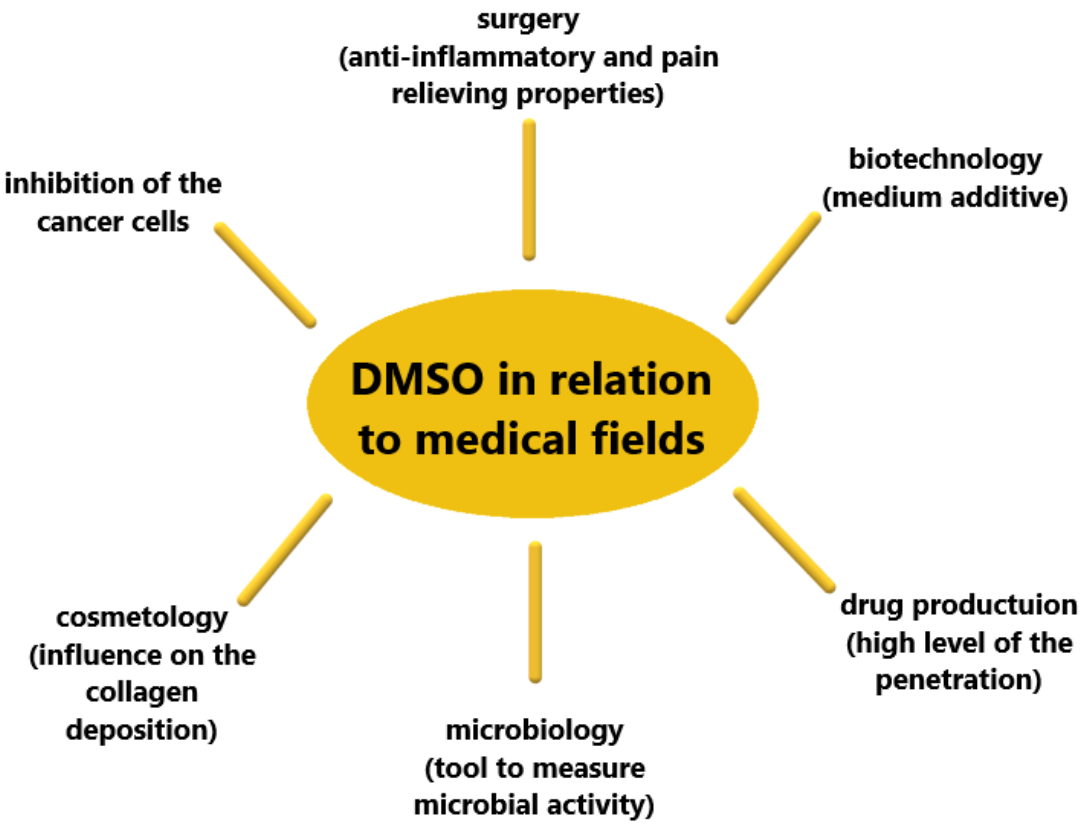

Figure 2 – The scheme of the application DMSO in medical fields

Organic synthesis is another area in which DMSO is widely used. The variation of organic synthesis is extremely huge. In this process DMSO is used as a source of the following radicals or synthons: — CH_3, — CH_2—, — CH —, — CHO, — CN, — SMe, — SO_2Me [136]. As can be seen, DMSO can be a source of many organic groups, in addition to the previously mentioned carbon, oxygen and sulfur [119]. Due to its versatility, DMSO is applicable in many well-known reactions such as Swarm, Parkih-Doering, Pfitzner–Moffatt and others [136; 137]. As example of using DMSO in organic synthesis, obtaining of D-melanin from the L-3,4-dihydroxyphenylalanine (L-DOPA) by oxidizing it can be mentioned [138]. The study of the reaction mechanism showed that DMSO undergoes an oxidation process, and the phenolic oxygen of melanin is sulfonated. D-melanin, after being obtained by this method, became insoluble after nucleophilic substitution of sulfonate groups [138]. In some cases, DMSO can serve as a catalytic system, thus in work [139] the KOH/DMSO system played the role of a superbasic catalytic system in the preparation of vinyl esters. Or it can be used in catalyst-free synthesis, like in study [140], where cyanohydrin carbonates were obtained from aldehydes. Products obtained in the process of organic synthesis in the presence of this reagent are usually used in pharmaceuticals, the production of dyes and agrochemicals [136].

DMSO is also widely used in inorganic synthesis. Here DMSO can play several roles. It can act as a common solvent, like in [141], where organic-inorganic perovskite ($CH_3NH_3PbI_3$) films were produced via spin coating approach. In [142], inorganic perovskite-related cesium lead bromides (Cs_4PbBr_6) were synthesized in water-dimethylsulfoxide-dimethylformamide (H_2O-DMSO-DMF) systems. Perovskites, in turn, are used in the conversion of solar energy [141; 142]. DMSO can act as a source of ligands for the formation of complex compounds of platinum group metals. For example, in studies [143; 144], complex compounds of the $[Ph_3PhCH_2P]^+[PdCl_3(DMSO)]^-$ DMSO, $[Ph_4P]^+[PtCl_3(DMSO)]^-$, $[Ph_4P]^+[PtCl_3(DMSO)]^-$ etc. types were obtained by mixing the initial components and concentrating them in DMSO. Complex compounds $[M(DMSO)_6][B_nH_n]$ (M = Zn(II), Cd(II)) types can be also obtained by the same way [145]. The complex compounds mentioned earlier are interesting for science from the point of view of the structure, formation and chemistry of the process, since they are poorly investigated and the studies on this topic is very rare[143–145].

In addition to the mentioned fields of application of DMSO, it is used in analytical chemistry [146; 147], physical chemistry [148; 149], electrochemistry [150] and photocatalysis [151; 152] to study the kinetics of reactions. DMSO is one of the most commonly used reagents for studying kinetics, since it can be used to easily and visually study the reaction mechanism. For this purpose, the OH attack reaction to DMSO is usually used (OH + $(CH_3)_2SO$) [146; 147].

1.3.3 Application of the DMSO in production of the multicomponent materials

In previous section brief details of application of DMSO in organic and inorganic synthesis were given. In this sub-chapter a short information about the most common multicomponent materials prepared with help of DMSO will be given.

The variety of the multicomponent materials, which can be produced with using of DMSO is extremely high. A big class of the multicomponent materials prepared with application of DMSO are materials based on kaolinite [153–156]. In the synthesis procedure kaolinite is impregnated in DMSO for modification and intercalation. Then it is washed (usually by methanol and the pores of the clay are doped with different components [153–155]. In [154], kaolinite is doped with Ag nanoparticles. The interlayer basal spacing can be explained by using special techniques (using of different solutions). Thus, in [155], DMSO–MeOH and potassium acetate (KAc)-aqueous systems are used for process of expanding and after that modified material is used for obtaining of polymethyl methacrylate (PMMA)-kaolinite intercalation composite. For obtaining of such composites PMMA or polystyrene (PS) polymers obtained by emulsion polymerization can be used [155; 156]. In general, kaolinite is used in these processes because it is an environmentally friendly material, it does not swell in water and it is possible to change the interlayer space between the layers (pores) of this clay [154].

DMSO can be also used as the media or solvent for dissolving polymers, to obtain complex polymer suspensions [157; 158]. Polymers are often dissolved in DMSO and can form complex systems, which consist of polymeric part and inorganic [157] or mineral part [153–155]. For instance, in [157] using DMSO as a solvent in the process of peroxodisulfate-induced polymerization of aniline improved the stability of the obtained polyaniline (PANI). Or DMSO can be used for obtaining of composite films from polyacrylonitrile (PAN) with GO, with high stability and electrical resistivity [158]. There can also be the alliance of polymer Poly(aniline-co-o-toluidine) and TiO_2, which form nanocomposite coatings. In this study the co-polymer, nanocomposite and homopolymer were dissolved in DMSO [159]. The other polymers, that can be used for obtaining of multicomponent materials by dissolving it in DMSO are PS [160], poly(1-vinyl-1,2,4-triazole) (PVT) [161], polyvinyl alcohol (PVA) [162] and others.

One of the most popular applications of DMSO in the synthesis of various multicomponent systems is its use as a solvent. The composition of the systems can be very defferent. It can be bismuth/bismuth oxybromide (Bi/BiOBr) composites prepared through one-step facial solvothermal approach [163]. In study [164], organic-inorganic nanocomposite based on Ag and polymers was prepared, with using DMSO and DMF not only as solvent, but also as a reducing agents of the Ag^0 ions. It large group that is represented by multicomponent systems based on graphene [165; 166]. Their diversity is large, however, most often oxides, sulfides or selenides of

metals are used to obtain these materials. From the oxides tin oxide (SnO_2) [165; 166] or manganese (II, III) oxide (Mn_3O_4) [167] can be mentioned. As examples of the sulfides and selenides, cadmium sulfide [168] and cadmium selenide [169] can be named.

All the mentioned materials are represented by a set of specific properties, which makes it possible to use them in various fields of science and technology.

1.4 Application of silver halides based multicomponent materials in photocatalysis

Before starting the discussion about the application of AgX in production of photocatalysts, a brief introduction regarding the reasons of these use should be given This chapter consists of general and basic information, and enumeration of substances used to produce multicomponent materials based on AgX for the processes of photocatalysis. Photocatalysis is extremely rich field of chemistry and gives possibility to purify waters and air, conduct the reduction of CO_2, suppress microbes and produce H_2. In general, photocatalysis is the process which caused by the flowing of chemical reactions under solar or visible light irradiation. AgX-based photocatalysts are actively studied and produced by scientists around the world.

AgX are inorganic compounds of crystalline form that exhibit the properties of semiconductors [34; 170]. These substances have different colors: silver chloride - white crystals; silver bromide - light yellow crystals; silver iodide - yellow crystals. They are represented by a positively charged Ag^+ ion and negatively charged X^- ion. AgX are highly photosensitive and applied in photographic film [170; 171]. The using of AgX solution for recording of a photo images dates back to 1720 [171]. Among many components, AgX play one of the most important roles in the formation of color photographs. The color film is a multilayer material with layers of gelatin on the surface of which the particles of AgX impregnated with various agents are present. During the exposure and development of the film, AgX particles are dissolved and removed from the gelatin layers. These same particles undergo a photolysis reaction (2) under the action of light and form silver atoms [171]:

$$Ag^+ Cl^- \rightarrow Ag^0 + X^0 \text{ [172]} \quad (2)$$

The key point of the photocatalytic activity are the presence of the semiconductor properties and the ability to create electron-hole pairs by phocatalysts under light irradiation [172]. After Fujishima and Honda discovered in 1972 that TiO_2 is capable of splitting water under the influence of light, there was a big leap in the development and production of new photocatalysts [173]. However, TiO_2 has a wide band gap (~3 eV), which indicates that no more than 5 % of all sunlight can photoactivate this compound and the absorption edge of this metal oxide is below 400 nm [174]. Scientists are faced with the task of increasing the efficiency of TiO_2 (by narrowing band gap) that will be able to overcome ultra violet (290-400 nm) and visible (400-700 nm) radiations

[174]. This goal was achieved using various methods, for example, doping TiO_2 with an anion or metal [174]. Numerous studies have shown that an increase in absorption does not always lead to an increase in the efficiency of the photocatalyst. This happens because the electrons and holes obtained during the photoreaction annihilate, forming so-called recombination centers. Moreover, these transformations occur before electrons and holes take part in a chemical reaction on the surface [174]. Thus, all this lead to an inefficiency of the TiO_2 photocatalysts [174]. Therefore, there is a need to develop materials that will be sensitive to the effects of visible light. AgX are able to demonstrate photocatalytic activity under visible light irradiation, even if their band gap is larger than visible light edge [175]. The band gaps of the AgX are given in Table 2.

Table 2 – The values of the band gaps of the AgX.

Silver halide (AgX)	The band gap (eV)
AgCl	3.00 – 3.28 [176; 177]
AgBr	2.60 – 2.80 [176; 177]
AgI	2.33 – 2.40 [177]

Thus, AgX are of great interest due to the photosensitivity and subsequently photocatalysis. The manifestation of photocatalytic activity is due to many factors, the most important ones include the method of production, morphology and size of synthesized particles. If we are talking about multicomponent systems, then the accompanying substances are also play big role [34; 170].

The first group of materials that are used as accompanying elements in multicomponent AgX materials are noble metals (their nanoparticles), such as Au, Ag [178–180]. These nanoparticles are called plasmon because they are represented by high UV-Vis absorption, due to their surface plasmon resonance (SPR) [178–180]. Thus, plasmon nanoparticles able to increase the UV-Vis absorption range of the AgX. One of the easiest ways to obtain Ag-AgX system is preparing the AgX by simple ion exchange reaction and further drying it at ambient conditions. The photosensitive AgX at ambient conditions under the effect of the day light produce Ag^0 [178]. The photocatalytic activity of the Ag-AgX system was studied with help of azo dyes (methyl orange (MO) and congo red (CR)). According to the results systems based on AgCl and AgBr were able degrade azo dyes, while AgI revealed the weak photocatalytic activity [178]. In [179] Ag/AgX (X = Cl, Br) photocatacalysts were obtained by a facile one-pot ultrasonic spray pyrolysis method. In this study simple ion exchange reaction between excess $AgNO_3$ and KX was studied, and initial reagents were ultrasonicated. Then the reaction mixture was heated in furnace at high temperature for formation of the Ag^0 from the residuals of the $AgNO_3$. The photocatalytic activity of the

synthesized samples was investigated by degradation of the MO and methylene blue (MB) molecules by photocatalysts under visible light irradiation. The results of the photocatalytic activity revealed that Ag/AgCl system is effective with MO and MB, while Ag/AgBr system was less active with MO, but more active with MB [179]. As for obtaining and using of the systems with Au, the study [180] can be mentioned, where Au/Ag/AgCl nanochains were prepared form the solutions of the $AgNO_3$, chloroauric acid ($HAuCl_4$) under effect of the laser beam. These materials are prospective candidates for visible light driven photocatalysts, as they revealed high phtocatalytic activity by degradation of MB. These systems with the plasmon nanoparticles can be prepared by numerous approaches with using different reagents (galvanic replacement, microemulsion, sonochemical and others) and successfully used in photocatalysis for organic dyes degradation, H_2 and O_2 evolution, reduction of CO_2 and nitrogen oxides (NO_x) conversion [34].

Metal oxides are widely used in photocatalysis. These compounds can be used separately or with other materials or co-catalysts for improving of their activity. The procedures of production and initial reagents varies from study to study, but the base methods remain unchanged. For example, in [181] AgX (I, Br) nanoparticles were modified by ZnO nanorods via impregnation method. The photocatalytic activity of the AgX/ZnO samples was studied by degradation of the MO and the samples based on the AgBr showed the highest activity. For these multicomponent systems simple ion exchange reaction between $AgNO_3$ and halide salt (K/NaCl) is usually used, like in [182]. TiO_2 is also actively used for synthesis of the photocatalysts like AgX/TiO_2 [183], which are used for decolorization of azo dyes. Other metal oxides which can be used together with AgX are (copper (II) oxide) CuO [184; 185] and (tungsten trioxide) WO_3 [186; 187].

Another big group of compounds that can be used together with AgX are layered double hydroxides (LDH). LDH are materials, which consist of two layers of metal hydroxides. One layer of the first metal hydroxide is applied on the layer of the second metal hydroxide with help of intercalation [188]. This class of inorganic host layered materials are represented by the common formula $[Me^{II}_{1-x}Me^{III}_x(OH)_2]^{z+}(A^{n-})_{z/n} * yH_2O$, where Me^{II} are divalent metals, like Mg^{2+}, Zn^{2+}, Fe^{2+}, Co^{2+}, Cu^{2+}, Ni^{2+}; Me^{III} are trivalent metals, like Al^{3+}, Fe^{3+}, Cr^{3+}, Ga^{3+}, In^{3+}; A^{n-} is the inorganic/organic anion incorporated into the layered region [188; 189]. LDH are widely used in photocatalysis because of high stability, thermal resistance, electrical conductivity, large surface area, the presence of more superficial hydroxyl ions (OH^-) and others [190]. Usually, for obtaining this type of materials $AgNO_3$ solution is added to Me^{II}-Me^{III}-LDH system prepared in advance [190–193]. AgX-Me^{II}-Me^{III}-LDH materials in one composition can show good ability for photocatalytic processes. For instance, such kind of materials are able to degrade pharmaceutical contaminants (tetracycline, ofloxacin, levofloxacin, and ciprofloxacin) from aqueous effluents

[190]. These materials are also effective in investigations based on application of the model solutions (organic dyes) [191; 192].

The most common substances used in photocatalysis are graphene, its oxide and carbon compound g-C_3N_4 [194; 195]. The application of graphene can be explained by its high carrier mobility. Moreover, it can be a good substrate for the growing of the nanomaterials, because it is represented by sp^2 hybridized 2D carbon sheet. As for GO, this compound can be a "builder" of new blocks when obtaining new hybrids. But the most attractive is reduced graphene oxide (r-GO), since due to its ability to extract excited charge carriers, it can increase the photocatalytic activity of the product [196]. g-C_3N_4 is also having a number of reasons of using in photocatalysis. Because it can shorten the migration distance for the charge carriers and thereby accelerate the charge carriers transport from the internal layers to the surface layers [197]; it has a high electronic conductivity and it do not require the high cost initial reagents [196]. These materials are able to enchase photocatalytic activity of the AgX by providing a new optoelectronic and plasmonic properties [196]. Joining of this materials with the AgX leads to high photocatalytic activity in the process of organic dyes decolorization [198–200], for hydrogen evolution [201] and for removing of the various pollutants [202].

Different inorganic salts are also used for obtaining of the multicomponent materials based on AgX. It can be metal sulfides (CdS, Ag_2S) [51; 203], silver orthophosphate (Ag_3PO_4) [204; 205], silver and calcium carbonate (Ag_2CO_3 and $CaCO_3$) [206; 207]. Such kind of materials are used for degradation of organic dyes and purifying water from pollutants [204–207]. In the Table 3 the types of multicomponent materials based on AgX and their application filed in photocatalysis are given.

Table 3 – Types of the multicomponent materials based on AgX and their application in various sub-fields of photocatalysis.

Multicomponent material	Application filed of photocatalysis	Reference
1	2	3
Ag-AgX (X = Cl, Br, I)	Photodegradation of azo dyes	[178]
AgX-loaded Ag_2CO_3 (X= Cl, I) composites	Photodegradation of MB	[207]
Au/Ag/AgCl nanochains	Photodegradation of MB	[180]

Continuation of Table 3

1	2	3
Ag-branched-nanowire/Pt nanoparticle/AgCl nanocomposite	H_2 evolution	[208]
AgCl/TiO_2 nanotubes	Photocatalytic reduction of nitrate to nitrogen	[209]
AgX nanoparticles-modified ZnO nanorod arrays	Photodegradation of MB	[181]
AgX/ZnO powders	Photodegradation of RhB, reactive orange and bisphenol A	[182]
AgBr/TiO_2 nanocomposite	Reduction of CO_2 to hydrocarbons	[210]
CuO/AgX (X = Cl, Br, or I) nanocomposites	Photodegradation of MB and 4-chlorphenol Photodegradation of the *E. coli* and *S. aureus*	[184]
Ag−AgCl/WO_3/g-C_3N_4 nanocomposites	Photodegradation of the trimethoprim (TMP)	[211]
Ag@AgCl/ZnAl-LDH sesame balls	Photodegradation of neonicotinoid pesticides	[212]
Ag/AgBr/Co–Ni–NO_3 LDH nanocomposites	Photodegradation of organic pollutants	[192]
AgX(Br, I)/CoCrNO$_3$LDH	Photodegradation of the tetracycline, ofloxacin, levofloxacin, and ciprofloxacin	[190]
C_3N_4/Ag/AgCl/$BiVO_4$ microstructure	Photocatalytic reduction of CO_2 to CH_4	[213]
Graphene sheets grafted Ag@AgCl hybrid	Photodegradation of RhB	[200]
rGO-supported AgI-TiO2 mesocrystals	Photodegradation of RhB	[214]
Ag–AgBr/TiO_2/RGO nanocomposite	Photodegradation of penicillin G	[215]
rGO/AgCl quantum dots	Photodegradation of the tetracycline	[216]
Ag/AgX (X=Cl, Br, I)/g-C_3N_4 composites	H_2 evolution	[201]
Ag@AgCl/g-C_3N_4 porous nanosheets	Photodegradation of RhB	[217]

Continuation of Table 3

1	2	3
$CaCO_3/Ag_2CO_3/AgI/Ag$ composites	Photodegradation of MO	[206]
Z-scheme CdS/AgBr-rGO nanocomposite	Photodegradation of RhB	[203]
$AgCl–Ag_2S$ nanocomposites	Photodegradation of MO	[218]
$Ag_3PO_4–AgX$ ($X= Cl^-, Br^-, I^-$)	Photodegradation of MB	[204]

As can be seen from the Table 3, the multicomponent materials based on AgX are very different. These materials are used in wide range of the photocatalysis sub-fields, what indicates their value and necessity for a large number of industries.

1.5 Application of sulfur based multicomponent materials in photocatalysis

This chapter will contain the basic information about application of the sulfur containing multicomponent materials in photocatalysis.

Sulfur is the chemical element with yellow color and with the atomic weight of 32.06. It is represented by non-metallic nature and has three forms: alpha, beta and gamma [219]. This element is odorless, tasteless and insoluble in water. The resource of sulfur is usually sulfates (SO_4^{2-}), sulfites (SO_3^{2-}) and sulfides (S^{2-}) [220]. Sulfur is one of the most common elements of the earth's crust [221] and it is an essential component of the living cells [220]. Sulfur can be found in minerals like chalcopyrite, sphalerite, gypsum, pyrite and others. It is also present in hydrogen sulfide (H_2S), oil, coal, natural gas and bitumen sands. Talking about the leading countries in the production of sulfur and the percentage of its production, it is as follows 13.5 % is belongs to Canada, 13 % - the USA, 12 % - Russia, 4.5 % each - Japan and Saudi Arabia, 4 % - Kazakhstan [219]. In addition to photocatalysis, sulfur is used in many fields, from agriculture to biomedicine [220; 222]. In Figure 3 the main fields in which sulfur is applicable are depicted. Thus, sulfur plays an important role in various fields of science, technology and industry.

In photocatalysis sulfur usually is used as doping agent for improving the activity of semiconductor photocatalysts and usually it is iused in ionic form [2; 4; 223–226]. In synthesis of sulfur containing multicomponent materials the precursors for obtaining sulfur are usually thiourea (CH_4N_2S), sodium sulfide (Na_2S), Na_2SO_3, commercial sulfur in α-S form (S_8) or H_2SO_4 [2; 223–226]. Sulfur based materials are successfully degrading organic dyes and pollutants, suppress microorganisms, able to initiate the reaction of water splitting for H_2 evolution, initiate CO_2 reduction and other [2–4; 223–237]. Using of sulfur as a photocatalytic agent is under the intensive

investigation. The analysis of the literature sources revealed that there are huge number of scientific articles, where sulfur is effective only with supportive "additives", like phosphorus (P), graphene, nitrogen (N), or photosensitive semiconductors [2; 4; 223–226]. However, sulfur has a great potential for application in photocatalysis. According to [2] α-S can increase photocatalytic degradation of the organic dyes of semiconductors, if is intimately contact is present between them. Under light irradiation α-S directly transfers the photo-excited electrons from the valence band (VB) to the conduction band (CB). Subsequently, these photo-excited electrons are migrating to semiconductor and are already driven by high carrier mobility of the semiconductor. As the final stage, holes can be absorbed directly by organic dyes or interact with water (or hydroxyl group) to form hydroxyl free radicals (•OH). And it is known that hydroxyl free radicals are strong oxidizers for the decomposition of organic dyes [2].

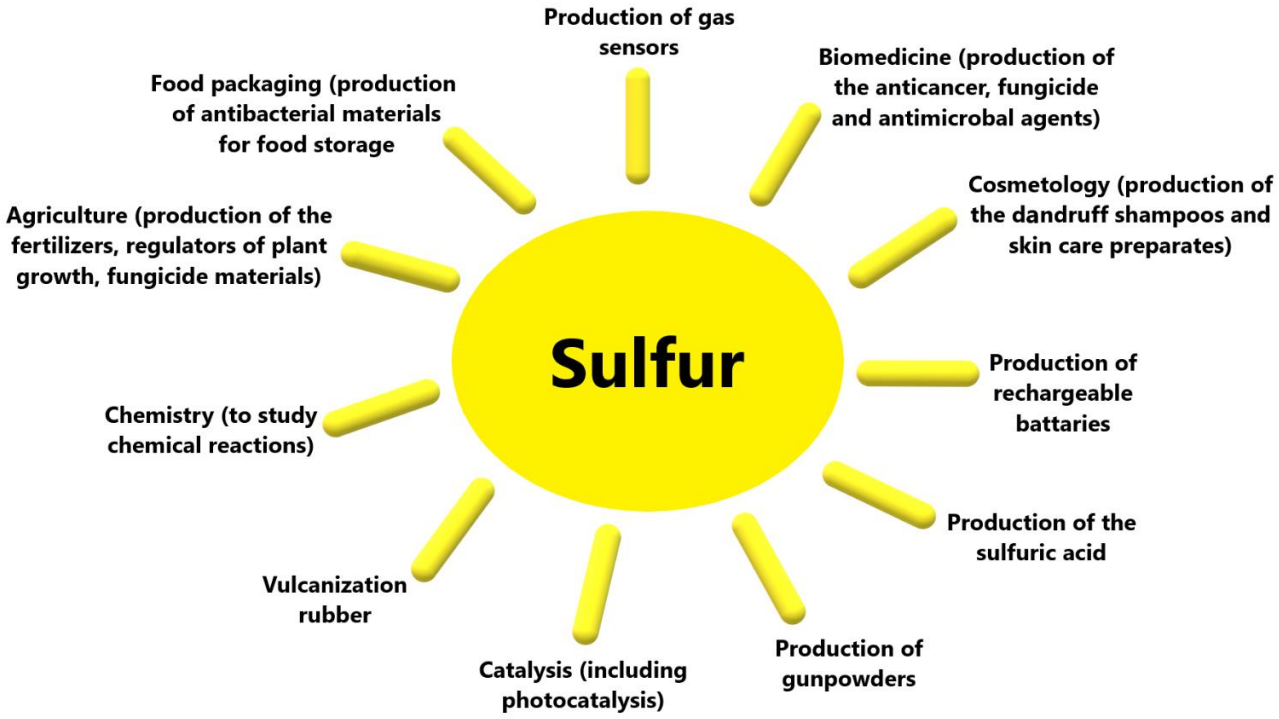

Figure 3 – The scheme of application fields of sulfur

According to [3] α-S is a prospective candidate for producing visible-light-driven photocatalysts. This material in addition to the ability to generate •OH radicals, can split water under UV-vis and visible light irradiation. This process is related to the photoelectrochemical process. However, why there is still no α-S-photocatalyst with high photocatalytic activity? Because this issue requires more attention. For example, in [3] it was concluded, that α-S needs to be modified for improving photocatalytic activity, because big size of the particles and its

hydrophobic nature leads to the low activity. For today, scientist have produced a big number of multicomponent materials, which are complex and sulfur plays a secondary role here. Table 4 contains basic information about the types of such materials and the sub-fields of their photocatalytic application.

According to Table 4, sulfur containing multicomponent materials are represented by a complex scheme in general. Co-doping by sulfur or other nonmetals gives possibility to obtain hydrogen, oxygen or reduce pollutants with higher effectiveness. TiO_2 or g-C_3N_4 are most popular semiconductors in production of sulfur doped materials.

Table 4 – Types of the multicomponent materials based on sulfur and their application in various sub-fields of photocatalysis.

Multicomponent material	Application filed of photocatalysis	Reference
1	2	3
g-C_3N_4 (SCN)/TiO_2 heterojunction	Photodegradation of CR	[4]
CdS/NS-rGO	H_2 evolution	[224]
α-S/MoS_2	Photodegradation of MB	[2]
P-S-codoped g-C_3N_4	Photodegradation of MB and phenol	[225]
Sulfur-doped anatase TiO_2	Photodegradation of Rhodamine 6G	[226]
TiO_2 codoped with bismuth and sulfur	Photodegradation of Indigo carmine	[227]
2D nonmetal hexagonal boron nitride nanosheets (h-BNNS)	Photodegradation of RhB and H_2 evolution	[228]
Sulfur-doped g-C_3N_4/Au/CdS	Photodegradation of RhB	[229]
Fe − S codoped TiO_2	Photodegradation of phenol	[238]
S-g-C_3N_4	Reduction elimination of UO_2^{2+} pollutant	[230]
Sulfur-doped g-C_3N_4/$BiVO_4$ composite	O_2 evolution	[231]
S-doped g-C_3N_4	CO_2 reduction	[232]
Indium sulfide nanotubes with sulfur vacancies (SV-In_2S_3)	Photocatalytic N_2 fixation	[233]
Sulfur-doped carbon on CdS	Photocatalytic H_2O_2 production	[234]
Sulfur-doped polyimide (SPI)	Photodegradation of MO	[235]

Continuation of Table 4

1	2	3
g-C_3N_4 nanosheets cowrapped elemental α-Sulfur heterojunction	Bacterial inactivation under visible light	[239]
Sulfur and potassium co-doped g-C_3N_4 (S + K-codoped g-C_3N_4)	H_2 evolution	[236]
Sulfur-doped covalent triazine-based frameworks (CTFs)	H_2 evolution	[237]
Heterostructured N,S-doped black TiO_2/g-C_3N_4(CN/NS-BT)	Photodegradation of RhB	[240]
Direct α-Fe_2O_3/sulfur-doped polyimide	Photodegradation of MO	[241]
Sulfur-doped carbon quantum dots loaded hollow tubular g-C_3N_4	Photocatalytic destruction of *Escherichia coli* and tetracycline degradation	[104]
Sulfur mediated graphitic carbon nitride/S-Se-graphene (CNS:S-Se-Gr)	Photodegradation of MB and H_2 evolution	[242]
Mesoporous sulfur (S)-doped Ta_2O_5 nanocomposites	Photodegradation of MB	[243]
Sulfur-doped and sulfur/nitrogen co-doped CsTaWO6	H_2 evolution	[244]
Sulfur-doped $SnFe_2O_4$/graphene nanohybrids (S-SFO/GR)	Photodegradation of chlorotetracycline	[245]
Sulfur-doped bismuth vanadate ($BiVO_4$)	Photodegradation of MB and formaldehyde	[246]
Tin oxide (Sn_3O_4) nanoflakes on sulfur-doped sodium tantalite ($NaTaO_3$) nanocubes	Photodegradation of RhB	[247]

1.6 Application of silver halides based multicomponent materials for inhibition of microorganisms

Before focusing on biological activity of AgX based multicomponent materials a short introduction to microbiology and definition of what are bacteria and fungi should be given. This

chapter will be devoted to the basic information about microbiology and influence of AgX on suppression of microorganisms.

Microbiology is the science that studies various microorganisms (microbes) and their interaction with the environment and living organisms. Microbiology is trying to find approaches to “fight microbes” and the possibilities of its practical implementation. As microorganisms we usually understand the live organisms with extremely small sizes; these include viruses, bacteria, fungi, protozoa and even some types of algae. In general, microorganisms are essential part of our ecosystem and without them the big chain of interaction of all species may suffer and disappear. However, scientists are concerned with microbes which able to cause various diseases [248].

Since one experimental part of this work is devoted to the study of the influence of the obtained materials on bacteria and fungi, information about these types of microorganisms will be provided here. Bacteria are single-celled microorganisms, which can be represented by spherical, spiral and sometimes filament morphology. They do not have a cell nucleus. Most of them can be seen with the help of optical microscope at high magnifications. This type of organisms is widely spread in nature and can be a reason of diseases of a living organism [248]. Bacteria can be Gram-positive and Gram- negative (the difference between them are given in Table 5 [249]).

Table 5 – The difference between Gram positive and Gram negative bacteria [249]

Parameters/characteristics	Gram-positive	Gram-negative
Cell wall	A single-layered, represented by smooth structure	A double-layered, represented by wavy structure
Cell wall thickness	About 20-30 nm	About 8-12 nm
Peptidoglycan layer	Thick (multilayered)	Thin (single-layered)
Teichoic acids	Present	Absent
Lypopolysaccharide	Absent	Present
Outer membrane	Absent	Present
Lipid content	Low	High
Resistant to antibiotics	Low	High

Fungi are separate kingdom and these microorganisms are different from plants and animal species [250]. The total amount of fungi is estimated to be about 1.5 million of species and it is the least studied species in the world [251]. Fungi play an essential role in environment, as these

organisms are taking part in biogeochemical cycling of carbon in nature. Fungi can be used in alcohol, bread, penicillin and biofertilizers production, and also in some industrial processes like detoxification of organic pollutants [252]. However, they also have a negative influence on living organisms. Consequently, there is a need for research on the suppression of the influence of fungi. Usually, fungi are spread by formation of numerous small spores, then the colonization of food source appears, what further flows to the formation of hyphae. This whole system is called mycelium. Not all fungi grow like hyphae, some of them grow like yeast cells [251]. Overall, fungi exhibit complex construction and even contain nuclei bounded by membrane with the chromosomes that contains DNA [250–252].

The fight against the above-mentioned microorganisms has been going on for a very long time, since they can be pathogenic and cause various diseases. This threat is hanging not only over people or animals, but also plants and structures frown by people. Bacteria and fungi are able to spread in water sources, food, sanitation stuff and other. In addition, more and more strains are becoming resistant to antibiotics and different antimicrobial or fungicidal agents which makes it worse [253; 254]. More than ever modern world needs in development of new materials as biological agents. For this aim, AgX are widely used, because these materials are able to inhibit various microbial strains. AgX can perform inhibition of microbes individually or there can be increasing of suppressing ability by mixing of these compounds with others. In [255] amorphous calcium phosphate modified with AgX nanoparticles was synthesized. Antimicrobial activity of the samples was investigated against *Staphylococcus aureus* (*S.aureus*) (Gram-positive) and *Pseudomonas aeruginosa* (*P.aeruginosa*) (Gram-negative) by the calculation of the minimum inhibitory concentration (MBC). Here the samples with AgI revealed the greatest resistance to growth of strains. Other halides were able to suppress bacteria, but at higher MIC. In [256] AgCl nanoparticles were biosynthezised with using of *Pulicaria vulgaris* extract (stabilizing and reducing agent). The inhibition of microorganisms was studied by disc diffusion method (DDM) and estimating of MIC, minimal bactericidal and fungicidal concentrations (MBC and MFC). Prepared AgCl nanoparticles showed inhibition ability against *S.aureus*, *E.coli*, *Candida albicans* (*C.albicans*), and *Candida glabrata* (*C.glabrata*) pathogens. Liu and his co-workers fabricated AgBr nanocubes and studied their antibacterial activity [254]. MIC and MBC values showed that AgBr nanocubes are excellent antibacterial agents. There are also scientific works devoted to the investigation of the biological activity of the different materials under solar or visible light irradiation (short information was given in Tables 3 and 4). In [257] chitosan/AgCl/ZnO nanocomposite was able to inactivate successfully *E.coli* and *S.aureus*, and in [258], Ag@AgI/Bi-BiOI nanoarchitectures exhibited disinfection property against *E.coli*. Table 6 provides

information about the variety of multicomponent materials based on AgX as biocidal (fungal) agents and more common methods for determining antimicrobial properties.

According to Table 6, it can be concluded that multicomponent materials based on AgX are strong antibacterial and antifungal agents. Analysis of the literature data revealed that in recent years, more and more investigations have been devoted to the photocatalytic inactivation of microorganisms. It also should be mentioned that AgX-based materials are used in the production of antimicrobial covers, agents, dressing and packaging materials and others [259–272].

The suppression of microorganisms by these materials can be explained by the following mechanism: Ag^+ ions are formed and released from AgX, which leads to the prevention of microbial cell reproduction. Moreover, Ag^+ is able to penetrate the cell walls and interact with protein and nucleic acid, which leads to disruption of bacterial cell reproduction [259]. As for fungal cells this is not a fully understood mechanism, however it is also can be explained by the action of Ag^+ ions with cell components of fungi [260; 261]. Sidorowicz and her colleagues proposed a hypothesis of mechanism of metal ions action against fungi [262]. In the first stage, ions penetrate to the cell walls of fungi, where subsequently the cell membrane is also destroyed. Then the formation of reactive oxygen species (ROS) occurs, which leads to oxidative stress, causing the formation of pores, leakage of cellular contents and programmed cell death (apoptosis). All this leads to the cessation of adenosine triphosphate (ATP) synthesis, DNA damage, changes in the composition of fatty acids and disruption of cell structure [262].

Table 6 – Multicomponent materials based on AgX as antimicrobial/antifungal agents and the methods used for determining biological activity.

Multicomponent material	Type of suppressed strain (Type of activity)	Method of determining of biological activity	References
1	2	3	4
Chitosan/AgCl–TiO_2 colloid	*S.aureus*, *E.coli* (Antibacterial)	AATCC 100 Antimicrobial fabric testing	[263]
AgBr-nanoparticles (NP)@CTMAB hybrid (AgBr-NP@CTMAB)	*C.albicans* (Antifungal)	Direct contact test (DCT)	[264]

Continuation of Table 6

1	2	3	4
TiO_2/AgBr nanocomposites	*Fusarium graminearum* (*F. graminearum*), *Botrytis cinerea* (*B.cinerea*), and *Sclerotinia sclerotiorum* (*S.sclerotorium*) (Antifungal)	Spore suspension method and microdilution method	[265]
Ag@AgI/agarose structure	*S.aureus*, *E.coli* (Antibacterial)	Serial dilution method and photocatalytic inactivation	[266]
Ag/AgX nanoparticles	*S.aureus*, *E.coli* and *C.albicans* (Antibacterial and antifungal)	AATCC 100–1999 test method for microbial counting	[267]
Ag/AgCl/TiO_2-coupled photocatalyst module	*E.coli* (Antibacterial)	Photocatalytic inactivation	[268]
Ag-AgCl/α-Fe_2O_3	*Aspergillus flavus* (*A.flavus*) (Antifungal)	Photocatalytic inactivation	[269]
Z-scheme TiO_{2-x}/AgI heterojunctions	*E.coli* and *F. graminearum* (Antibacterial and antifungal)	Photocatalytic inactivation	[273]
Co@AgCl nanoparticles	*Bacillus subtilis* (*B. subtilis*), *Proteus mirabilis* (*P.mirabilis*), *C.albicans and Aspergillus niger* (*A.niger*) (Antibacterial and antifungal)	Well diffusion method	[270]
AgCl-TiO_2 nanoparticles	*Chromobacterium violaceum* (*C.violaceum*) (Antibacterial)	Disc diffusion method (DDM)	[271]
Ag@AgCl/ZnO	*E.coli, P.aeruginosa, Streptococcus salivarius* (*S.salivarius*), *S.aureus* and *C.albicans* (Antibacterial and antifungal)	Standard dilution method (Microdilution method)	[272]

Continuation of Table 6

1	2	3	4
Spherical Ag/AgCl nanoparticles	*E.coli*, *B.subtilis*, *P.aeruginosa*, *S.aureus*, *P. aeruginosa* 48 and *P. aeruginosa* B 52 (Antibacterial and antifungal)	Microdilution method	[261]

1.7 Application of sulfur based multicomponent materialsfor inhibition of microorganisms

In the section 1.5, it was already mentioned that due to the ability of sulfur to inactivate microbes, it can be used in medicine, biotechnology, construction industry, agriculture and other fields [222]. However, the nature of its behavior was not described yet. This chapter will be devoted to the brief discussion about its effect on microbial cells, types of multicomponent materials based on sulfur and their inhibition of microorganisms.

According to literature sources, sulfur can suppress microorganisms in nano-state more effectively [222]. If we talk about the mechanism of suppression of various strains, then a certain scheme can be indicated here. When sulfur particles are exposed to microorganisms, first there is a strong attraction between the cells of microbes, which leads to the dilution of the cytoplasm and further destruction of the cell, due to the greater penetration of sulfur particles into bacterial cells. Also, the effect of sulfur nanoparticles may be associated with their binding to ribosomes and further inhibition of the translation process. The effect of DNA binding to sulfur particles is also not excluded, which can also lead to the irrevocable destruction of the microorganism cell [222]. The mechanism of suppression of microorganisms by sulfur nanoparticles is not yet fully understood phenomenon, which requires more detailed study. For a greater manifestation of biological activity, sulfur is mixed with other components. For instance, in [274] sulfur nanoparticles were capped with chitosan and their antimicrobial activity was compared with elemental sulfur and sulfur containing salts. It was shown that chitosan capped sulfur nanoparticles were more effective in suppression of *E.coli*, *S.aureus, A. flavus* amd *C.albicans*. Also Ezati and her co-workers have obtained carbon dots doped with nitrogen, sulfur and boron. These materials were tested against different strains and in the case of sulfur-doped carbon dots it revealed excellent results in inhibiting of *E.coli* and *Listeria monocytogenes* (*L.monocytogenes*) [275]. Table 7 provides information on the types of sulfur-based multicomponent materials used as antimicrobial agents and on the methods used for determining antimicrobial activity.

Table 7 – Multicomponent materials based on sulfur as antimicrobial/antifungal agents and the methods used for determining biological activity.

Multicomponent material	Type of suppressed strain (Type of activity)	Method of determining of biological activity	References
1	2	3	4
Sulfur nanoparticles capped with chitosan	*E.coli*, *S.aureus, A. flavus* amd *C.albicans* (Antibacterial and antifungal)	DDM and Microdilution method	[274]
Carbon dots doped with sulfur, nitrogen and boron	*L. monocytogenes, E. coli, A.niger, F.solani*, *Penicillium citrinum* (*P.citrinum*), *Rhodotorula rubra* (*R.rubra*) (Antibacterial and antifungal)	Microdilution method	[275]
Carrageenan-Based Antimicrobial Films Integrated with Sulfur-Coated Iron Oxide Nanoparticles (Fe_3O_4@SNP)	*E.coli*, *L.monocytogenes* (Antibacterial)	Viable total colony count method	[276]
Starch-capped sulphur nanoparticles	*Clavibacter michiganensis* subsp. *Sepedonicus* (*C. sepedonicus*) (Antibacterial)	Propidium iodide fluorescent dye staining method and DDM	[277]
Ag deposited phosphorus and sulfur co-doped g-C_3N_4 (PSCN) composites	*E. coli* (Antibacterial)	Photocatalytic inactivation	[278]
rGO-S, and rGO-S/Se	*S.aureus* and *Enterococcus faecalis* (*E.faecalis*) (Antibacterial)	Turbidometeric and (hematopoietic functional assay) CFU assays	[279]

Continuation of Table 7

1	2	3	4
Alginate-based multifunctional films incorporated with sulfur quantum dots	*E. coli, L. monocytogene, A. niger, Penicillium chrysogenum* (*P. chrysogenum*) (Antibacterial and antifungal)	DDM	[280]
Carbon-sulfur co-doped ZrO_2 nanocomposites	*Salmonella typhi* (*S.typhi*), *P. aeruginosa, E.coli* (Antibacterial)	DDM	[281]
Carrageenan-based antimicrobial films incorporated with sulfur nanoparticles	*L. monocytogenes, E. coli* (Antibacterial)	DDM	[282]

According to Table 9 it can be concluded that sulfur is widely used as antimicrobial agent. Also it is utilized in the production of different coatings and film materials for covering and protection from pathogens. Analysis of the literature sources revealed that separate using of sulfur in nano-state gives better results in suppression of different strains.

2 EXPERIMENTAL PART

In this work bicomponent materials are studied. In the further text their name will be as micro-/nano-structures based on sulfir and silver halides (AgX).

2.1 Reagents and techniques

2.1.1 Chemical reagents and their descriptions

Descriptions of the reagents which was used for conducting experiments are given in Table 8.

Table 8 - Descriptions of reagents

№	Name and coding of reagents and nutrient media	Manufacturer	Purity/pH
1	Silver nitrate	Sigma Aldrich, Germany	≥99.0 %
2	Sulfur	Sigma Aldrich, Germany	99.998%
3	Dimetylsolfoxide (DMSO)	Sigma Aldrich, Germany	Chemically pure
4	Ammonia chloride	Sigma Aldrich, Germany	≥99.0 %
5	Ammonia bromide	Sigma Aldrich, Germany	≥99.0 %
6	Ammonia iodide	Sigma Aldrich, Germany	≥99.0 %
7	Orange II sodium salt	Sigma Aldrich, Germany	≥85.0 %
8	Mueller-Hinton Agar (MHA) (M173)	HiMedia, India	pH (at 25 °C) 7,3±0,1
9	Mueller-Hinton broth (MHB) (M391)	HiMedia, India	pH (at 25 °C) 7,4±0,2
10	Sodium chloride	Mikhailovsky Reagent Plant, Russia	Chemically pure
11	Ethanol	Talgar spirt, Kazakhstan	96.0 %
12	Concanavalin A (C0412)	Sigma, USA	-

2.1.2 Apparatus for solvothermal synthesis

For solvothermal synthesis in DMSO media apparatus which consists of three-neck flask, backflow condenser, thermometer, oil bath, and magnetic stirrer was used. In Figure 4 full details installation scheme are given.

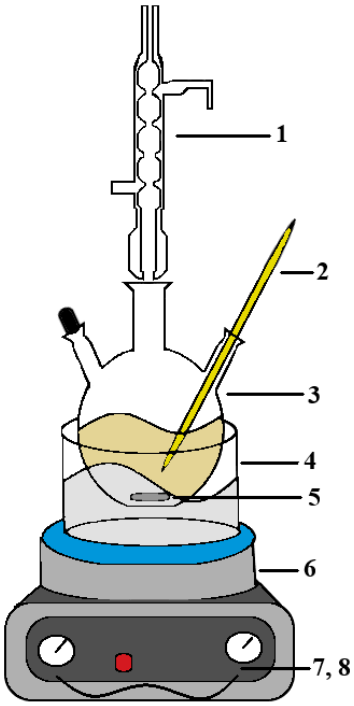

1 – backflow condenser; 2 – thermometer; 3 – three-neck round bottomed flask; 4 – oil bath; 5 – stirrer; 6 – magnetic stirrer with heating; 7, 8 - mixing speed controller and temperature controller.

Figure 4 – Apparatus for solvothermal synthesis

2.2. Solvothermal synthesis of the S/AgX (X = Cl, Br, I) micro-/nano-structures in DMSO media. Precipitating of sulfur at room temperature (method 1)

Solvothermal synthesis of S/AgX in DMSO media was conducted with help of installation exhibited in Figure 4. Accordong to the mass ratio of components the compositions of micro-/nano-structures were the next: 90 wt.% of sulfur and 10 wt. % of AgX; 70 wt. % of sulfur and 30 wt. % of AgX. To obtaining of 2.5 g of S 90 wt. %/AgX 10 wt. %, 2.25 g of S and 0.25 g of AgX was taken. The required amount of $AgNO_3$ and NH_4X was calculated in accordance with a simple ion exchange reaction (2):

$$AgNO_3 + NH_4X = AgX + NH_4NO_3 \quad (2)$$

For example, 0.2972 g of $AgNO_3$ and 0.0926 g of NH_4Cl were taken to obtain 10 % S/AgCl. The remaining calculations for all compositions were performed in the same way, based on the reaction (1). The initial solutions of $AgNO_3$ and NH_4X were prepared in advance in 50 mL of DMSO.

In typical experiment, 100 mL of DMSO with necessary amount of sulfur was transferred into the flask. Under constant stirring the reactional mixture was subjected to the heating. When

sulfur is totally dissolved (120°C) dropwise adding of NH_4X solution in DMSO is performed. After adding of the 1/10 of volume of NH_4X, the reactional mixture is kept at high temperature (120°C) for 15 minutes. Then heating is stopped and when temperature drops to 80°C, dropwise adding is done of $AgNO_3$ and last part of NH_4X solutions under constant stirring. The resulting mixture was left for 12 hours for complete precipitation of the sulfur. Then, the mixture was stirred and centrifuged (4000 rpm, 10 min), washed 2 times with deionized water and dried for 12-14 hours, at 70°C.

2.3 Solvothermal synthesis of the S/AgX (X = Cl, Br, I) micro-/nano-structures in DMSO media. Precipitating of sulfur by water (method 2)

The procedure of the solvothermal synthesis in DMSO media by method two is similar to the procedure described in previous paragraph. But after adding of $AgNO_3$ and NH_4X solutions, sulfur was precipitated with help of water in a volume ratio DMSO to water 1:1. In Figure 5 the scheme of the two methods of synthesis is given.

In further text, sampls were denote as S/AgX (90:10) 1, 2 and S/AgX (70:30) 1, 2, where 1 and 2 is method of sulfur precipitation.

2.4 Solvothermal synthesis of the pure sulfur and silver halides

The procedure of obtaining of pure substances was similar to two previous paragraphs. For sulfur synthesis the step of adding $AgNO_3$ and NH_4X solutions was skipped. As the result there was two types of sulfur, obtained by sedimentation at room temperature and with water.

For pure AgX synthesis, the processes of diluting and precipitating of sulfur were skipped.

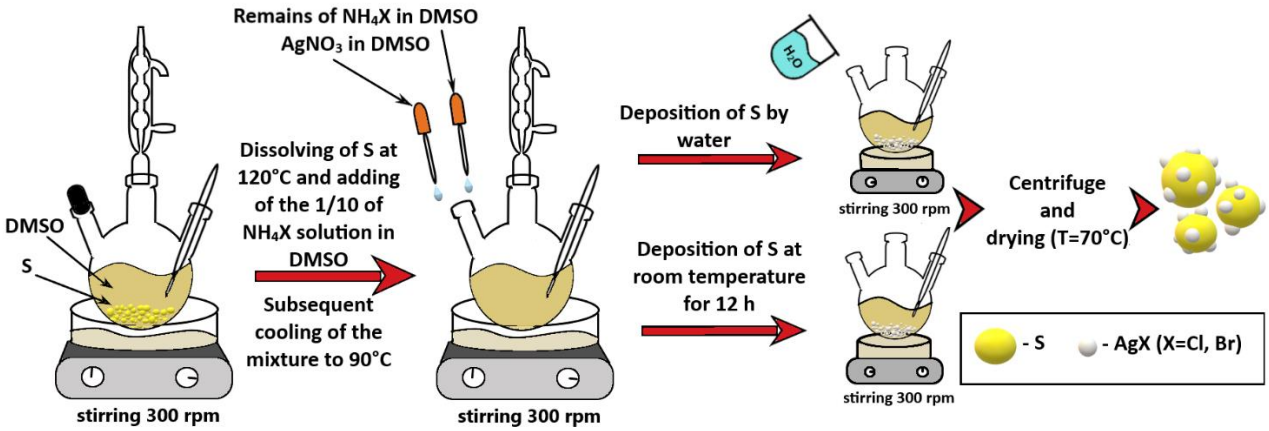

Figure 5 – The scheme of the two methods of synthesis of the S/AgX

The synthesis conditions were selected experimentally. The preparation was carried out both in an aqueous medium [283] and in a DMSO-water medium [284]. The difference between the method of obtaining described in the dissertation differs from [284] by using aqueous solutions of salts to obtain silver halides.

2.5 Characterization methods and techniques

2.5.1 X-ray diffraction (XRD) analysis

The structural investigation of the samples was conducted by XRD analysis.

The XRD of the S/AgX micro-/nano-structures was done on MiniFlex 600 X-ray diffractometer (Rigaku, Japan). The conditions of the analysis were the next: the CuKα irradiation (λ = 0.15405 nm); the X-ray tube voltage is 40 kV; the tube current is 15 mA; the goniometer movement step is 0.02 2 Θ. For processing of X-Ray patterns was used the ICCD-PDF2 release 2016 database was used.

2.5.2 Raman spectroscopy

Raman spectroscopy of the S/AgX samples was performed on Solver Spectrum (NT MDT Instruments, Russia) spectrometer using an 1800/500 diffraction grating, which provides a spectral resolution of 1 cm^{-1}. The Raman spectra were excited by a He-Ne laser with a wavelength of 633 nm and processed with help of Origin Lab program. Analysis was conducted in The Nanotechnological Laboratory of Open Type, of Al-Farabi Kazakh National University.

2.5.3 X-ray photoelectron spectroscopy (XPS)

X-ray photoelectron spectroscopy (XPS) was conducted for analyzing of the elemental composition and chemical and electronic states of the atoms of the synthesized samples, using NEXSA X-ray photoelectron spectrometer (Thermo Scientific, USA) equipped with double-focusing, hemispherical analyzer with 128 channel detector.

2.5.4 Scanning electron microscopy (SEM)

SEM and EDAX (elemental mapping) analyses of S/AgX samples were carried out on the scanning electron microscope Quanta 3D 200i (FEI, Netherlands). Conducting carbon adhesive tape served as a substrate for the samples. Analyses were conducted in The Nanotechnological Laboratory of Open Type, of Al-Farabi Kazakh National University.

2.5.5 High resolution transmission electron microscopy (HRTEM) and energy dispersive X-ray spectroscopy (EDS) (EDS elemental mapping)

Transmission electron microscopy (TEM) was conducted on Themis-Z 3.1 instrument (TFS, USA) equipped with X-FEG-monochromator and CS/S double corrector, accelerating voltage 200 kV. Energy dispersive X-ray spectroscopy (EDS) results were obtained with help of Super-X EDS detector (energy resolution about 120 eV) in HAADF-STEM and TEM modes. Before analysis,

the samples were treated by ultrasonic dispersion in hexane. The sample suspensions were deposited to a carbon film supported on a copper mesh.

2.5.6 Surface area analysis

Surface area analysis was performed by automated gas sorption station Anton Paar Autosorb IQ. Before performing analysis samples were degassed 12 hours at 45 °C.

2.5.7 Thermogravimetric analysis (TGA) and differential scanning calorimetry (DSC)

Thermogravimetric analysis (TGA) and differential scanning calorimetry (DSC) were conducted for determining of the real mass ratio between sulfur and AgX in micro-/nano-structures, as well as their thermal properties. Analyses were performed with help of simultaneous thermal analyzer NETZSCH STA 449 F3 Jupiter (Germany), in an inert atmosphere (N_2), from room temperatures up to 550°C with a heating rate of 10°C/min.

2.6 Photocatalytic activity

In typical experiment, 20 mg of the sample was dispersed in 40 mL of the Orange II 10 mg/L solution. Then solution was sonicated for 5 minutes, before starting light irradiation. The adsorption-desorption equilibrium test was conducted for 60 minutes to reaching stabilization of the samples. After stabilizing the process of light irradiation (15 mW/cm^2) was started. A 300 W OsramVita−lux lamp equipped with a UV filter ($\lambda \geq 420$ nm) served as source of light. The sampling occurred every 30 minutes. Then the suspension was centrifuged (10000 rpm for 3 min) to remove the powder of the sample. The filtrate was analyzed by measuring its optical density in the maximum absorption band (484 nm for Orange II) using a UV-Vis spectrophotometer (SPh 56, Russia). Each photocatalysis study was conducted twice to confirm the results. The photocatalytic degradation of organic dye for almost all samples was fitted with the Pseudo-first order kinetics, equition (1):

$$\ln (C_0/C) = kt \quad (1)$$

Where C_0 and C are initial and final concentrations of model solution in moment of time t and k (min^{-1}) is the apparent rate constant [283; 284]. The k was founded from the slopes of the straight-line portion of the plots. To prove the kinetic order of dye degradation reaction correlation coefficient R^2 was found.

In addition, stability of the photocatalysts was studied. The process was repeated during five cycles. In each cycle after the sampling and measuring, sample was washed by deionized water and reused in the next cycle.

2.7 Biological activity

Microbiological tests were performed at the Scientific Center of Anti-infectious Drugs (Almaty, Kazakhstan). The preparatory process was carried out by the degree applicant personally. The work with microorganisms was carried out by the staff of the scientific center, but the doctoral student observed the process.

2.7.1 The test strains

The following bacterial strains of American Type Culture Collection (ATCC) were used for the tests of biological activity:

• *Staphylococcus aureus* (*S.aureus*) ATCC 6538-P (collection sensitive strain);

• *Candida albicans* ATCC 10231 (collection sensitive strain);

• *Escherichia coli* (*E.coli*) ATCC 8739 (collection sensitive strain);

• *Pseudomonas aeruginosa* (*P.aeruginosa*) ATCC 9027 (collection sensitive strain);

• *Erwinia amylovora* (*E.amylovora*) (phytopathogenic strain).

Reference strains from ATCC were used as studied strains for investigation of antimicrobial activity. The *E.coli* strain ATCC 8739 is a sensitive strain recommended for the study of bactericides and antiseptics. The *S.aureus* strain ATCC 6538-P is a reference strain for studying antibiotic sensitivity, as well as for studying the bactericidal properties of antimicrobial agents. *P.aeruginosa* strain ATCC 9027 is the recommended reference strain for studying the effectiveness of bactericides The reference strain *C.albicans* ATCC 10231 is a sensitive strain recommended for the study of fungicides. The *E.amylovora* strain was isolated in 2019 from the leaves of a fruit tree with signs of fire blight.

In addition, the test strain of *S.aureus* (subsp. aureus) ATCC®BAA-39™ - MRSA was used, which has a SCC mec type III - mec complex in the staphylococcal cassette chromosome mec - SCCmec. It contains genes encoding msrA1 (exchange of antibiotic resistance proteins); pls (surface factor of methicillin resistance) and ccr (resistance to non-lactam antibiotics). The main component of the mec complex is the structural mec gene (methicillin-binding protein), which encodes the synthesis of an additional penicillin-binding protein-PBP2a, that has a low affinity for beta-lactam antibiotics (penicillins, cephalosporins, monobactams, carbapenems). Type III of this complex causes multidrug resistance, since this cassette contains additional resistance determinants located on the integrated plasmids pUB110, p1258, pT181, as well as on the transposon Tn554.

The test strain of *Escherichia coli* ATCC®BAA-196™ produces extended-spectrum beta-lactamases (ESBL) - enzymes produced by microorganisms which are capable to inactivate β-lactam antibiotics of various classes, including penicillins and cephalosporins of I-IV generations. *E. coli* has a multidrug resistance mediated by β-lactamase of class A encoded in the TEM-10 plasmid.

The sensitivity of microorganisms was studied on standard nutrient media [285, 286].

2.7.2 Preparation of a suspension in saline solution 0.9% NaCl

To prepare suspensions of microorganisms of the necessary concentration, a DEN-1 densitometer (Biosan, Latvia) was used designed to measure the optical density (turbidity). The suspension was prepared in saline solution (0.9% NaCl). 5 ml of saline solution was added to the test tube, which was placed in a densitometer and the optical density was measured.

First, a suspension was prepared with a concentration of 1.5 × 108 CFU/mL. For bacteria, this concentration corresponds to a turbidity of 0.5 McFarland units; for fungus - 2.5. From these suspensions, ten-fold dilutions were made by transferring 1.0 ml of the suspension to 9.0 mL of sterile saline. Thus, a dilution of 1.5×106 CFU/mL for bacteria and 5×106 CFU/mL for fungi was obtained.

2.7.3 Method of twofold serial dilutions

For the next experiments water suspensions of the micro-/nano-structures with concentration 10 mg/mL were used.

Testing was carried out on a liquid nutrient medium: Muller-Hinton broth. 0.5 mL of Muller-Hinton broth was added to the wells of the 48-hole plate. In the first well of the row, 0.5 ml of the sample solution was added, and a 1:1 dilution was obtained. 0.5 mL was mixed and transferred to the second will of the row and diluted twice. Thus, the dilution in the second well was 1:2. Double serial dilutions up to 1:128 were prepared in the same way. 0.05 ml of test strains of microorganisms were added to all test tubes. For each row of dilutions, two controls were set: control of the media and control of strain growth. The procedure was repeated for all test samples in two repetitions.

The samples were incubated for 48 hours at a temperature of (22 ± 1) °C for fungi, 18-24 hours at (37 ± 1) °C for bacteria. At the end of the incubation time, seeding was performed on Petri dishes to determine live cells. After seeding, the Petri dishes were placed in a thermostat for incubation for 48 hours at (22 ± 1) °C for fungi, 18-24 hours at (37 ± 1) °C for bacteria.

The results were taken into account by the presence of visible growth of microorganisms on the surface of a dense nutrient medium. The minimum bactericidal/fungicidal concentration (MBC/MFC) was considered the smallest dilution in which there was no growth of microorganisms [286].

All experiments were performed in three repetitions.

2.8 Statistical analysis

All photocatalytic experiments were repeated two times. The statistical analysis included average values, error bar and standard deviation. The results were processed with the help of Microsoft Excel program, using the following formulas [287]:

$$\bar{x} = \frac{\sum_{i=1}^{n} x_i}{n} \quad (2)$$

Where $\bar{x}$ is average value, n is total number of *x* values.

$$S = \sqrt{\frac{\sum_{i=1}^{n} (x_i - \bar{x})^2}{n-1}} \quad (3)$$

Where S is standard deviation, $\bar{x}$ is average value, n is total number of *x* values

The calculated data were represented by the average of two independent photocatalytic experiments and standard deviations were displayed through error bars in the graphs.

All experiments dealing with determination of biological activity were conducted in three repetitions. In the method of twofold serial dilutions used by us, the statistically processed data coincide with repetitions and only absolute values are included in the results [285, 286]. If the repetitions do not match, then the percentage of error is very large and the test is considered invalid. In this regard, microbiological test data are presented with absolute data without additional graphical representation of standard deviations.

3 RESULTS AND DISCISSIONS

3.1 Characterization

3.1.1 XRD analysis

XRD patterns of the S/AgX micro-/nano-structures, pure sulfur and corresponding AgX are given in Figures 6, 7 [288] and 8 respectively [289]. Multicomponent materials are represented by clear and visible peaks of cubic AgX, and with an increase in the amount of AgX, the intensity of its peaks increases. There is also presence of elemental sulfur peaks, where peak at 23.1° is more noticeable. In addition, in the range of 2Θ values between 25 to 30° are also markable peaks corresponding to sulfur. According to [2] the set of these values indicate that sulfur is performed in α-form or it is α-octa-sulfur. In addition, it is also possible to observe an increase in the intensity of sulfur peaks with an increase in its percentage content. Other peaks associated with sulfur are not so noticeable, which indicates the need for additional analyses, such as Raman spectroscopy and EDX, to confirm the presence of all components.

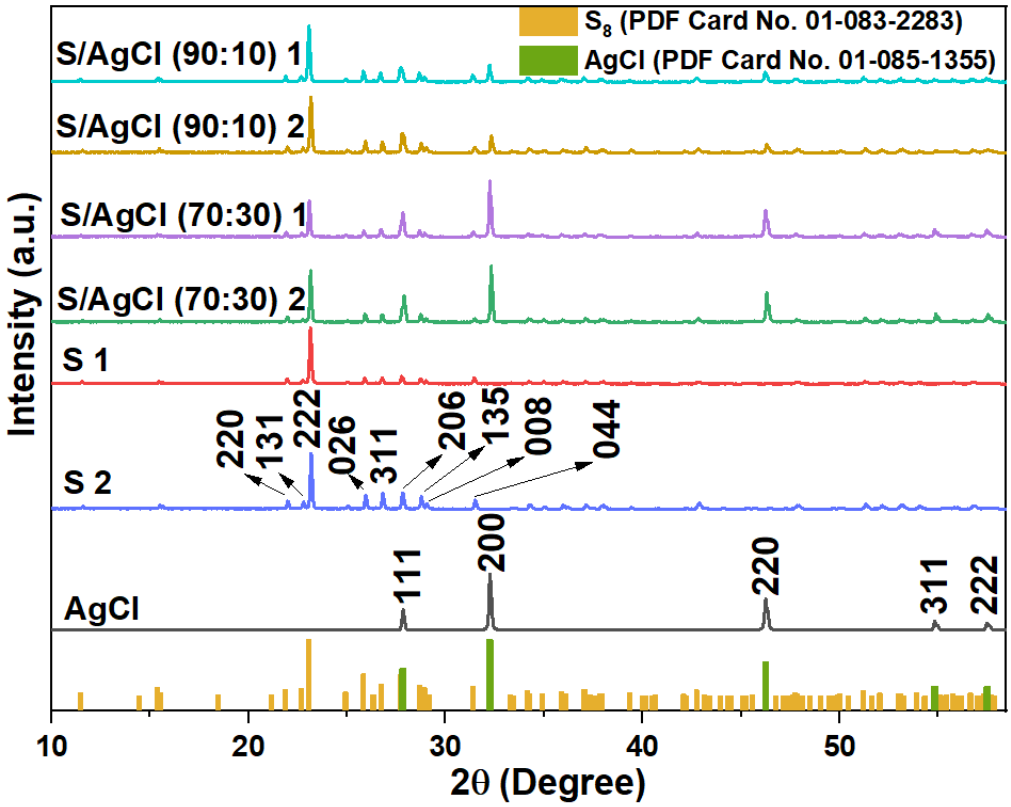

Figure 6 - XRD patterns of the S/AgCl (90:10) 1, 2; S/AgCl (70:30) 1, 2; pure S 1, 2 and AgCl [290]

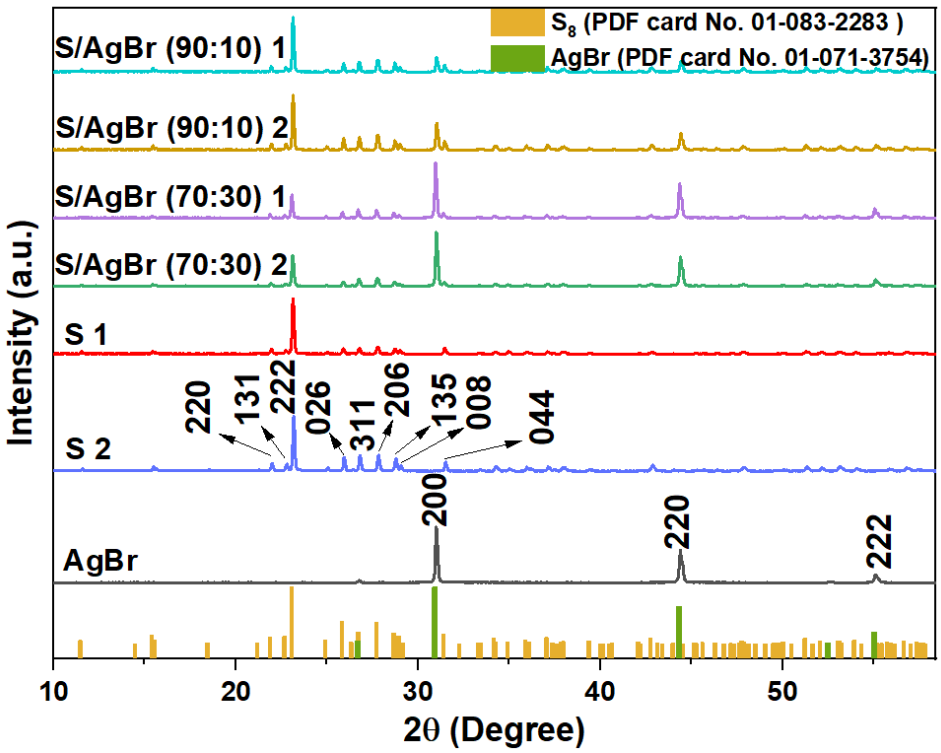

Figure 7 - XRD patterns of the S/AgBr (90:10) 1, 2; S/AgBr (70:30) 1, 2; pure S (1, 2) and AgBr [290]

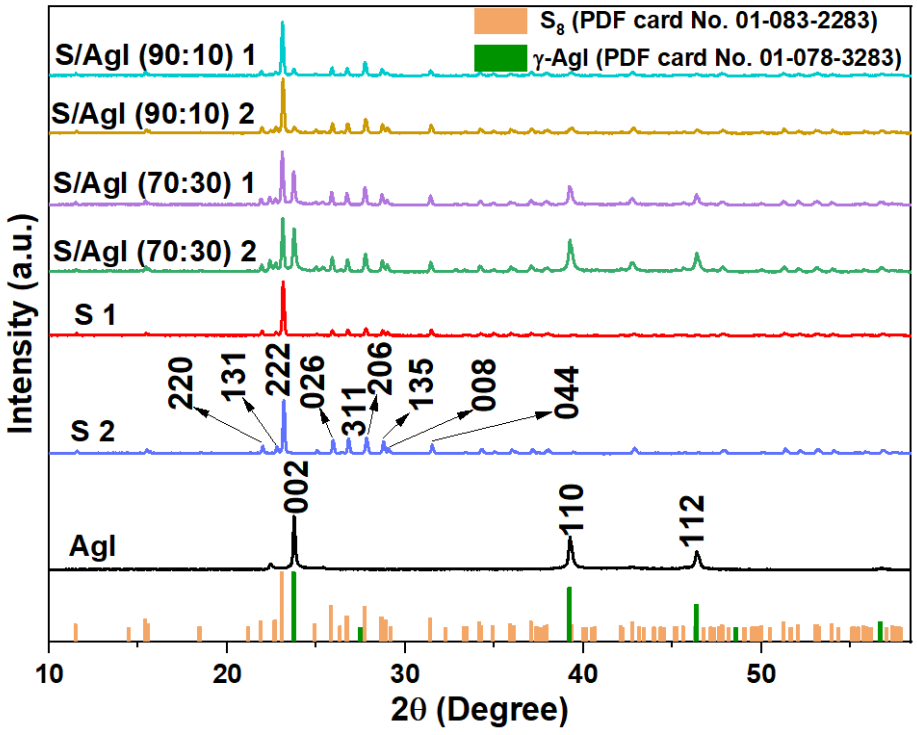

Figure 8 - XRD patterns of the S/AgI (90:10) 1, 2; S/AgI (70:30) 1, 2; pure S (1, 2) and AgI [290]I

3.1.2 Raman spectroscopy

Raman spectra for all micro-/nano-structures, pure sulfur and corresponding AgX are given in Figures 9, 10 [291] and 11 [292] respectively.

The results for samples based on AgCl are presented in Figure 9. According to analysis, there are can be highlighted three Raman modes at 75, 86 and 240 cm^{-1} for pure AgCl. The peaks at 75 and 240 cm^{-1} wavenumbers are related to AgCl, while the peak at 86 cm^{-1} is characteristic for elemental Ag, which can be formed under influence of the laser, because of the photosensitivity of AgCl and its decomposition [172]. Typically, AgCl forms a face-centered cubic lattice structure in which halogen atoms can act as binding or bridging ligands between Ag ions or as terminal atoms. As given in [172], the bridged halogen is represented by a lower stretching frequency than the terminal halogen, so it can be supposed that the peaks at 75 cm^{-1} and 240 cm^{-1} wavenumbers attributed to the bridging and terminal binding of Ag-Cl, respectively.

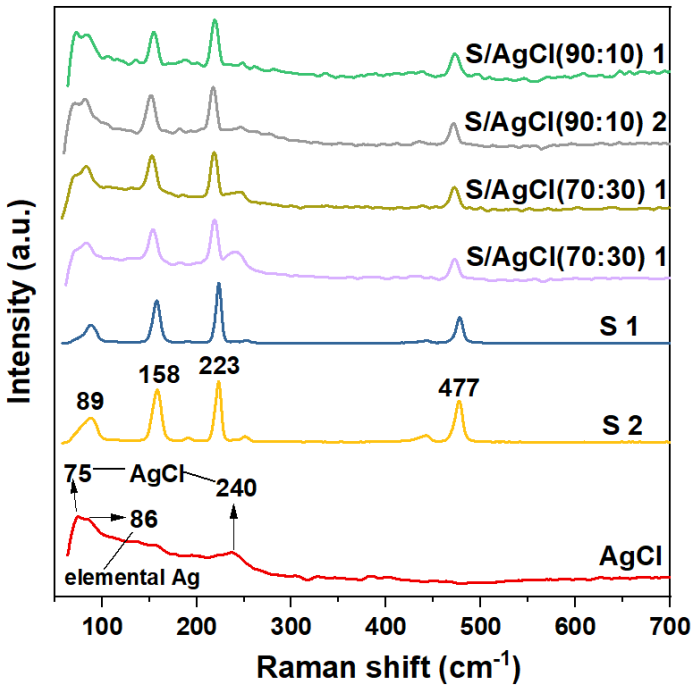

Figure 9 - Raman spectra of the S/AgCl, pure S 1, 2 and AgCl [290]

Figure 10 is depicted Raman spectra for S/AgBr (90:10) 1, 2, S/AgBr (70:30) 1, 2, pure AgBr and S (1, 2). Pure AgBr represented by three characteristic peaks at about 70, 130 and 180 cm^{-1}. Peaks at 70 and 130 cm^{-1} can be attributed to Ag lattice vibrations. The peak at 180 cm^{-1} is conditioned by stretching of the Ag–Br bond, which is echoes with results for AgCl (considering the difference in mass [44]). S/AgBr demonstrate a combination of S and AgBr peaks with unchanged positions.

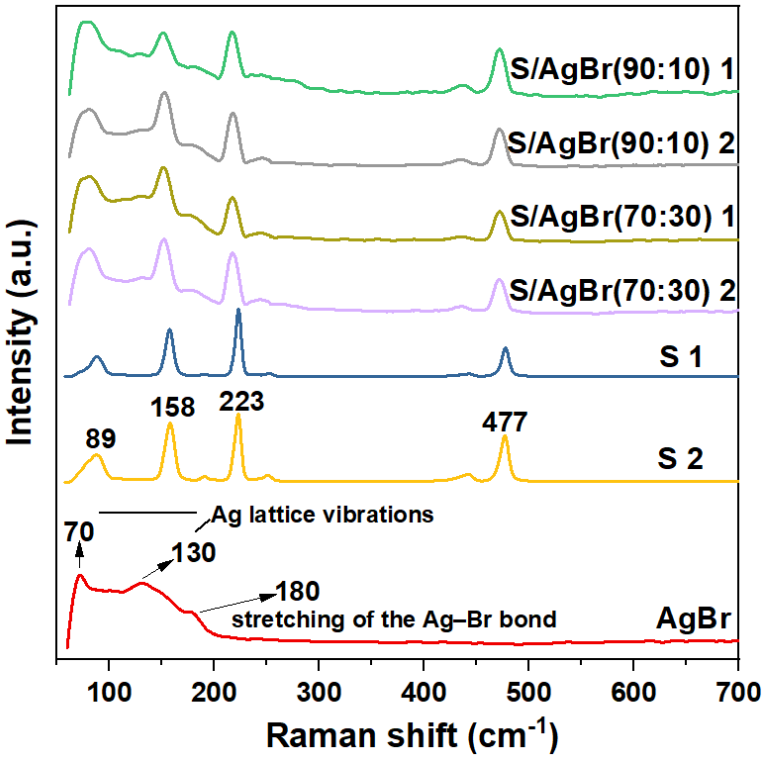

Figure 10 - Raman spectra of the S/AgBr; pure S 1, 2 and AgBr [290]

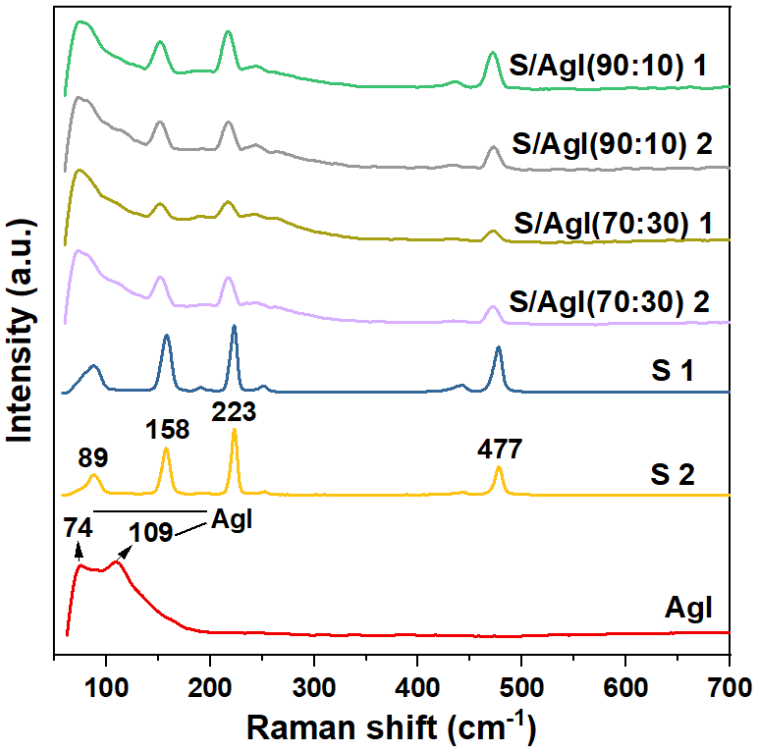

Figure 11 - Raman spectra of the S/AgI; pure S (1, 2) and AgI [290]

In Figure 11 the Raman spectra of S/AgI (90:10) 1, 2, S/AgI (70:30) 1, 2 micro-/nano-structures pure compounds are shown. For pure AgI can be highlighted two peaks at 74 and 109 cm^{-1}. The four clear peaks at 89, 158, 223 and 477 cm^{-1} are attributed to sulfur. The results of analysis are analogue to [172; 291]. S/AgI as other samples demonstrate a combination of S and AgI peaks with unchanged positions.

3.1.3 XPS analysis

For this method of analysis samples with the 30 % AgX content were chosen. The survey spectrum revealed that samples represented by Ag, Cl, Br and S pointing out that these were main elements (Figure 12 a, b) [290]. The presence of the O 1s can be explained by the adhesion of oxygen molecules to the surface of materials, while C 1s was indicated because of using a carbon tape for fixing the powders. In Figure 12 c and d [290] Ag 3d spectra of of AgCl, S/AgCl (70:30) 1, 2 and AgBr, S/AgBr (70:30) 1, 2 samples are shown, respectively. In general, for Ag 3d spectra two main peaks are noticeable, at about 367.0 and 373.0 eV relating to Ag $3d_{3/2}$ and Ag $3d_{5/2}$, respectively, alongside two minor peaks deconvoluted from the main ones. The smaller peaks are visible because of the presence of metallic Ag^0. This is proven by the spin energy separation of two mean peaks being up to 6.0 eV [293]. Metallic Ag can be formed because of photosensitivity of the AgX, what leads to their photoreduction into metallic Ag and free halogen gases on the surface of materials. This process was the most significant for the sample S/AgCl (70:30) 1 where the Ag in its elemental form is predominant. However, elemental Ag was not identified by XRD for all samples, what means that photoreduction is taking place only on the surface of the materials [288]. In Figure 12 e [290] spectra of Cl 2p with peaks at 197.0 and 199.0 eV is shown [294]. For S/AgCl (70:30) 1 micro-/nano-structure chlorine binding energies are significantly shifted, what explained by the photosensability of the samples. Br 3d spectra (Figure 12 f) [290] revealed similar signals at ~ 67.7 and 68.6 eV [295] for all three micro-/nano-structures. S 2p spectra (Figure 12 g) [290] of all micro-/nano-structures showed low-intensity signals of sulfur at about 163.0, 164.7 and 170.0 eV corresponding to S $2p_{3/2}$, S $2p_{1/2}$ and S bonds with other elements (mostly oxygen), respectively [293; 294].

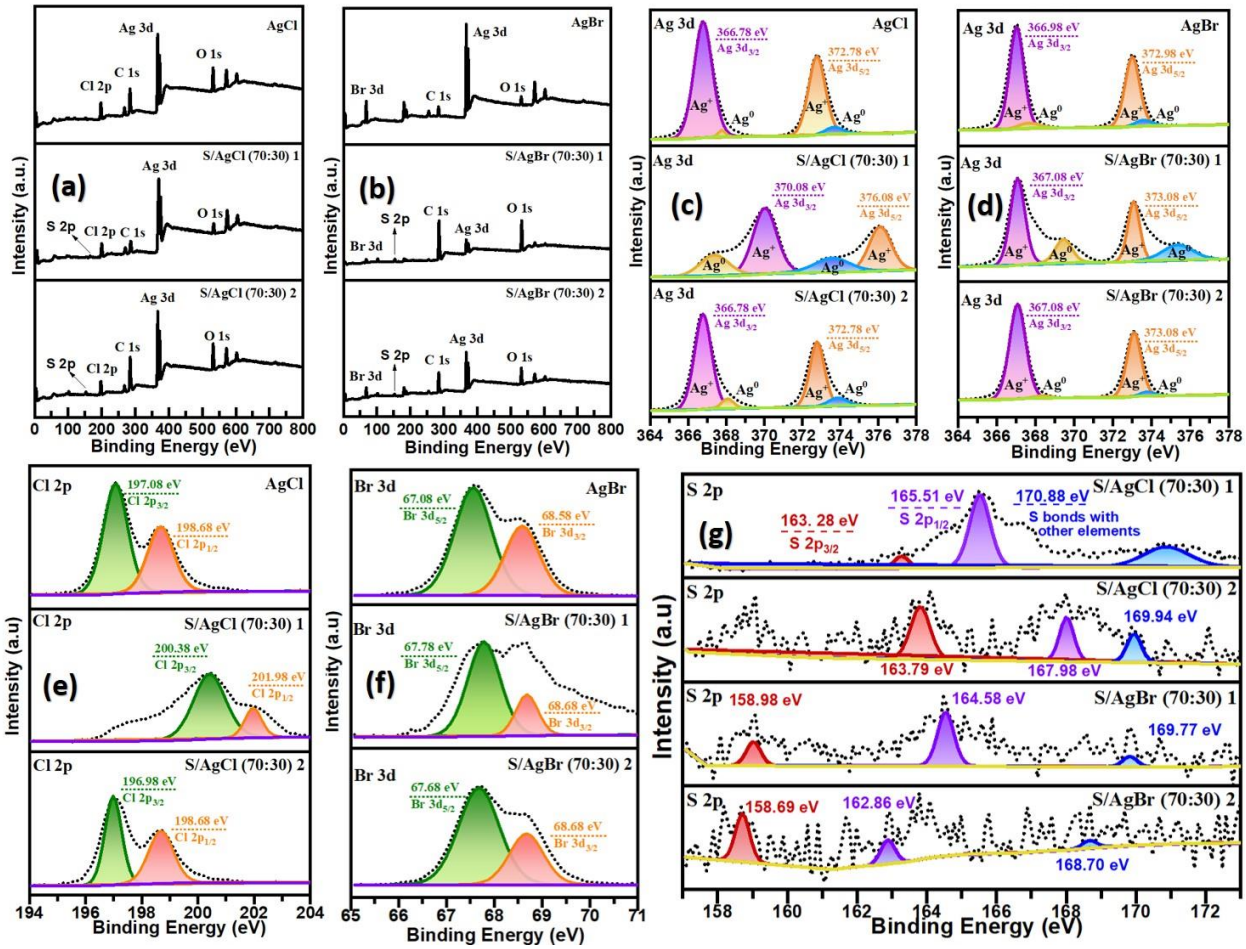

Figure 12 - XPS spectra of the AgCl, S/AgCl (70:30) 1, 2 and AgBr, S/AgBr (70:30) 1, 2 (a-b) – elemental survey; (c-d) – Ag 3d spectra; (e) – Cl 2p spectrum; (f) – Br 3d spectra; (g) – S 2p spectra [290]

3.1.4 SEM analysis

The size and morphology of the micro-/nano-structures were studied by means of SEM. SEM of the S/AgX samples and pure compounds are given in Figures 13-18 [290; 291]. All S/AgX micro-/nano-structures have the same morphology – large and dark particles, which are mostly covered by the smaller grains with the light color. The images with the highest magnifications are demonstrate the specific morphology of the AgX particles (Figures 13-18 b, c, e, f). It also was found, that two methods gave the different size of sulfur particles. Thus, the method 1 produced bigger grains with irregular form (from 20 to 50 μm), than method 2 (from 10 to 25 μm). The presence of water apparently leads to the production of smaller particles. Since sulfur is formed during long spontaneous precipitation, the particles grow together and form one large agglomerate in the case of the 1st method. While in the case of the 2nd method, water partly disperses these agglomerates. The AgCl grains (Figure 13, 14) in the synthesized micro-/nano-structures are

almost spherical or cylindrical with smooth surface; their size is represented by range between 2 and 4 μm. At the lower magnifications the heterogeneous system of the prepared samples can be seen (Figure 15, 16 a, d).

Figures 17 and 18 are show SEM of S/AgBr (70:30) 1, 2. For these samples sulfur forms more plate grains with approximate size from 30 to 70 μm (Figure 15 a, c, e, j). While AgBr particles represented by spherical form and smooth surface; the average size is fluctuated from 0.7 to 2 μm (Figure 16 b, d, f, h). The results of the study at the lowest magnifications are given in Figure 18 a-d, here the heterogeneous nature of the samples are noticeable.

The results for the S/AgI samples are given in the Figures 19, 20. The S/AgI (90:10) 1 have grains sulfur with the range from 20 to 50 μm (Figure 17 a-c) and for the S/AgI (90:10) 2 - from 10 to 20 μm (Figure 17 d-e). AgI grains prepared by the 1st method have clear, smooth triangle and hexagonal form with the 0.5 - 3 μm size. While the 2nd method gave irregular particles with size from 0.3 to 0.9 μm. As for the 30 % samples, here the same tendency with the sulfur. The AgI particles produced by the 1st method represented by triangular and hexagonal form with smooth surface. The 2nd method gave irregular shape AgI particles with loose surface. The size of AgI in the S/AgI (70:30) 1 is in the range from 0.2 to 0.6 μm and for S/AgI (70:30) 2 from 0.4 to 1 μm (Figure 18 (a-c) and (d-f)).

In general, microimages show that AgX particles are represented by grains of several microns in size, however the closest investigation reveales even smaller grains. For example, Figure 13 f, Figure 14 f or Figure 16 f show particles from 100 to 200 nm. Given that the second method allows to obtain particles of two micro-/nano-structures smaller in size, this suggests that the DMSO-water system can create certain conditions for particle stabilization.

In Figure 19 SEM images of the pure AgX are given (AgCl in Figure 19 (a-c) [290], AgBr in Figure 19 (d-f) [290] and AgI in Figure 19 (g-i)). Pure compounds are particles with the regular form, mostly spherical and homogeneous system. The surface area of the grains is smooth and fine. The average size of the particles ranges from 1 to 3 μm.

In addition the SEM of the sulfur prepared by two methods was conducted. Figure 20 (a-c) [290] demonstrates SEM microimages for the S 1 sample, while Figure 20 (d-f) [290] – for the S 2 sample. According to analysis, both methods gave large particles of the sulfur with textured surface and recticular structure. The sulfur particles prepared by method 1 seem to exhibit a porous morphology.

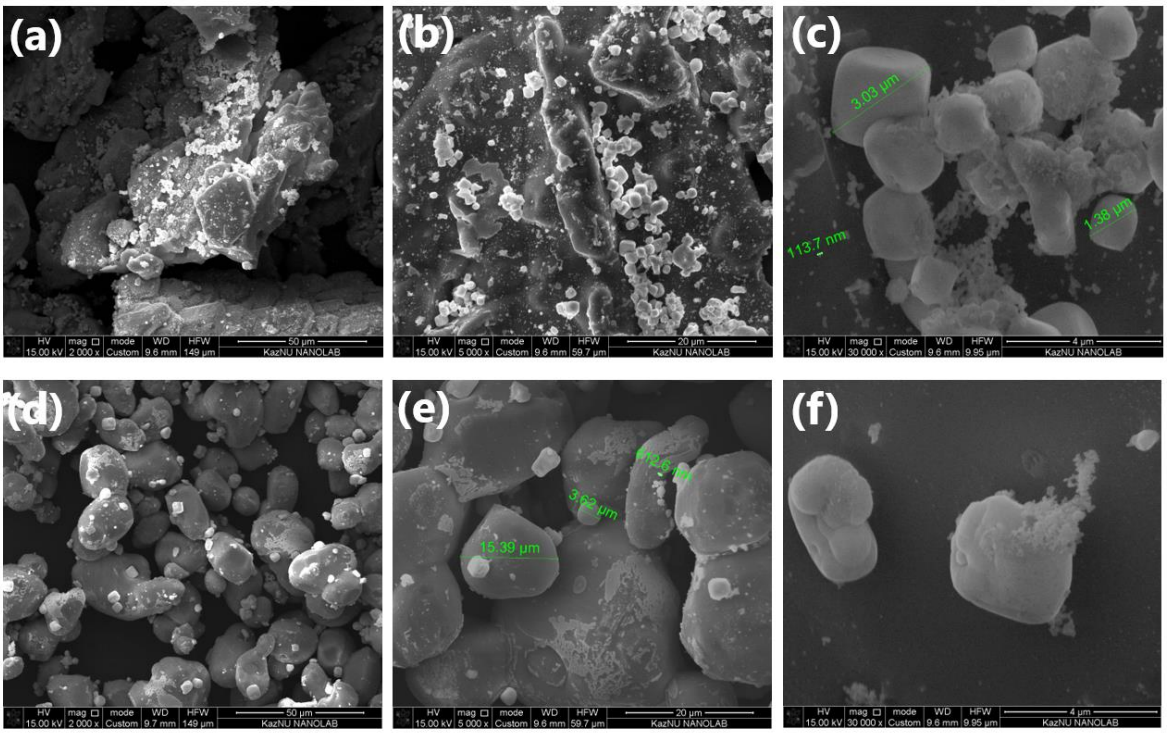

Figure 13 – SEM of the samples: (a-c) – S/AgCl (90:10) 1; (d-f) – S/AgCl (90:10) 2
Magnifications: (a, d) – 2000x; (b, e) – 5000x; (c, f) – 15000x [290]

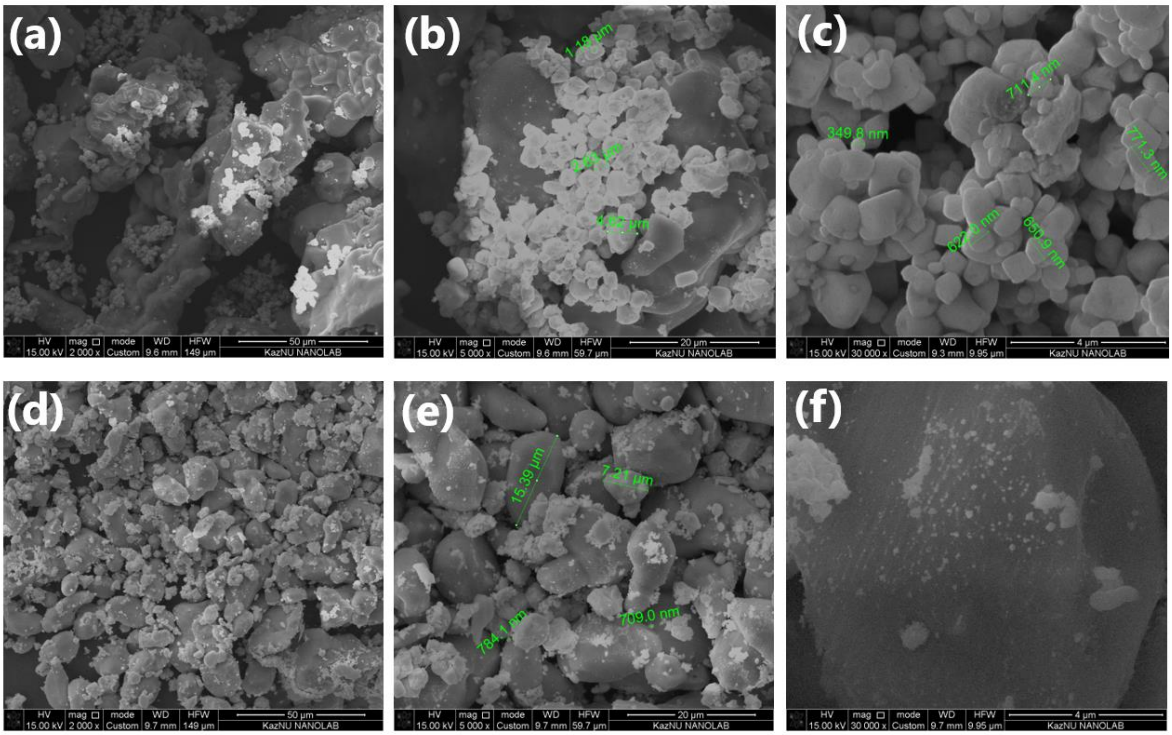

Figure 14 – SEM of the amples: (a-c) – S/AgCl (70:30) 1; (d-f) – S/AgCl (70:30) 2
Magnifications: (a, d) – 2000x; (b, e) – 5000x; (c, f) – 15000x [290]

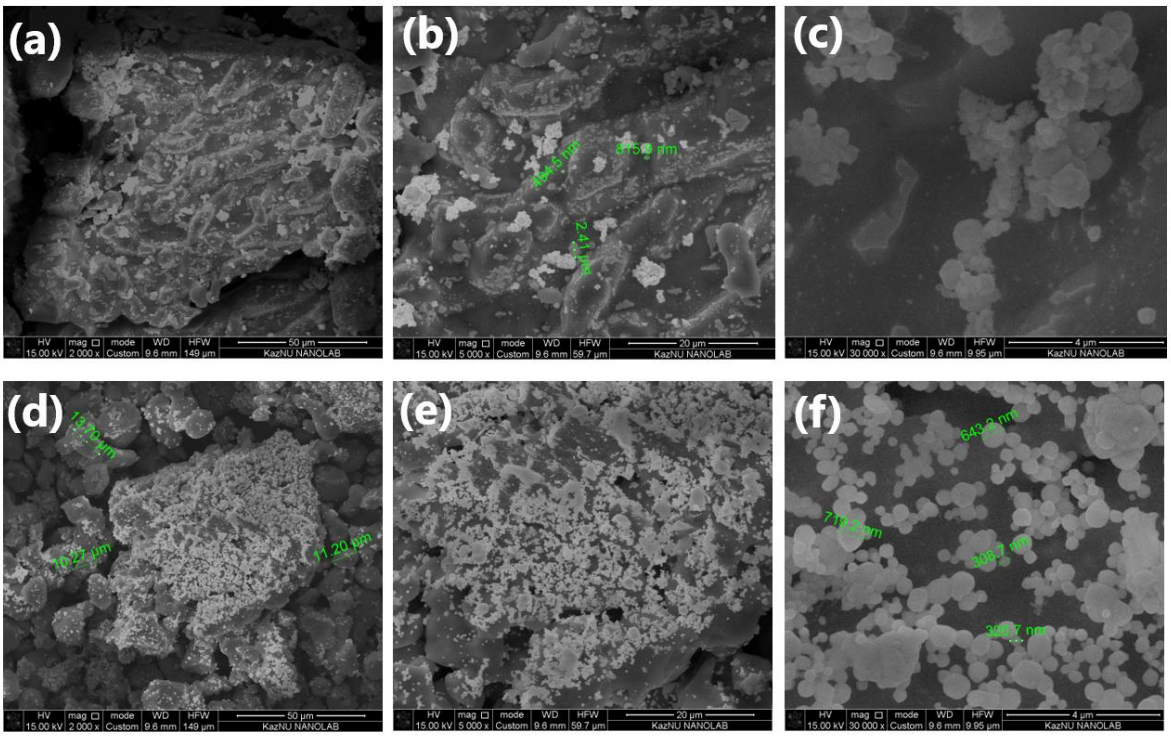

Figure 15 – SEM of the samples: (a-c) – S/AgBr (90-10) 1; (d-f) – S/AgBr (90-10) 2
Magnifications: (a, d) – 2000x; (b, e) – 5000x; (c, f) – 15000x [290]

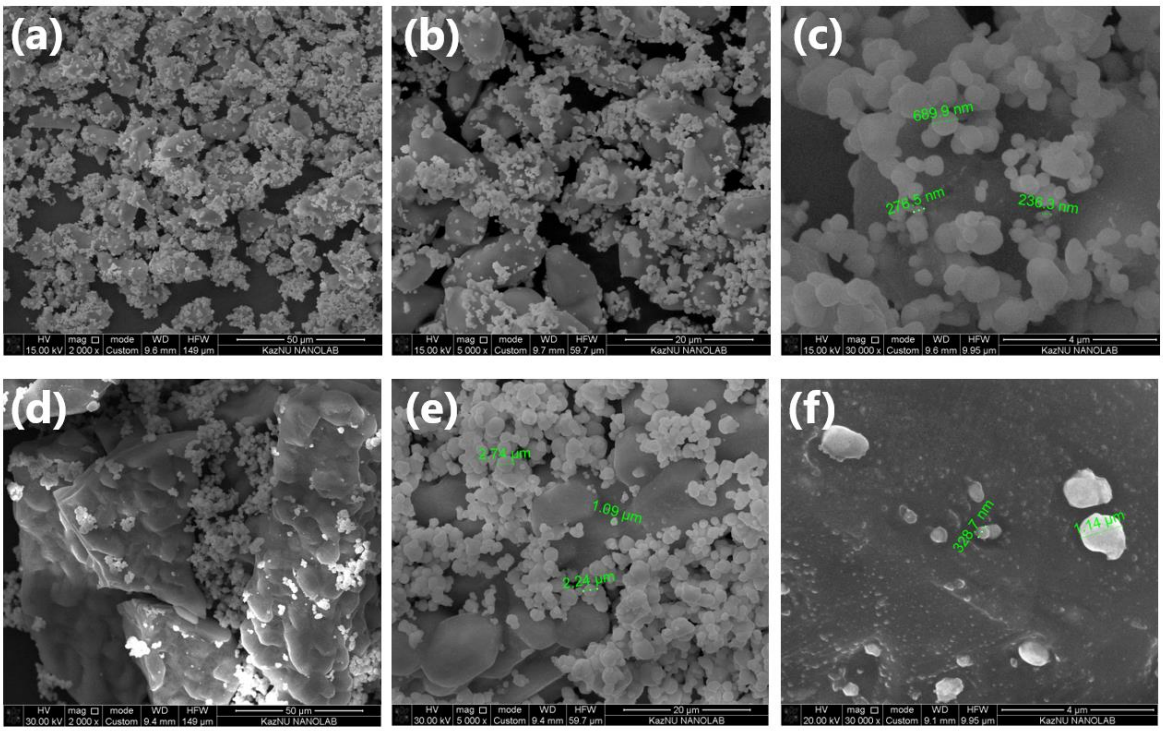

Figure 16 – SEM of the samples: (a-c) – S/AgBr (70:30) 1; (d-f) – S/AgBr (70:30) 2
Magnifications: (a, d) – 2000x; (b, e) – 5000x; (c, f) – 15000x [290]

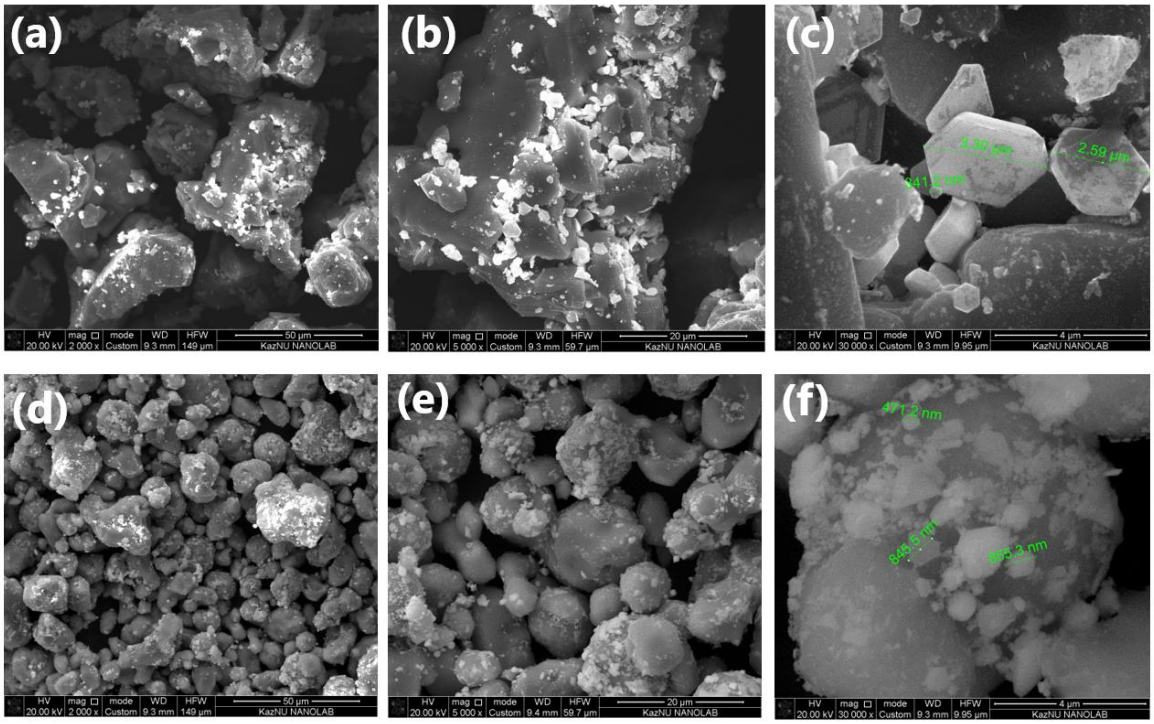

Figure 17 – SEM of the samples: (a-c) – S/AgI (90:10) 1; (d-f) – S/AgI (90:10) 2
Magnifications: (a, d) – 2000x; (b, e) – 5000x; (c, f) – 15000x [291]

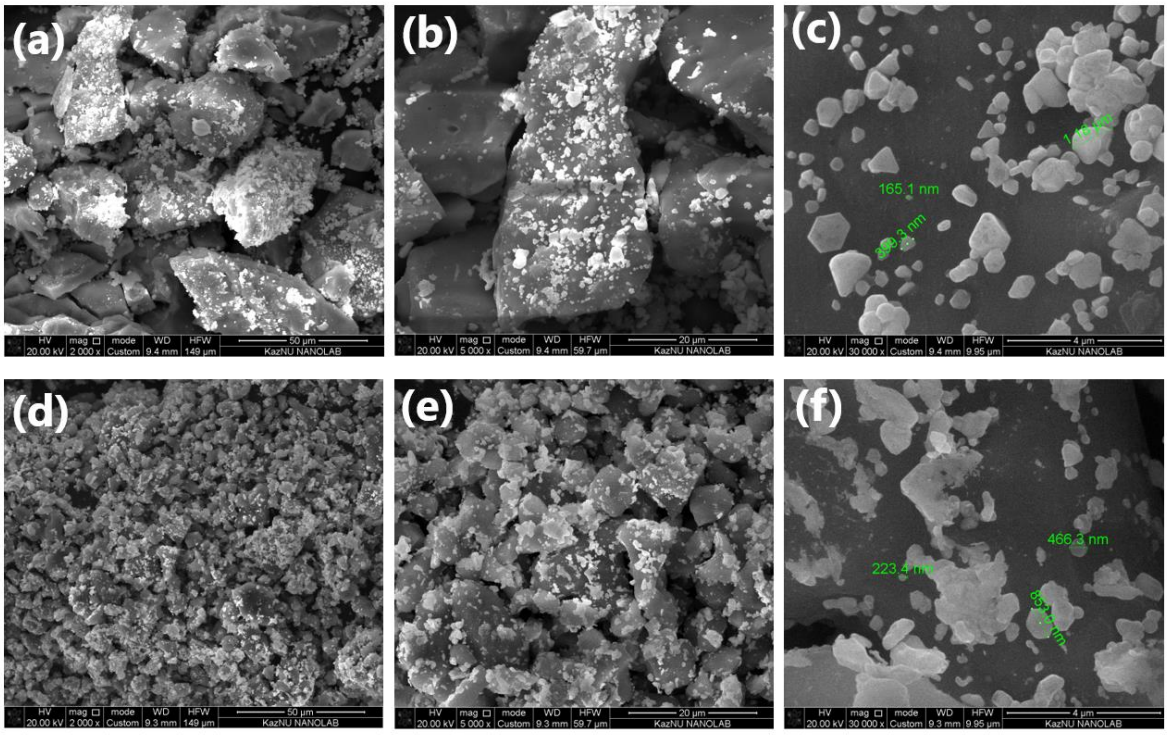

Figure 18 – SEM of the samples: (a-c) – S/AgI (70:30) 1; (d-f) – S/AgI (70:30) 2
Magnifications: (a, d) – 2000x; (b, e) – 5000x; (c, f) – 15000x [291]

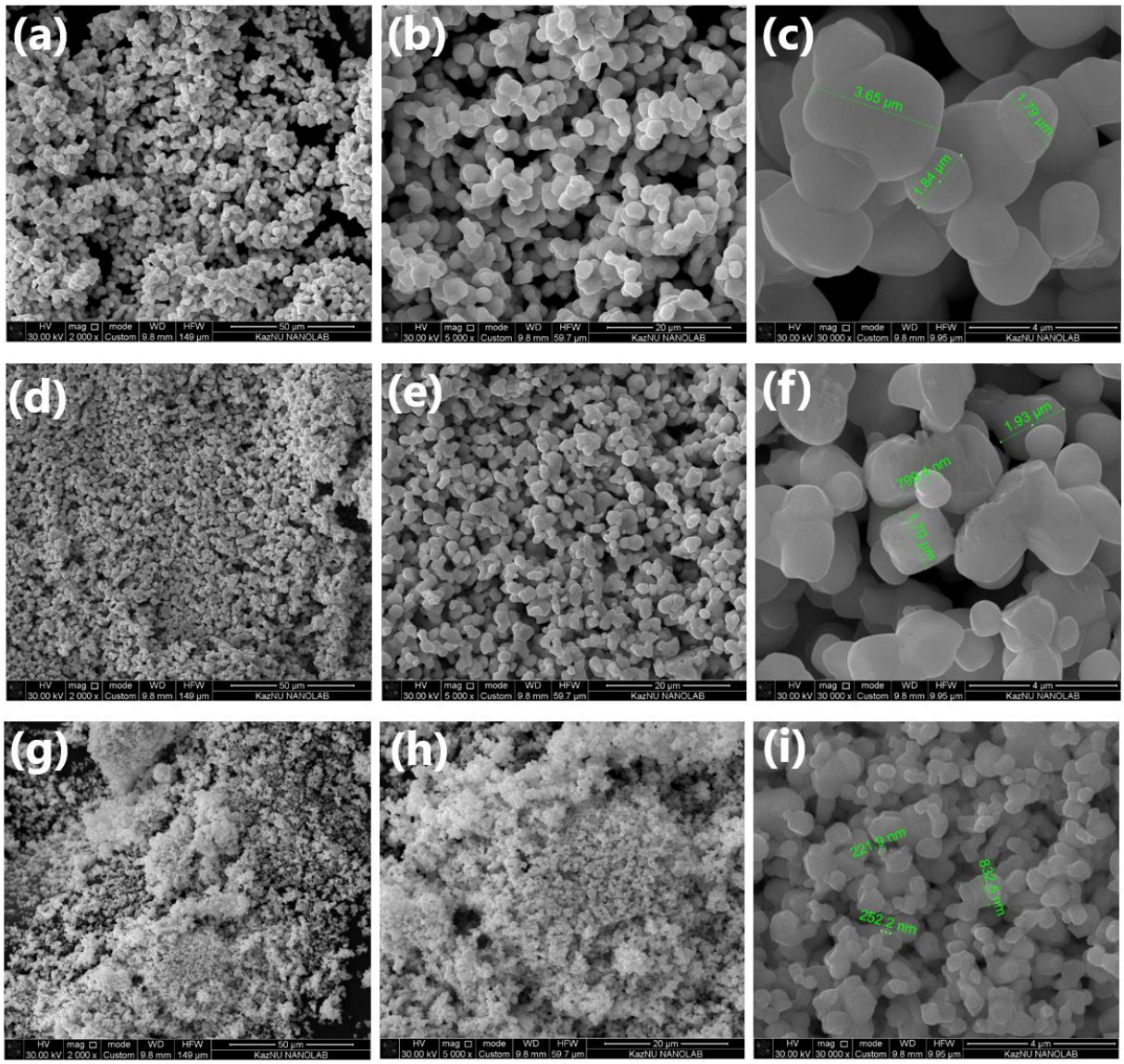

Figure 19 – SEM of the samples: (a-c) – AgCl; (d-f) – AgBr; (g-i) – AgI
Magnifications: (a, d, g) – 2000x; (b, e, h) – 5000x; (c, f, i) – 15000x [290]

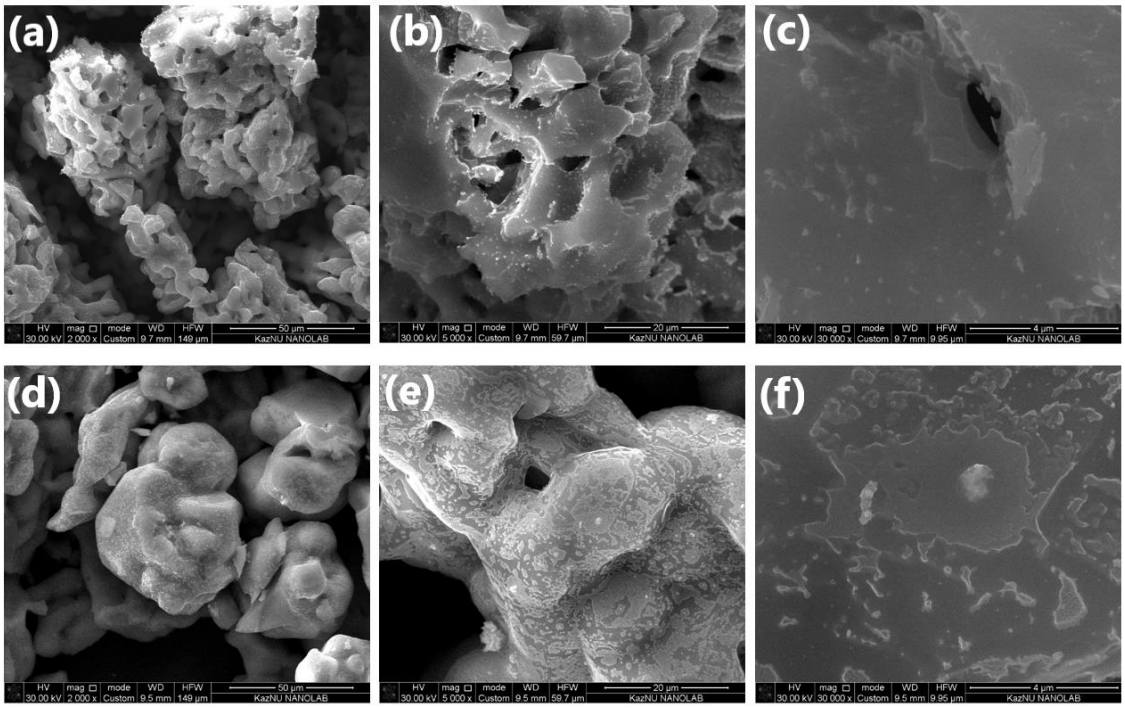

Figure 20 – SEM of the samples: (a-c) – S 1; (d-f) – S 2
Magnifications: (a, d) – 2000x; (b, e) – 5000x; (c, f) – 15000x [290]

3.1.5 HRTEM/EDS elemental mapping

For analysis S/AgCl (70:30) 2 and S/AgBr (70:30) 1 were chosen. Figure 21 [290] demonstrates HRTEM for the S/AgCl (70:30) 2 and Figure 22 [290] - for the S/AgBr (70:30) 1.

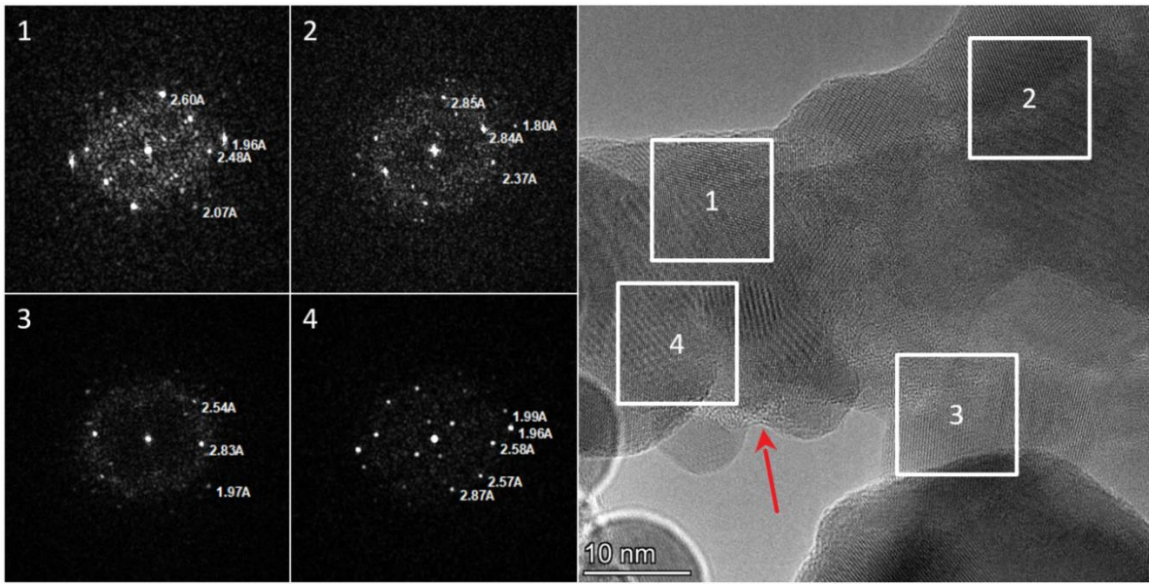

Figure 21 - HRTEM of the S/AgCl (70-30) 2: (1-4) – corresponding Fourier diffractograms with the indicated observed interplane distances [290]

The S/AgCl (70:30) 2 micro-/nano-structure have dense micron-sized aggregates of grains from 5 to 100 nm with a highly developed system of dense intergrain boundaries. Separate particles are rarely observed. According to images of HR, the crystal structure of the grains is observed. The surface of the sample is mostly free from any contamination, but in some cases amorphous near-surface layers up to 5 nm thick are observed (in Figure 23 it marked by red narrow). The interplanar distances (in Figure 23 it marked by numbers from 1 to 4) in the range 2.35–2.37 Å can be related to the cubic crystal lattice of Ag (PDF#87–0597); the distances with the 2.24 Å and 2.50 Å are attributed to hexagonal Ag (PDF#87–0598), and the range 2.77–2.83 Å can be regarded to AgCl (PDF#85–1355).

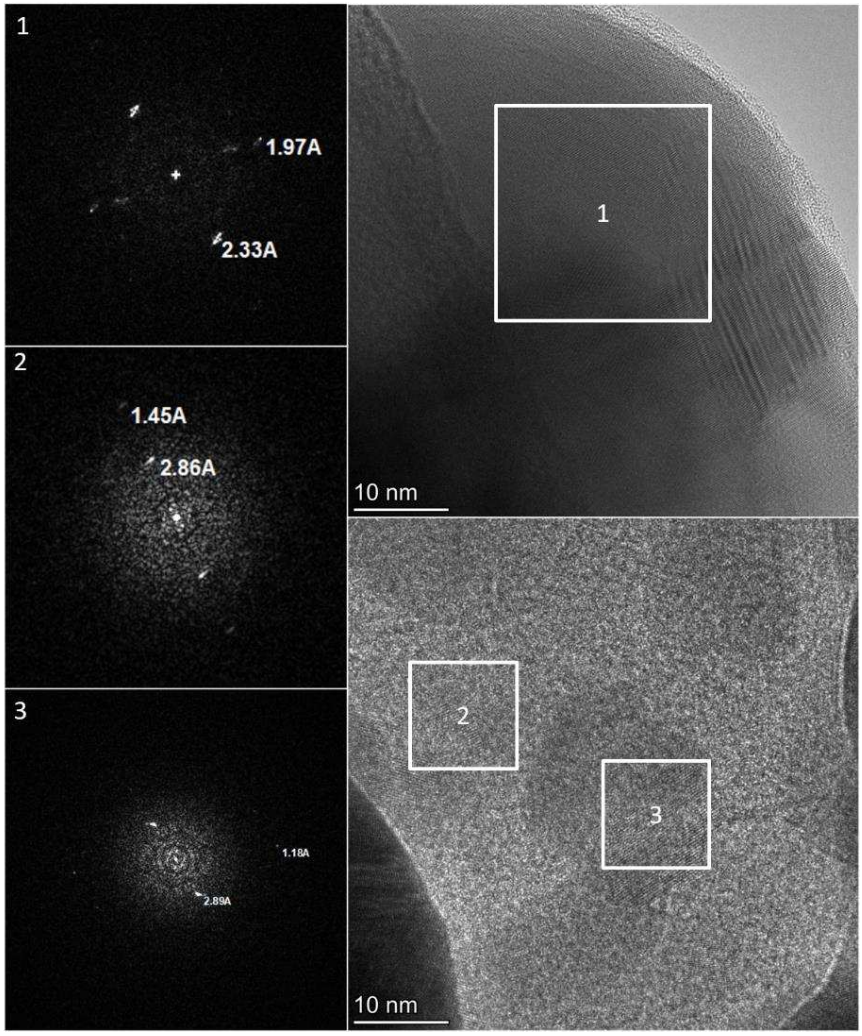

Figure 22 - HRTEM of the S/AgBr (70:30) 1: (1-4) – corresponding Fourier diffractograms with the indicated observed interplane distances [290]

The S/AgBr (70:30) 1 (Figure 24) represented by large aggregates of crystalline grains and an amorphous matrix. Because of the high vacuum conditions and the action of high-energy

electrons's stream, sample quckly changes the original morphology and structure. This is why, it is impossible to show the "initial" state at HR, because these images of the already changed sample. Moreover, sometimes spontaneous formation of the particles from an amorphous matrix is occurs, due to prolonged exposure to electron beam. The observed interplanar distances for large single-crystal particles are close to that of cubic Ag (PDF#87–0597), and for the particles in an amorphous matrix to those of AgBr (PDF#06–0438).

In Figures 23 and 24 [290] EDS elemental mapping of the samples is shown. With help of this analysis the elemental distribution was investigated. Results revealed that morphology of the particles almost the same for both methods. According to elemental mapping, large agglomerates is sulfur, which covered by smaller grains of the AgX. AgX particles are randomly distributed over the sulfur surface, and the presence of nanoparticles up to 100 nm in size is visible. In addition, in Figure 25 (a-b) [290] the spectra of the studies multicomponent materials are given.

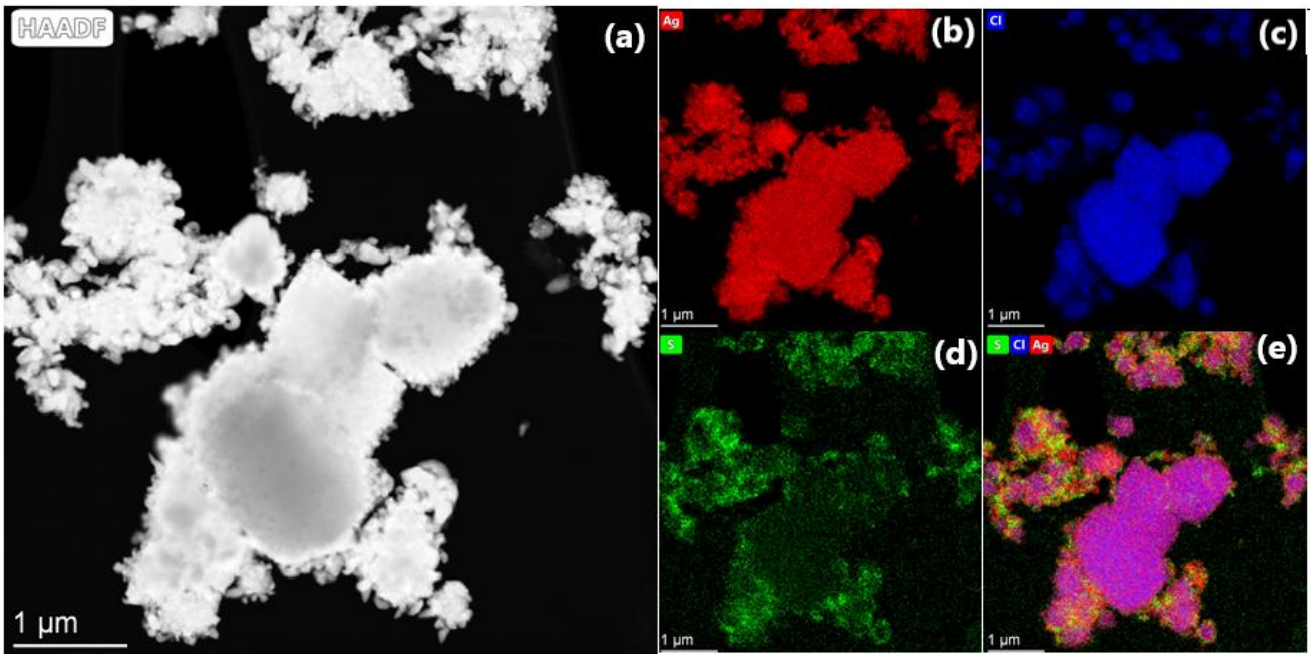

Figure 23 - TEM elemental mapping of the S/AgCl (70:30) 2: (a) - EDS layered image; b – EDS image of Ag distribution; (c) - EDS image of Cl distribution; (d) - EDS image of S distribution: (e) - EDS distribution of the all elements [290]

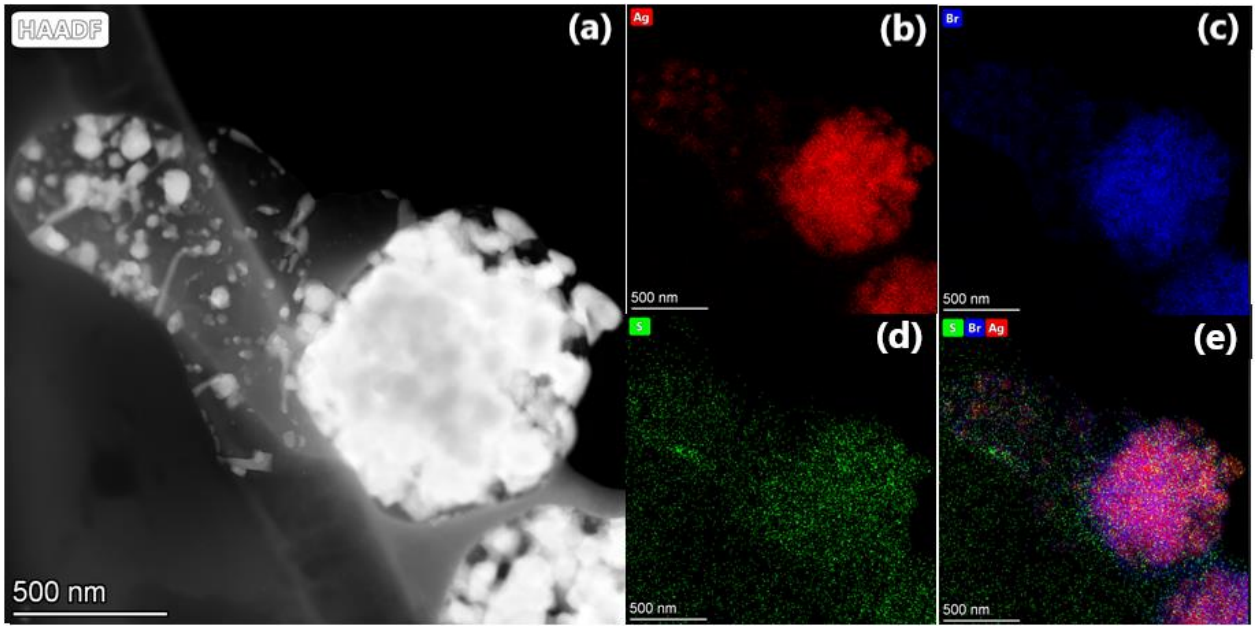

Figure 24 - TEM elemental mapping of the S/AgBr (70:30) 1: (a) - EDS layered image; b – EDS image of Ag distribution; (c) - EDS image of Br distribution; (d) - EDS image of S distribution: (e) - EDS distribution of the all elements [290]

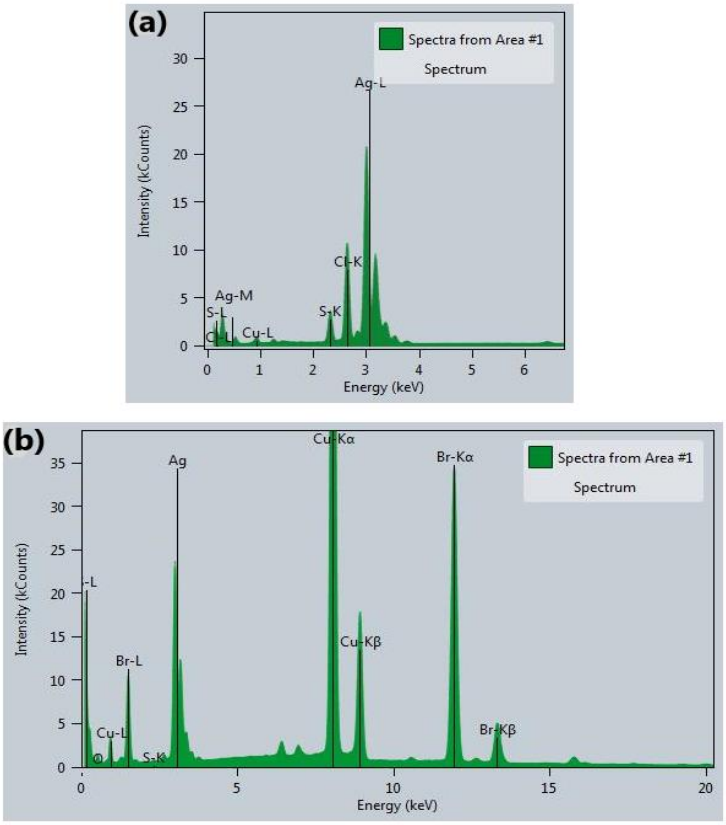

Figure 25 - EDS spectra of samples: (a) – S/AgCl (70:30) 2 and (b) – S/AgBr (70:30) 1 [290]

Based on the SEM, TEM and TEM-EDS elemental mapping, the next conclusion can be done: dilution of the reaction mixture solution with water provokes the formation of smaller sulfur grains. The dilution of the system of micro-/nano-structures in DMSO with anti-solvents like water [296; 297] influenced on morphology and particle size. According to our experiments, 1:1 dillution already leads to the positive effect. Moreover, DMSO molecules, even with low dilution with anti-solvents, increased the number of sulfur particles formed, and therefore it can be assumed that DMSO molecules are a micelle-forming component of the system, since they have an affinity for the sulfur surface. As for the DMSO–water system, the micelle structure consists of stable complexes of these components, which, given the hydrophobicity of sulfur particles and provides them the highest protection against aggregation. Thus, it can be concluded that DMSO has the properties of a surfactant [297; 298] due to the possibility of stabilizing sulfur particles, and it also leads as solvent of the system. The application of two methods of precipitation makes it possible to demonstrate this feature clearly.

3.1.6 Specific surface area analysis

Two samples of 30 % micro-/nano-structures based on AgCl and AgBr were analyzed by the low-temperature nitrogen adsorption. Results are represented in Figure 26 (a, c) for S/AgCl (70:30) 1 and in Figure 26 (b, d) for S/AgBr (70:30) 1 [290]. According to IUPAC classification of isotherms, both curves given in Figure 26 a and b related to type III of isotherms, which indicate that of weak adsorbent–adsorbate interactions on a non-porous or macroporous adsorbents. Specific surface area (S_{BET}) was calculated with help of the part of adsorption isotherm in the 0.05-0.35 range of relative pressure. Thus, for the S/AgCl (70:30) 1 the S_{BET} was 1.6 m^2/g and for the S/AgBr (70:30) 1 - 0.6 m^2/g. Such low values can be explained by incomplete cleaning of pores from DMSO due to low outgassing temperature (45°C), selected for analyeie. In addition increasing of the temperature also leads to the evaporation of sulfur. It is also possible to notice the presence of mesopores in the structure of the samples, since there is no overlap of the adsorption and desorption parts of the isotherms. The results obtained were also confirmed by measuring the pore size distribution (Figure 26). It was found that both samples are represented by the presence of very small pores that have a radius less than 100 Å, i.e. 10 nm which corresponds to fine mesopores. In addition, the pores of the S/AgBr (70-30) 1 sample are slightly smaller than those of the S/AgCl (70:30) 1 and their radius is 3 and 6 nm, respectively. The results of the surface area analysis are summarized in Table 9.

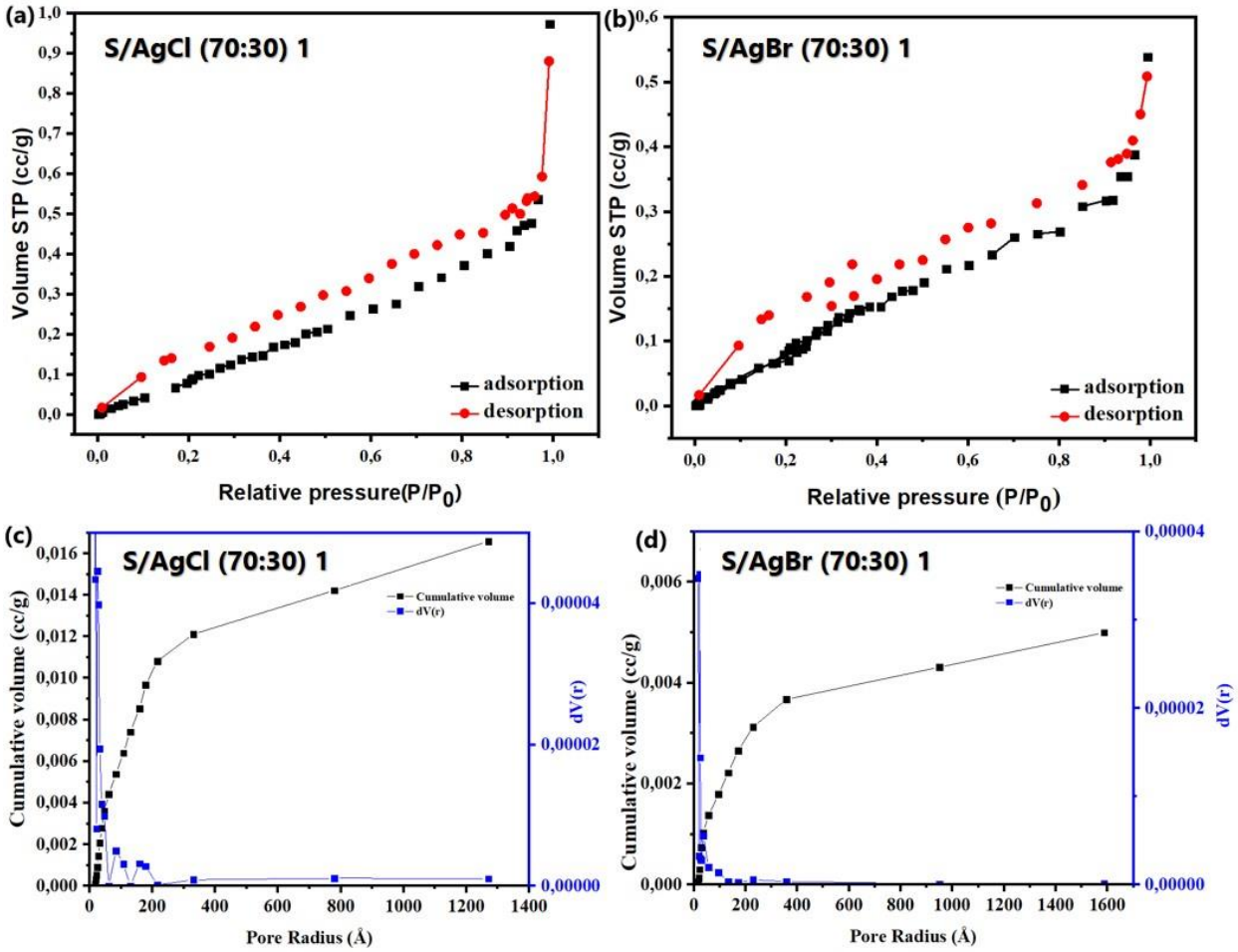

Figure 26 - Nitrogen adsorption–desorption curves of the samples: (a) – S/AgCl (70:30) 1 (b) – S/AgBr (70:30) 1. Pore size distribution curves of the samples: (c) – S/AgCl (70:30) 1 and (d) – S/AgBr (70:30) 1 [290]

Table 9 – Brunauer – Emmet – Teller (BET) cpecific surface areas, isotherm types (pore types) and pore size of the samples

Sample	BET surface area (m^2/g)	Isotherm type (pore type)	Pore size (nm)
S/AgCl (70:30) 1	1.6	Type III (macroporous)	6
S/AgBr (70:30) 1	0.6	Type III (macroporous)	3

3.1.7 TGA-DSC

TGA-DSC was conducted for investigation of the thermal properties, as well as to determine the actual content of sulfur and AgX (X=Cl, Br) in the S/AgX (70:30) 1, 2 micro-/nano-structures The results are given in Figure 27 [290] TG analysis showed that theoretical data converge with practical data and the content of elemental sulfur is 70 % in all samples. The exception was the sample S/AgCl (70:30) 2, in which the mass content of sulfur was equal to 66 %. From the data

obtained, it can be seen that the beginning of sulfur evaporation of this sample starts at 220°C, and its complete evaporation is achieved at 300°C, which corresponds to the literature data of nanosulfur evaporation [99]. The mass losses of the studied objects vary slightly, which indicates different degrees of sulfur-halide binding. For example, for S/AgBr (70:30) 1, the sulfur evaporation process lasts the longest and the sulfur leaves the sample composition only at 400°C, despite the fact that the heating rate and the mass of the samples were the same in all cases.

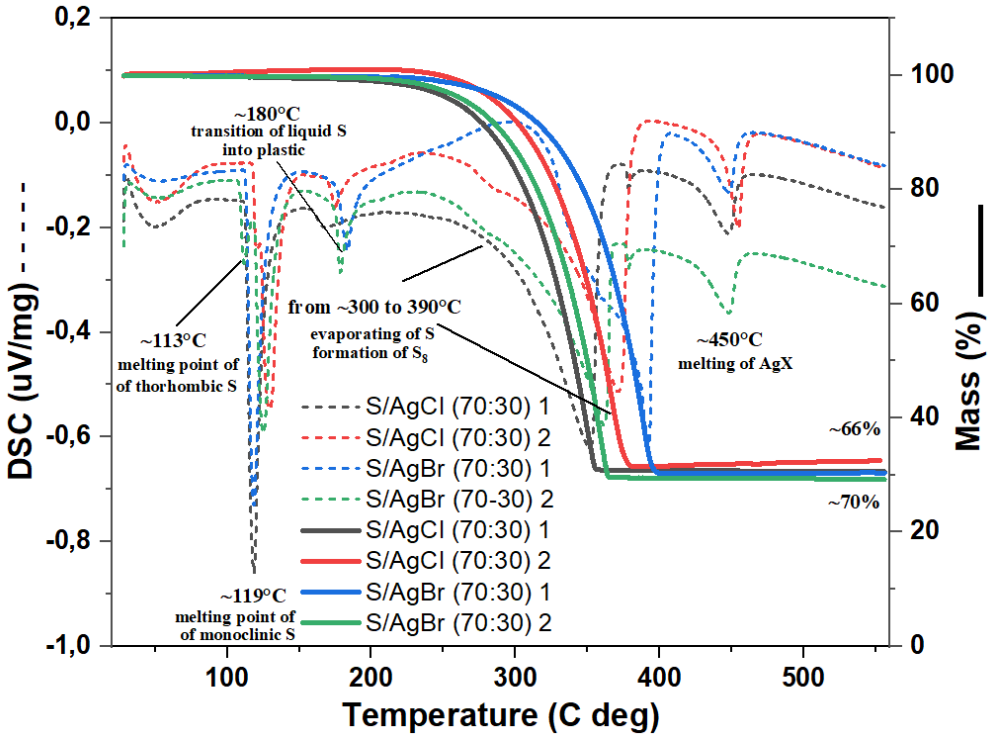

Figure 27 - TGA-DSC of the S/AgX (70:30) 1, 2 [285]

The DSC curves are expressed by several endothermic processes, each of which is responsible for certain phase transitions. For all samples, there is a small peak at 113°C and a rather large peak at 119°C [78]. These two peaks correspond to the melting points of orthorhombic and monoclinic sulfur, respectively. At room temperature, sulfur is in a rhombic form, but at temperatures above 96°C it turns into a monoclinic form. The presence of a small amount of rhombic sulfur is explained by the fact that when it is heated at a rate of 10°C/min, sulfur does not have time to completely turn into monoclinic until 113°C and begins to melt. The difference between 113°C and 119°C is only 6°C, which when heated at a speed of 10°C/min leads to overlapping peaks, since the system heats up from 113°C to 119°C in just 36 seconds. Another endothermic effect is observed at a temperature of about 180°C, which corresponds to the transition of liquid sulfur into plastic. The endothermic effect at the range from 300°C to 390°C is

the largest and corresponds to the evaporation of sulfur from the samples with the formation of sulfur molecules (gaseous S_8) [78]. Subsequent endothermic effects apply only to AgX since all elemental sulfur completely evaporates at 400°C. The endothermic effect at about 450°C indicates melting of AgX nanoparticles [78]. In conclusion, the results of the TGA-DSC show that the samples consist of ≈70% elemental sulfur and ≈30% AgX.

3.2 Application

3.2.1 Photocatalytic activity

Figures 28-33 (a-d) demonstrates absorbance spectra of the S/AgX micro-/nano-structures. It can be seen that for every sample the twice repeating of the photocatalytic experiments was done. While comparison of the photocatalytic activity of the investigated and corresponding reference powders are given in Figures 34, 35 (a-b) [290] and 36 [291]. After number of photocatalytic experiments, we noticed that pure AgCl and AgBr are higly active. Then, AgCl and AgBr based samples were compared with the effective mass of pure AgX for parity of the process. For instance, 6 mg of pure AgX was taken for 30 % samples and 2 mg for 10 % samples. For AgI based materials this procedure was skipped, because their activity was low in all cases.

According to Figure 34 (a) S/AgCl (90:10) 1, 2 and pure sulfur were not active during the whole period of light irradiation. As for pure AgCl, effective mass of it is effective only on 50 %.

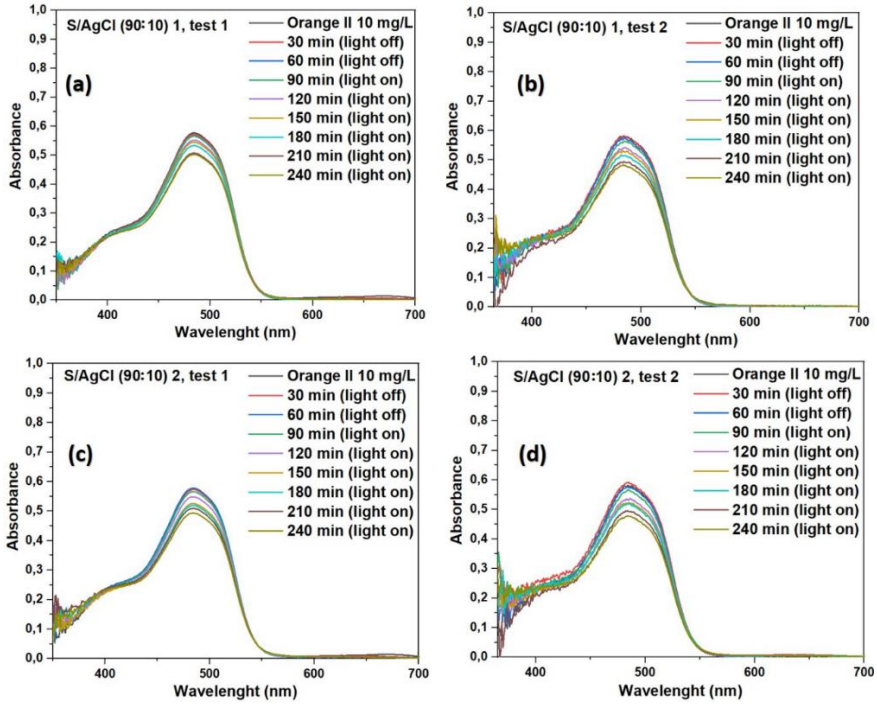

Figure 28 - Absorbance spectra of the: S/AgCl (90:10) 1 (a) – test 1; (b) – test 2; S/AgCl (90:10) 2 (c) – test 1; (d) – test 2

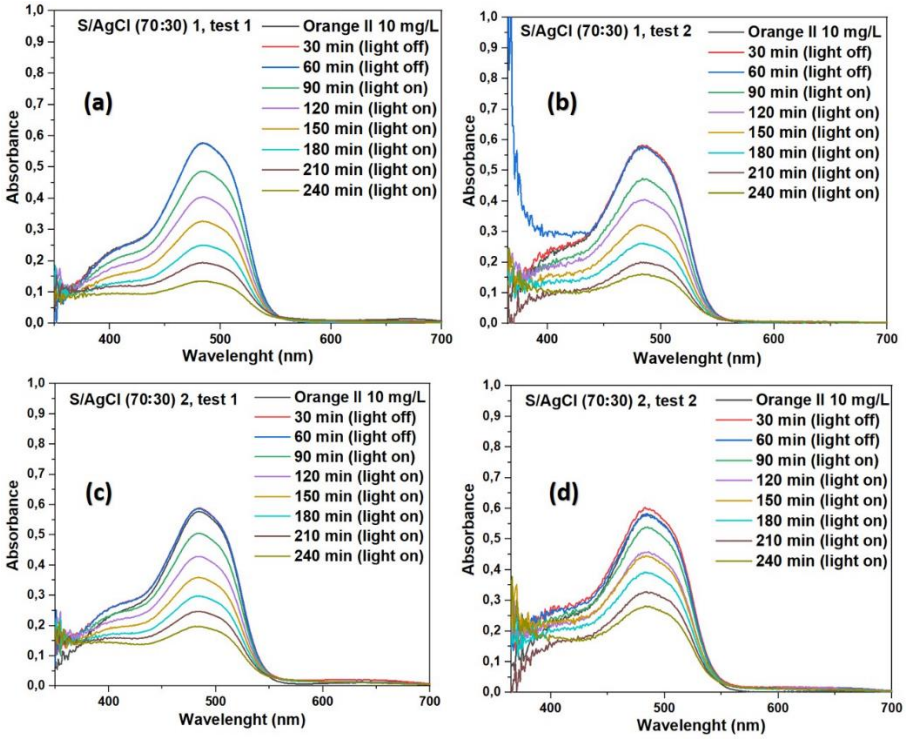

Figure 29 - Absorbance spectra of the: S/AgCl (70:30) 1 (a) – test 1; (b) – test 2; S/AgCl (70:30) 2 (c) – test 1; (d) – test 2

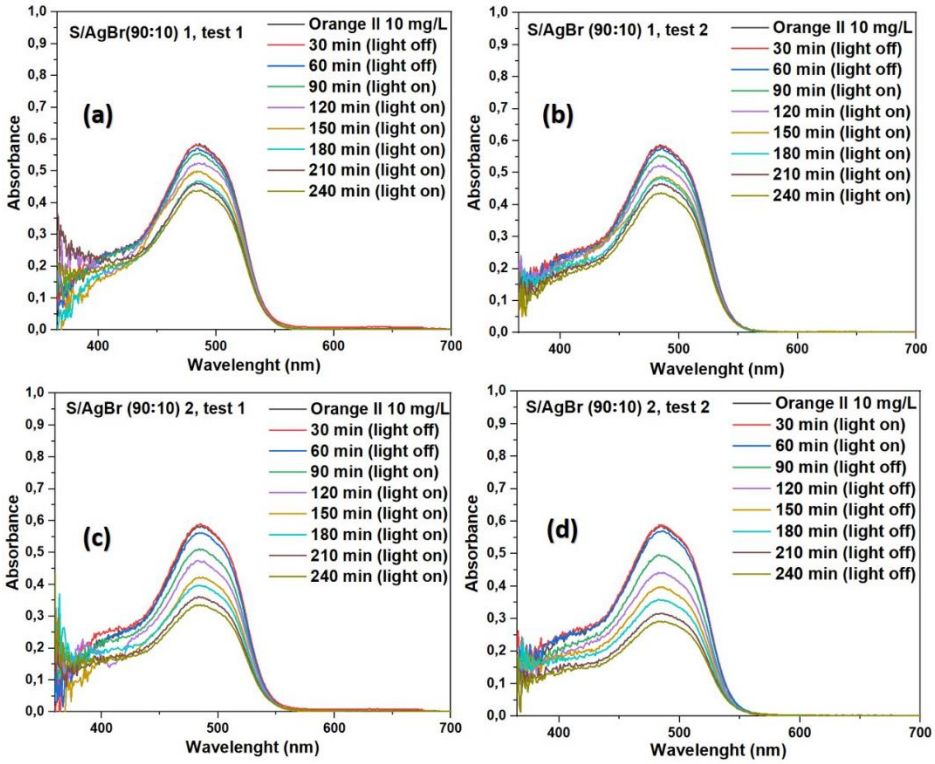

Figure 30 - Absorbance spectra of the: S/AgBr (90:10) 1 (a) – test 1; (b) – test 2; S/AgBr (90:10) 2 (c) – test 1; (d) – test 2

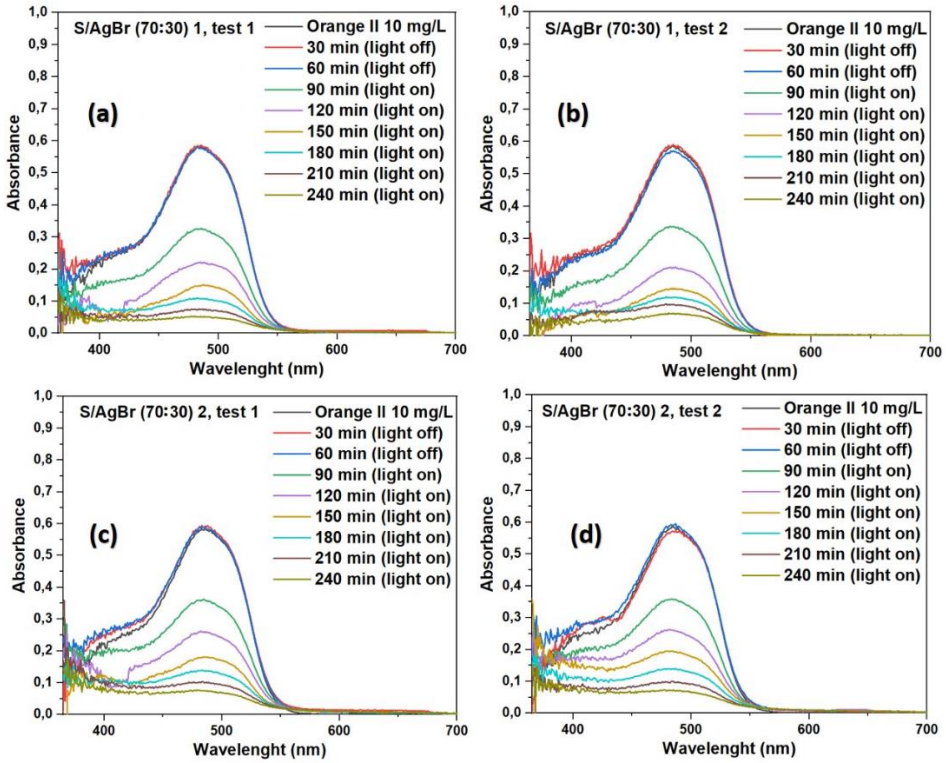

Figure 31 - Absorbance spectra of the: S/AgBr (70:30) 1 (a) – test 1; (b) – test 2; S/AgBr (70:30) 2 (c) – test 1; (d) – test 2

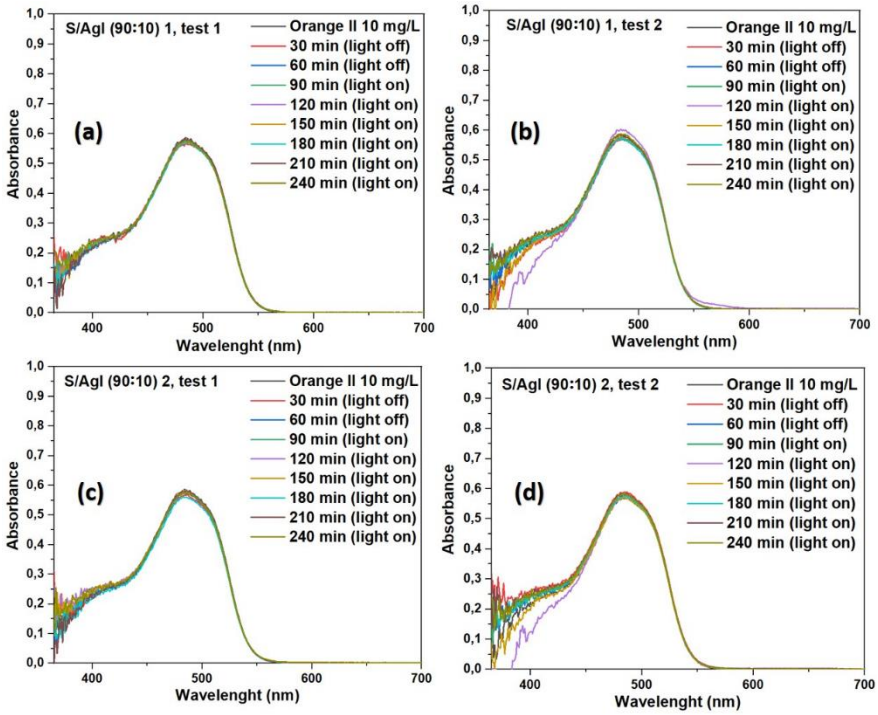

Figure 32 - Absorbance spectra of the: S/AgI (90:10) 1 (a) – test 1; (b) – test 2; S/AgI (90:10) 2 (c) – test 1; (d) – test 2

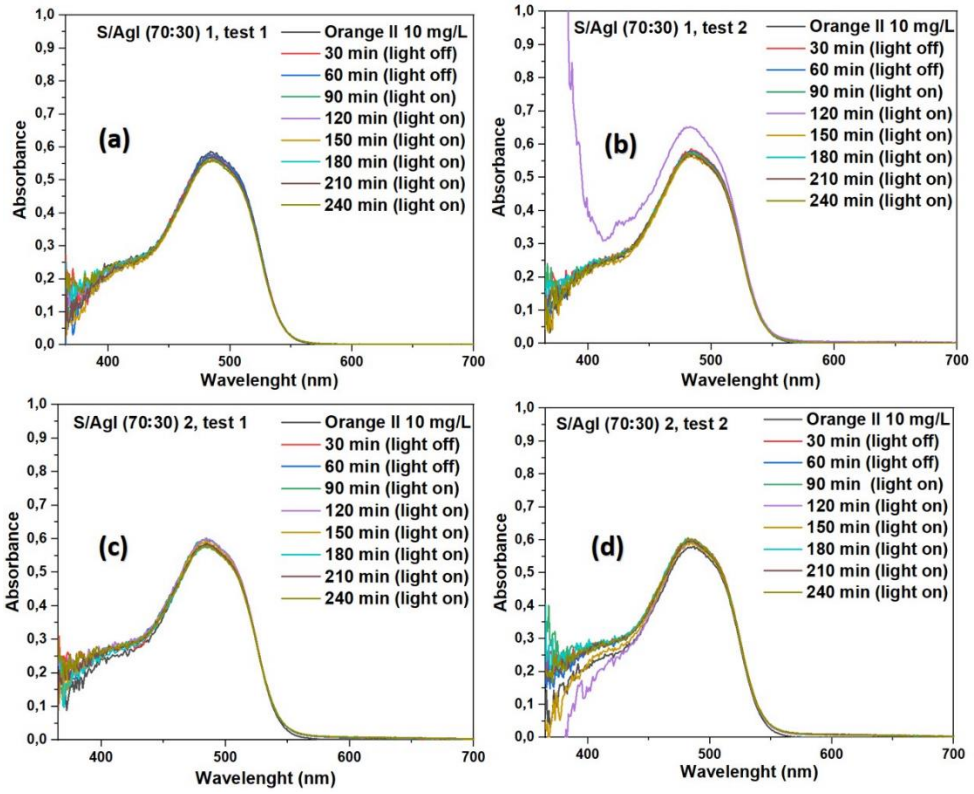

Figure 33 - Absorbance spectra of the: S/AgI (70:30) 1 (a) – test 1; (b) – test 2; S/AgI (70:30) 2 (c) – test 1; (d) – test 2

Results for the S/AgCl (70:30) 1, 2 are given in Figure 34 (b). Graph shows that pure AgCl is able to degrade almost 87 % of Orange II molecules, during the 180 min of light exposure. While in [294], AgCl was more active; such difference can be explained by using of the less amount of silver halide effective mass. Among all AgCl based samples, the S/AgCl (70:30) 1 had the greatest activity, degrading about 70 % of the organic dye molecules. S/AgCl (70:30) 2 was even less active, degrading near 50 % of the model solution.

Figure 35 (a-b) reveales data about photocatalytic activity of AgBr based samples. 10 % samples were less active among all AgBr based multicomponent materials, however, S/AgBr (90:10) 1 was less active than S/AgBr (90-10) 2 (Figure 35 (a)). Pure AgBr with effective mass 6 mg degraded about 80 % of organic dye (Figure 35 (b)). S/AgBr (70:30) 1, 2 were more active than S/AgCl (70:30) 1, 2 samples. For example, in [299] AgBr based micro-/nano-structures are show higher photocatalytic activity and explained by the smaller sizes of the nanocomposite graines. This applies to our results as well, since SEM analysis exibited that S/AgBr particles are in general smaller than those of S/AgCl. S/AgBr (70:30) 1, 2 micro-/nano-structures were effective on about 87 %. While pure AgBr is more active than AgCl and was able to degrade about 94 % of Orange II molecules. However, in study Cui and his collegues [172], pure AgBr showed average

photocatalytic activity with azo dyes. Such difference can pointed that the solvothermal synthesis approach is more suitable for obtaining AgBr with high photocatalytic activity. 30 % AgBr micro-/nano-structures exhibited the strongest ability of organic dye degrading. The result for both samples were approximately the same, but sample prepared by method 1 was more active on 1-2 %, than sample prepared by method 2.

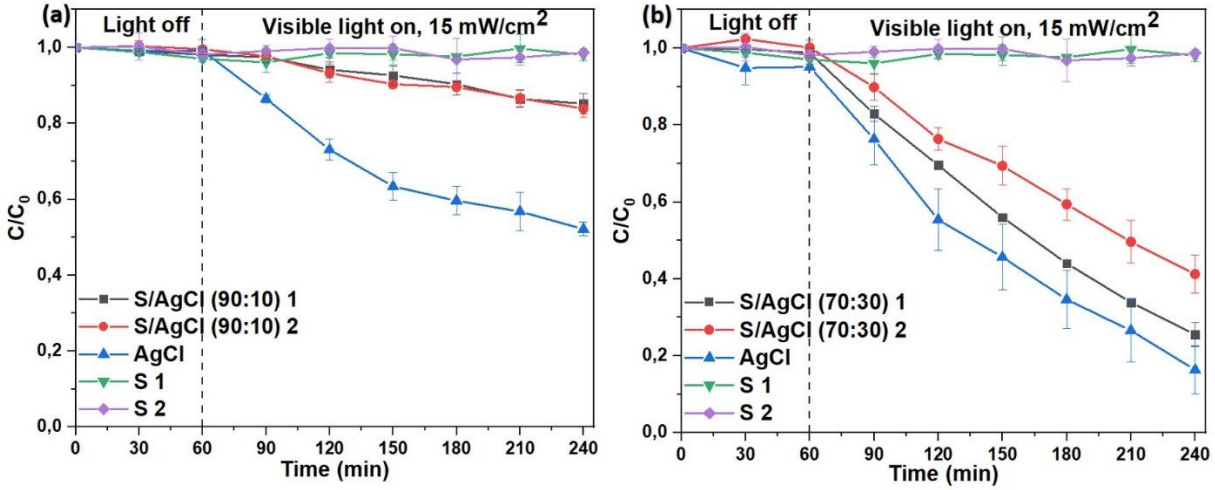

Figure 34 - Comparison of the photocatalytic activity of the samples: (a) – S/AgCl (90:10) 1, 2, AgCl and S 1, 2; (b) – S/AgCl (70:30) 1, 2, AgCl and S 1, 2 [290]

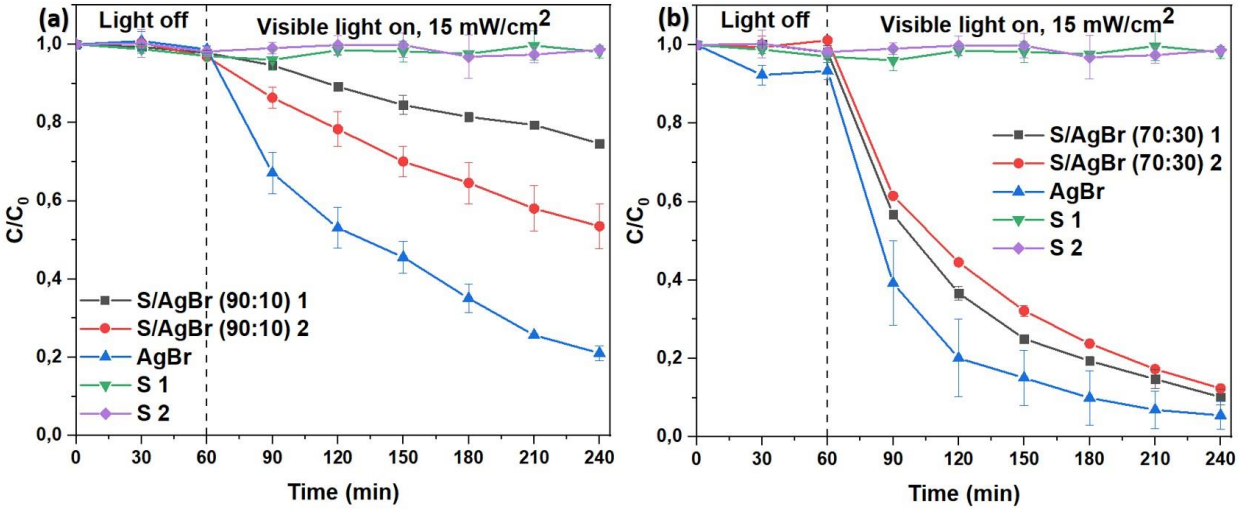

Figure 35 - Comparison of the photocatalytic activity of the samples: (a) – S/AgBr (90:10) 1, 2, AgBr and S 1, 2; (b) – S/AgBr (70:30) 1, 2; AgBr and S 1, 2 [290]

In Figure 36 comparison of the photocatalytic activity of the all AgI based micro-/nano-structures, pure AgI and sulfur are given. Only pure AgI was active and after 180 min of the visible light irradiation sample degraded near 99 % of Orange II molecules. However, for pure AgI was not applied the practice with the effective masses, like for AgCl and AgBr. This is why, AgI is less active halide. While S/AgI of all compositions do not show photodegradation higher than 7 %, like pure sulfur.

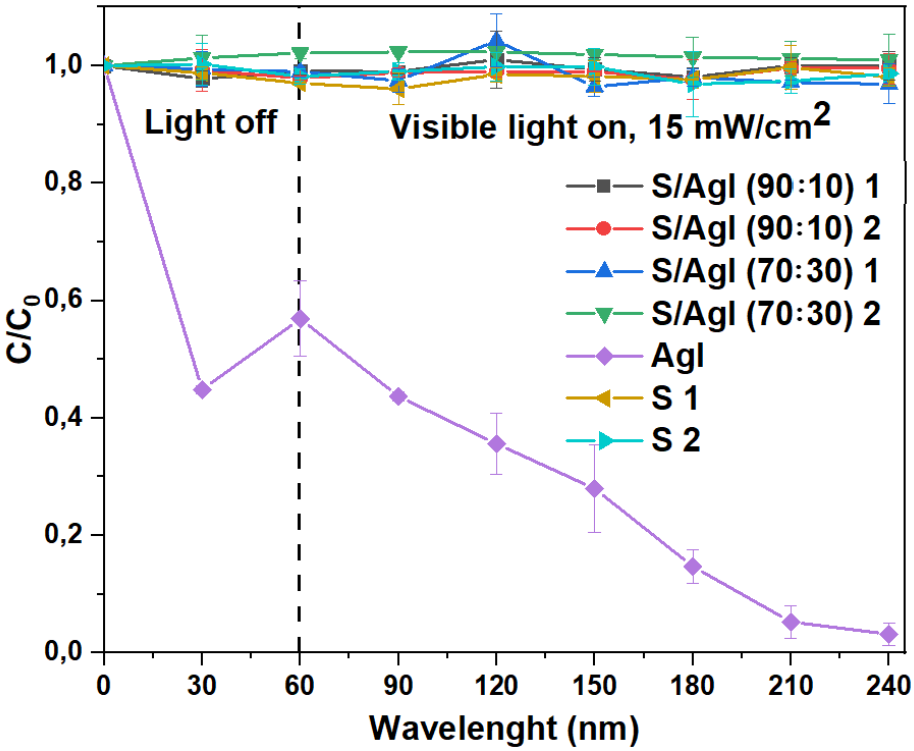

Figure 36 - Comparison of the photocatalytic activity of the S/AgI (90:10) 1, 2; S/AgI (70:30) 1, 2; AgI and S 1, 2 [291]

For kinetics study were chosen micro-/nano-structures based on AgCl and AgBr, as AgI based samples did not show any activity during the photocatalytic tests. The photocatalytic degradation of Orange II by chosen micro-/nano-structures was accepted as a pseudo-first-order reaction. It was found according to a simplified Langmuir–Hinshelwood model $\ln (C_0/C) = kt$, where C_0 and C are initial and final concentrations of Orange II solution, respectively, at time t and k (min^{-1}) is the rate constant of the reaction [25]. There are also were tested other kinetics models, but the pseudo-first order turned out to be the most suitable for this process. The k value was found from the constructed graphs. For proving of the kinetic order of organic dye degradation the correlation coefficient R^2 was used. Figure 37 (a-b) [290] demonstrates the possible pseudo-first order kinetics for photocatalytic degradation of Orange II by S/AgCl and S/AgBr samples.

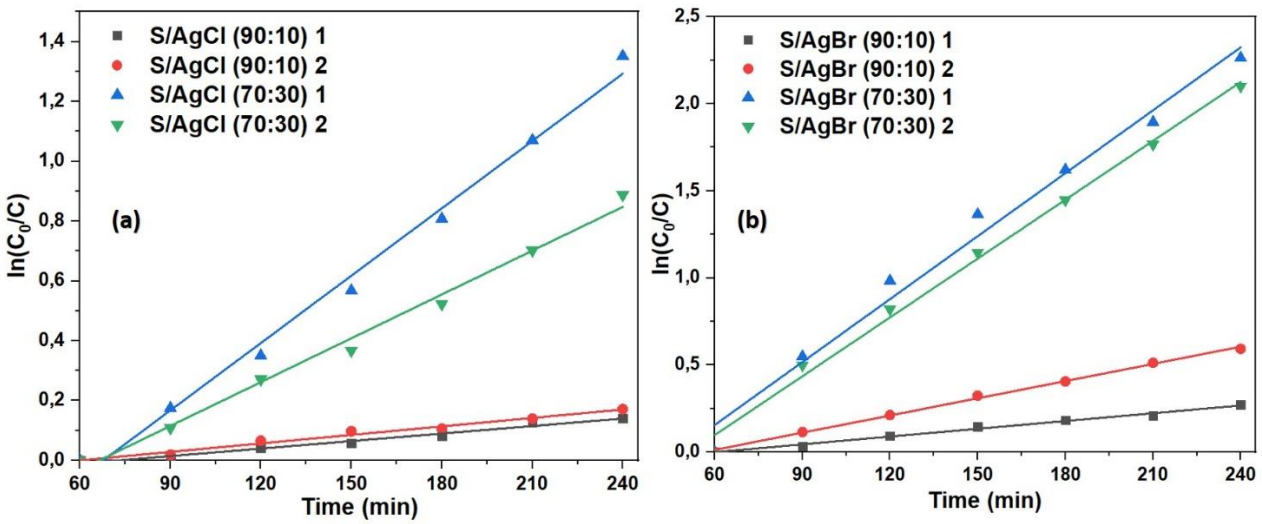

Figure 37 - Pseudo-first-order kinetics for photocatalytic degradation of the Orange II by samples: (a) – S/AgCl (90:10) 1, 2 and S/AgCl (70-30) 1, 2; (b) – S/AgBr (90:10) 1, 2 and S/AgBr (70:30) 1, 2 [290]

The values of the k and R^2 for all samples are summarized in Table 9. According to Table 9 the photocatalytic reaction of organic dye degradation with the S/AgBr (70:30) 1, 2 are in 1.5 times faster than with the S/AgCl (70:30) 1, 2. (90:10) micro-/nano-structures based on AgBr and prepared by methods (1) and (2) were in 1.8 and 3.5 times more active than S/AgCl (90:10) 1, 2 respectively. The highest values of the k were highlighted with the blue color in Table 9. In general, samples prepared by 2nd method showed higher *r* values than samples synthesized be the 1st method.

Table 10 – Pseudo-first-order rate constants of photocatalytic degradation of the Orange II for all samples [290]

Sample	The rate constant, k min^{-1}	R^2
1	2	3
S/AgCl (90:10) 1	(8.35±0.58) 10^{-4}	0.97
S/AgCl (90:10) 2	(9.44±0.56) 10^{-4}	0.98
S/AgCl (70:30) 1	(7.50±0.31) 10^{-3}	0.99
S/AgCl (70:30) 2	(4.88±0.20) 10^{-3}	0.99
S/AgBr (90:10) 1	(1.49±0.66) 10^{-3}	0.98

Continuation of Table 10

1	2	3
S/AgBr (90:10) 2	(3.39±0.67) 10^{-3}	0.99
S/AgBr (70:30) 1	(12.05±0.69) 10^{-3}	0.98
S/AgBr (70:30) 2	(11.27±0.37) 10^{-3}	0.99

The next step of the study was the estimation of the stability of the prepared samples, because stability of the photocatalysts is the essential property for practical application. For this investigation S/AgCl (70:30) 1, 2 and S/AgBr (70:30) 1, 2 samples were chosen, as these materials manifested the greatest photocatalytic activity. The photocatalytic performance of the (70:30) samples based on AgCl and AgBr in the first five reuse cycles is shown in Figure 38 [290]. The photocatalytic activity reduced from the first run to the fifth run only slightly, what could be the reason of the washing out of the powders during the process. However, the results indicate that all studied micro-/nano-structures are stable.

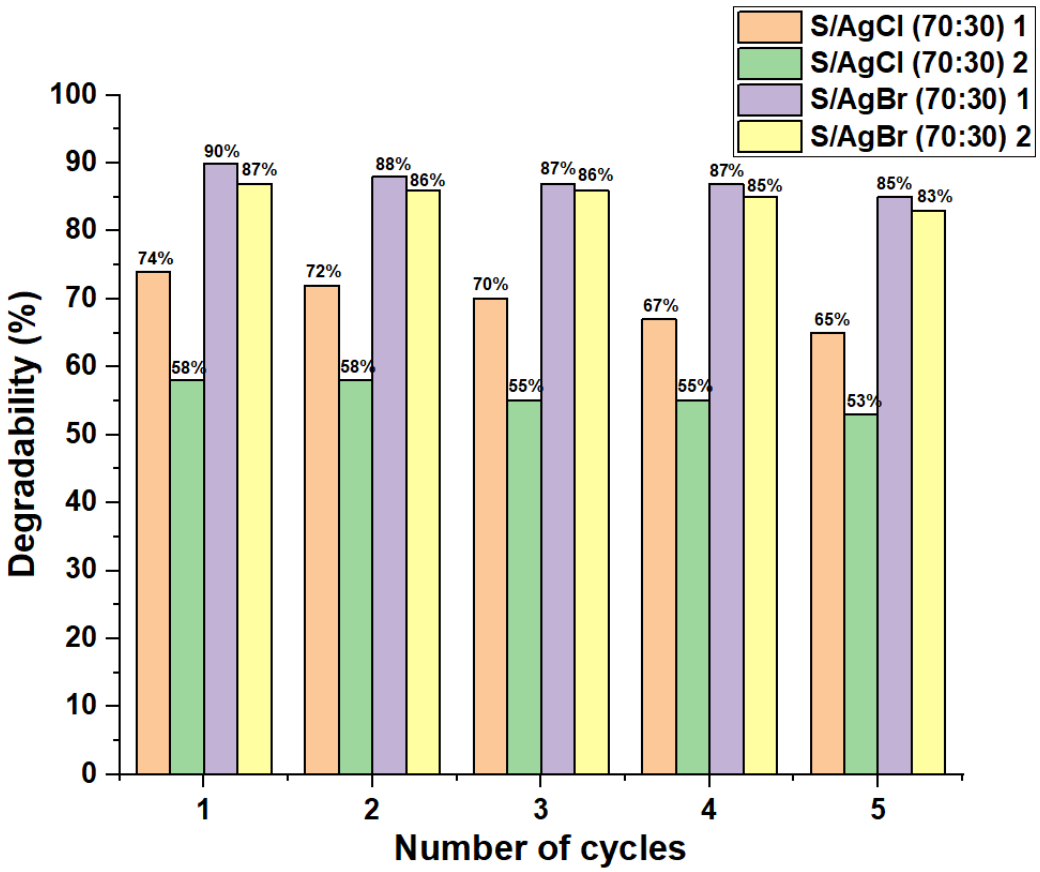

Figure 38 - Photocatalytic performance of the S/AgCl (70:30) 1, 2 and S/AgBr (70:30) 1, 2 in the first five reuse cycles [290]

Based on all the results of the testing of S/AgX micro-/nano-structures as photocatalysts, there can be introduced the mechanism of the process (Figure 39). The mechanism was proposed for S/AgBr (70:30) 1, 2, as these samples were the most active. AgBr forms e^- and h^+ pairs under visible light irradiation. Then on the surface of the AgX the trapping of the excited electrons by O_2 and H_2O is occurred. As the result, the $O_2^{\bullet-}$ and $OH^{\bullet-}$ radicals are generated. $O_2^{\bullet-}$ and $OH^{\bullet-}$ radicals interact with Orange II molecules and decompose them. The hole on AgX surface provokes the oxidation of Br^- ions to Br^0 atoms. The atoms of elemental Cl or Br can easily oxidize dyes and became reduced to Br^- ions again [300–302].

In conclusion we can highlight S/AgBr (70:30) 1, 2 micro-/nano-structures as the most prospective compositions, which are able to save about 90 % of photocatalytic activity. It also should be noted that the results obtained require further study in order to understand the nature and mechanism of prepared micro-/nano-structures action.

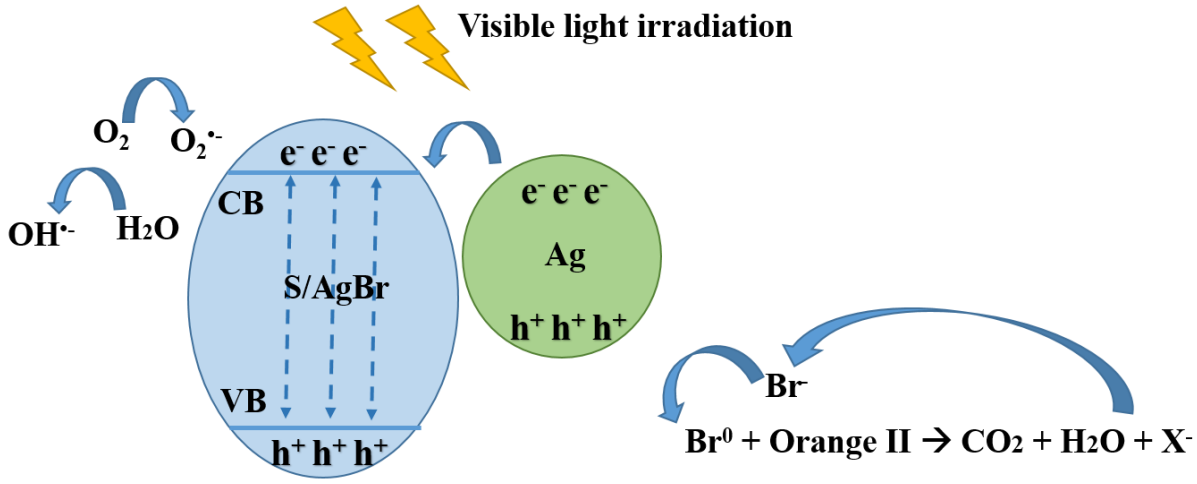

Figure 39 - Proposed mechanism of photocatalyst under visible light irradiation

3.2.2 Biological activity

The minimum bactericidal concentration (MBC) and minimum fungicidal concentration (MFC) were used as estimated value of the biological activity (Figures 40, 41 Tables 10, 11 [290]). During the experiment implementation it was found that S/AgI (90:10) 1, 2, S/AgI (70:30) 1, 2, pure sulfur and AgI unable to suppress microorganisms, this is why in common graph they are not given. According to literature sources, the main factor in the manifestation of pathogen suppression is nanoscale [303]. The methods developed by us make it possible to obtain sulfur in micro-sized scales, which makes it difficult for it to penetrate into the cells of microorganisms. In general, almost all synthesized AgCl and AgBr based samples were active against all tested strains.

As for AgI based micro-/nano-structures, it can be supposed that between sulfur and AgI appears synergetic effect with the strong bond, which cannot be destroyed during the experiments. It is also known, that in AgX compounds Ag^+ ions active antimicrobial agent. Apparently, Ag^+ cannot be formed in the tested suspension, what indicates that combination of sulfur and AgI is not suitable for demonstration of the biological activity. In general, almost all AgCl and AgBr based samples were active against almost all test strains. Only S/AgCl (90:10) 2 was not active against *E. coli* ATCC 8739 and *S. aureus* ATCC BAA-39, S/AgBr (90:10) 1 was not able to suppress *S. aureus* ATCC BAA-39 and *E. coli* ATCC BAA-196, and S/AgBr (90:10) 2 was unable to inactivate virus *E. amylovora, S. aureus* ATCC BAA-39 and *E. coli* ATCC BAA-196 strains. All S/AgCl(Br) micro-/nano-structures showed the lowest MFC and high effectiveness against *C.albicans* ATCC 10231. In our case, the method of solvothermal synthesis yields sufficiently large sulfur particles, which, apparently, do not allow AgX to completely counteract microorganisms. Pure AgBr inhibited only *C. albicans* ATCC 10231; AgCl inhibited *C. albicans* ATCC 10231, *P. aeruginosa* ATCC 9027 and *E. coli* ATCC BAA-196. Thus, pure AgX revealed the lowest activity than S/AgCl(Br) (90:10) and (70:30) 1, 2 samples. Samples with 70:30 % content showed biological activity at lower dilutions than samples with 90:10 % content. MBC/MFC were calculated relying on the concentration of the test samples10 mg/mL (10000 µg/mL) and dilutions. For instance, the dilution 1:1 will correspond to 5000 µg/mL, 1:2 will correspond to 2500 µg/mL and etc. The tables with MBC/MFC values of the all samples are represented in Tables 10 and 11. Figure 42 [290] show the activity of S/AgCl (70:30) 1, 2 and S/AgBr (70:30) 1, 2 against *C. albicans* ATCC 10231 after seeding pathogens on the agar surface by method of two-fold serial dilutions.

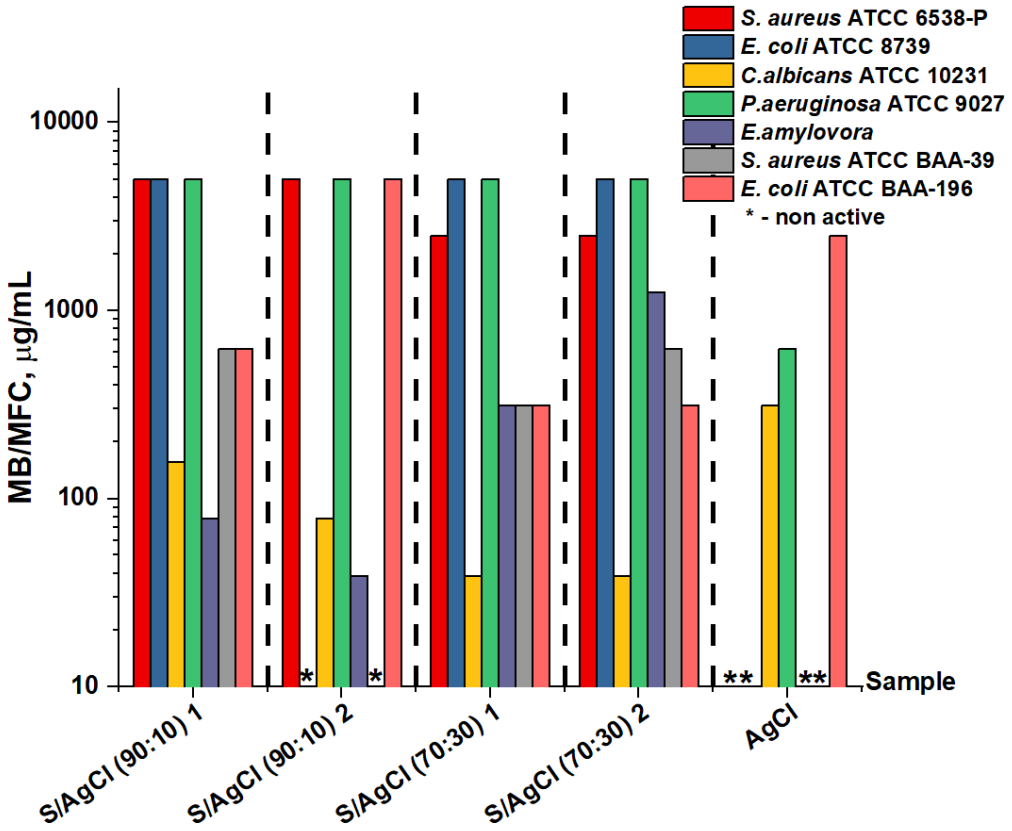

Figure 40 - Comparison of the biological activity of the S/AgCl samples and AgCl [290]

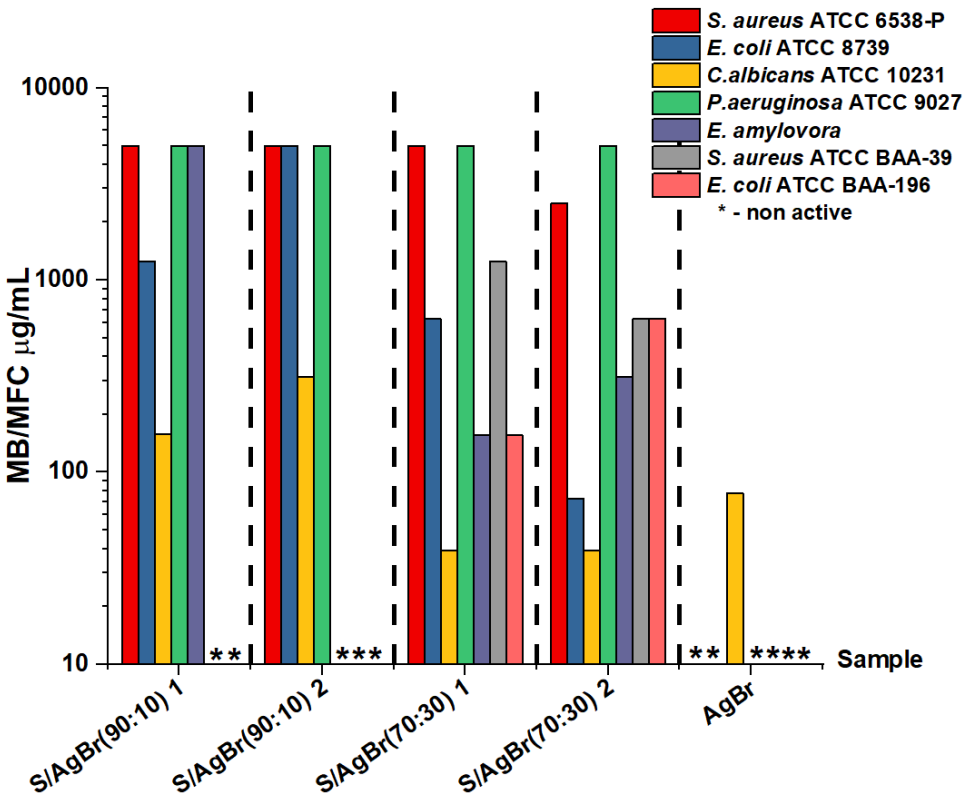

Figure 41- Comparison of the biological activity of the S/AgBr samples and AgBr [290]

Table 11 – Minimum bactericidal/fungicidal concentrations of the S/AgCl (1, 2) 10, 30, 50 %, AgCl and S (1, 2), µg/mL [290].

Test strain	S/AgCl (90:10) 1	S/AgCl (90:10) 2	S/AgCl (70:30) 1	S/AgCl (70:30) 2	AgCl	S 1	S 2
S. aureus ATCC 6538-P	5000	5000	2500	2500	NA	NA	NA
E. coli ATCC 8739	5000	NA	5000	5000	NA	NA	NA
C.albicans ATCC 10231	157	78	39	39	313	NA	NA
P.aeruginosa ATCC 9027	5000	5000	5000	5000	626	NA	NA
E. amylovora	78	39	313	1250	NA	NA	NA
S. aureus ATCC BAA-39	626	NA	313	626	NA	NA	NA
E. coli ATCC BAA-196	626	5000	313	313	2500	NA	NA
NA – non active							

Table 12 – Minimum bactericidal/fungicidal concentrations of the S/AgBr (1, 2) 10, 30, 50 %, AgBr and S, (1, 2) µg/mL [290].

Test strain	S/AgBr (90:10) 1	S/AgBr (90:10) 2	S/AgBr (70:30) 1	S/AgBr (70:30) 2	AgBr	S (1)	S (2)
1	2	3	4	5	6	7	8
S. aureus ATCC 6538-P	5000	5000	5000	2500	NA	NA	NA

Continuation of Table 12

1	2	3	4	5	6	7	8
E. coli ATCC 8739	1250	5000	626	78	NA	NA	NA
C.albicans ATCC 10231	157	312	39	39	78	NA	NA
P.aeruginosa ATCC 9027	5000	5000	5000	5000	NA	NA	NA
E. amylovora	5000	NA	156	313	NA	NA	NA
S. aureus ATCC BAA-39	NA	NA	1250	626	NA	NA	NA
E. coli ATCC BAA-196	NA	NA	156	626	NA	NA	NA
NA – non active							

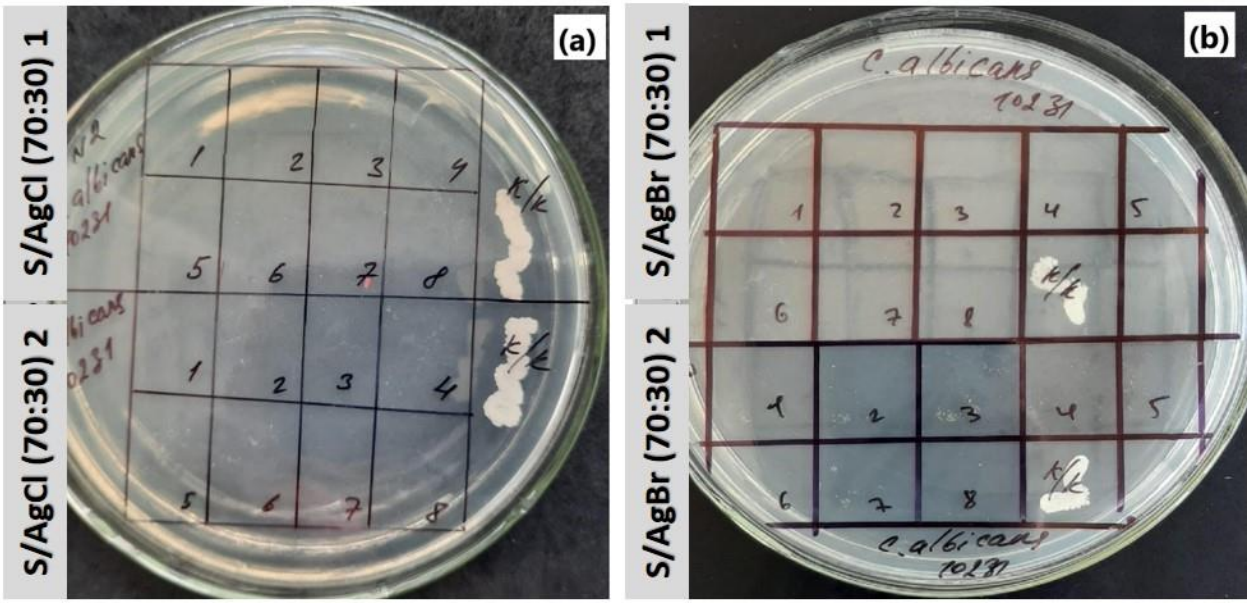

Figure 42 – Samples after seeding pathogens on the agar surface by method of two-fold serial dilutions: (a) – S/AgCl (70:30) 1, 2 and (b) – S/AgBr (70:30) 1, 2 [290]

According to the obtained results, testing of the prepared micro-/nano-structures based on sulfur and AgX as photocatalytic and antimicrobial agents gave certain results. The combination of the sulfur and AgI is not suitable for manifesting of any type of activity. S/AgCl(Br) (90:10) 1,

2 have shown weak photocatalytic and antibacterial/antifungal properties. While S/AgCl(Br) (70:30) 1, 2 are able to degrade organic dye molecules and suppress microorganisms. However, S/AgBr (70:30) 1, 2 are having prospective future as multipurpose multicomponent material, applicable in photocatalysis and microbiology.

In the case of photocatalytic properties, taking into account the effective masses, pure AgCl and AgBr have slightly great activity than the micro-/nano-structures themselves. In this case, when the two components are mixed, passivation of halides by sulfur occurs. Which is why there is a slight difference in the activities of reference samples and multicomponent materials. While the study of biological activity showed that AgCl and AgBr are able to suppress certain pathogens, and sulfur did not show any results at all. The mixing of the two components has led to the fact that synthesized samples of almost all compositions are able to suppress strains taken as part of the experiment. This may indicate a synergistic effect between sulfur and halides, despite the results of SEM, TEM, TEM-EDS elemental mapping and XPS. Clearly, this study requires further and deeper study. But within the framework of this work, one of the tasks was to test synthesized samples for their use in photocatalysis and microbiology, which was actually done.

4 APPLIED ASPECTS

4.1 Development of the principal technological scheme of producing S/AgBr (70:30) micro-/nano-structures

The process of producing of S/AgX micro-/nano-structures on a laboratory scale was given in chapter 2, paragraph 2.5. AgX based materials tend to decompose in daylight, so their storage requires special conditions. It should be noted that we don't need a big amount of photocatalyst for conducting photocatalytic process, because its consumption is extermelly small. The developed principal scheme for production of S/AgBr is designed for a 20-liter pilot plant (R-620 (SELECTA, Spain)) and given in Figure 43.

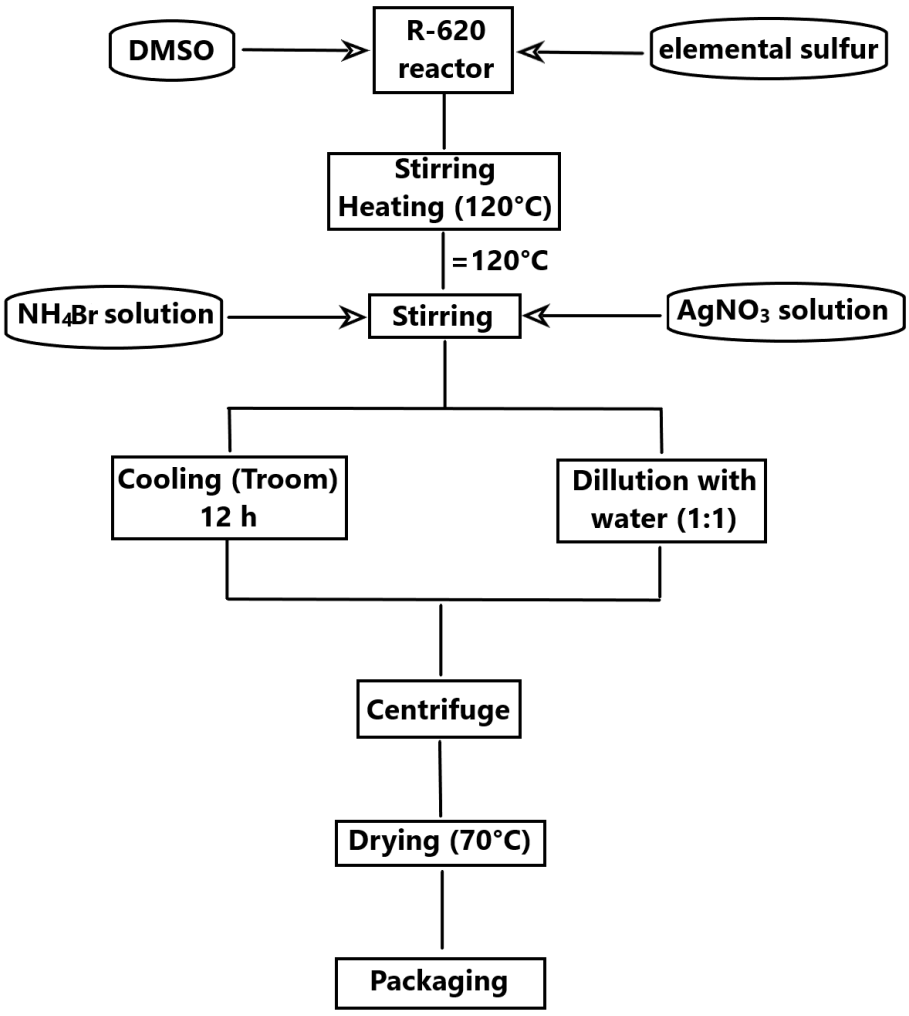

Figure 43 – Principle scheme of production of S/AgBr (70:30) 1, 2 micro-/nano-structures

The principle scheme (Figure 43) is presented on the example of obtaining a product based on AgBr, since this type of micro-/nano-structures was selected as one of the best samples with

the best photocatalytic and antimicrobial properties. All masses are given for producing of 125 g of S/AgBr (70:30) 1, 2. According to the principle scheme, reactor is filled with the 5 liters of DMSO at the first stage. Then, 87.50 g of elemental sulfur is put in 5000 mL of DMSO and the heating and stirring of the process is started. After the dissolution of sulfur at 120°C, the portion and altering pouring of NH_4Br (20.00 g in 250 mL of DMSO) and $AgNO_3$ (33.91 g in 250 mL of DMSO) is conducted. Depending on the method sulfur precipitation, under constant stirring the cooling (12 h) of the system or dilution with water is carried out. Dilution of reaction mixture with water requires 5500 mL of distilled water (volume ratio of reactional mixture to water is 1:1). Obtained product is centrifuged, dried (70°C, 24 h) and packed.

4.2 The material balance of obtaining of S/AgBr (70:30) micro-/nano-structures

The material balance of obtaining of the S/AgBr (70:30) 1 micro-/nanostructure for which sulfur was deposited at room temperature (method 1), is shown in Table 12. The material balance for S/AgBr (70:30) 2, where sulfur was deposited with help of water is given in Table 13.

Table 13 - Material balance of the S/AgBr (70:30) 1 micro-/nano-structure obtaining

Income		Expenses	
Item	Unit	Item	Unit
	g		g
Elemental sulfur (S)	87.50	S/AgBr	125.00
Silver nitrate ($AgNO_3$)	34.00		
Ammonia bromide (NH_4Br), (excess)	19.50	NH_4NO_3	16.00
DMSO	6050.00	DMSO	6050.00
Total	6191.00		6191.00

Table 14 - Material balance of the S/AgBr (70:30) 2 micro-/nano-structure obtaining

Income		Expenses	
Item	Unit	Item	Unit
	g		g
Elemental sulfur (S)	87.50	S/AgBr	125.00
Silver nitrate ($AgNO_3$)	34.00		
Ammonia bromide (NH_4Br), (excess)	19.50	Ammonia nitrate (NH_4NO_3)	16.00
DMSO	6050.00	DMSO	6050.00
Distillate water	5000.00	Distillate water	5000.00
Total	11191.00		11191.00

4.3 Cost estimation for the production of 125 g S/AgBr (70:30) micro-/nano-structures

The cost of the product was compared with commercial AgBr, since the photocatalysts and antimicrobial agents on the market do not have a composition similar to ours. Pure AgBr can be used both as a photocatalyst and as an antimicrobial agent, while pure sulfur cannot be used. Information about prices is publicly available on manufacturers' websites. For calculations the data from the Merck website were taken [304].

For the estimation of the production costs of 125 g S/AgBr (70:30) 1, 2 micro-/nano-structures was chosen, since these samples showed the best results on photocatalytic and biological activities. Table 12 provides information about cost estimation for the production of mentioned above samples. For the calculations the expenses for raw materials, salary and others were taken into account. According to Table 12, the price for the products production using methods 1 and 2 is very similar, because method of precipitation 2 (method 2) requires using of distillate water. Commercial AgBr of manufacturer Merck costs 2070 US dollars, which in tenge is about 963,157.00. As can be seen, the obtained products are 3.5 times cheaper, than commercial AgBr of Merck production Thus, S/AgBr micro-/nano-structure seems to be the best out of the studied once.

In conclusion, it can be said that the production and sale of the product synthesized by us is represented by sufficiently convincing profitability and prospects.

Table 15 - Cost estimation for the production of 125 g S/AgBr (70-30) 1, 2 micro-/nano-structures

Expenses	S/AgBr (70:30) 1		S/AgBr (70:30) 2	
	Amount, g (mL)	Expenses, tg	Amount, g	Expenses, tg
Elemental sulfur (S)	87.50	87.50	87.50	87.50
Silver nitrate ($AgNO_3$)	33.91	15,260.00	33.91	15,260.00
Ammonia bromide (NH_4Br), (excess)	20.00	484.50	20.00	484.50
DMSO	5500	242,281.00	6000	242,281.00
Distillate water	-		7000	560.00
Employee salary	-	10,000.00	-	10,000.00
Other	-	5,000.00	-	5,000.00
Total amount		273,113.00		273,673.00

CONCLUSIONS

Based on the results of the study , the following conclusions can be drawn:

1. Sulfur and silver halides micro-/nano-structures were synthesized in DMSO medium at 120 °C. Two methods of sulfur deposition have been developed: 1) sulfur precipitation by cooling the reaction mixture for 12 hours to room temperature; 2) sulfur precipitation by diluting the solution of the reaction mixture with water at a volume ratio of DMSO:water 1:1.

2. The study of synthesized sulfur and silver halides micro-/nano-structures by physico-chemical characterization methods was carried out. The results of the analyses showed that sulfur and silver halides are present in the micro-/nano-structures, the samples are represented by a heterogeneous system where sulfur grains are covered with silver halide particles. When sulfur is precipitated by cooling the reaction mixture to room temperature, sulfur particles with a size of 20 to 50 μm are formed, while dilution of the reaction mixture solution with water leads to the formation of smaller sulfur particles with a size of 10 to 25 μm. Silver halides, regardless of the method of sulfur deposition method, exhibit the particle size in the range from 1 to 4 μm.

3. SEM, TEM and TEM-elemental mapping showed that dilution of the system of micro-/nano-structures in the DMSO medium with water prevents agglomeration of sulfur particles. The DMSO–water system, due to the DMSO property as a surfactant, forms micelles consisting of stable complexes of these components, and the hydrophobicity of sulfur particles provides protection against aggregation.

4. The photocatalytic, antibacterial and antifungal properties of synthesized micro-/nano-structures were investigated. It was found that synthesized sulfur and micro-/nano-structures based on sulfur and silver iodide do not have significant photocatalytic activity. Sulfur and silver chloride/bromide micro-/nano-structures with a composition of 90:10 wt. % also showed low photodegradation ability of organic dye. Micro-/nano-structures with a content of sulfur:silver halide 70:30 wt. % were more active, and samples based on silver bromide exhibited about 90% degradation of the organic dye. The stability study of samples based on sulfur and silver chloride/bromide with a ratio of 70:30 wt.% showed that these samples remain functional during five cycles of the photocatalytic process.

The study of antimicrobial activity showed that synthesized sulfur and samples based on sulfur and silver iodide are inactive. The remaining samples were able to suppress almost all the test strains studied, and sulfur and silver chloride/bromide micro-/nano-structures with a composition of 70:30 wt.% are able to suppress pathogenic microorganisms at the lowest values of the minimum bactericidal/fungicidal concentration. Samples based on sulfur and silver bromide

with a composition of 70:30 wt.% have good prospects of application as functional materials, in photocatalysis and biomedicine.

5. The principal scheme of micro-/nano-structures obtaining was developed. The material balance of the process was calculated.

REFERENCES

1. Xue W., Huang D., Wen X., Chen S., Cheng M., Deng R., Li B., Yang Y., Liu X. Silver-based semiconductor Z-scheme photocatalytic systems for environmental purification//J. Haz. Mat. - 2020. - Vol. 390. - P. 122128.

2. Hu C., Zheng S., Lian C., Chen F., Lu T., Hu Q., Duo S., Zhang R., Guan C. α-S nanoparticles grown on MoS_2 nanosheets: A novel sulfur-based photocatalyst with enhanced photocatalytic performance//J. Mol. Catal. A Chem. - 2015. - Vol. 396. - P. 128-135.

3. Liu G., Niu P., Yin L., Cheng H.-M. α-Sulfur Crystals as a Visible-Light-Active Photocatalyst//J. Am. Chem. Soc. - 2012. - Vol. 134, No. 22. - P. 9070-9073.

4. Rockafellow E.M., Stewart L.K., Jenks W.S. Is sulfur-doped TiO2 an effective visible light photocatalyst for remediation?//Appl. Catal. B: Environ. - 2009. - Vol. 91, No. 1. - P. 554-562.

5. Beyth N., Houri-Haddad Y., Domb A., Khan W., Hazan R. Alternative Antimicrobial Approach: Nano-Antimicrobial Materials//Evid Based Complementary Altern. Med. - 2015. - Vol. 2015. - P. e246012.

6. Liang J., Deng J., Li M., Tong M. Bactericidal activity and mechanism of AgI/AgBr/$BiOBr_{0.75}I_{0.25}$ under visible light irradiation//Colloids Surf. B. - 2016. - Vol. 138. - P. 102-109.

7. Sharma S., Dutta V., Raizada P., Hosseini-Bandegharaei A., Thakur V.K., Kalia S., Nguyen V.-H., Singh P. Recent advances in silver bromide-based Z-scheme photocatalytic systems for environmental and energy applications: A review//J. Environ. Chem. Eng. - 2021. - Vol. 9, No. 2. - P. 105157.

8. Rakhshan N., Mansournia M., Jookar Kashi F. Plant extract-strategy using Teucrium Polium stems to green synthesize Ag/AgCl bionanocomposite imprinted on Fe3O4/kaolinite and potentials in catalytic and chemosensor applications//Arab. J. Chem. - 2022. - Vol. 15, No. 4. - P. 103719.

9. Tun P., Wang K., Naing H., Wang J., Zhang G. Facile preparation of visible-light-responsive kaolin-supported Ag@AgBr composites and their enhanced photocatalytic properties//Appl. Clay Sci. - 2019. - Vol. 175. - P. 76-85.

10. Vosmanská V., Kolářová K., Pišlová M., Švorčík V. Reaction parameters of in situ silver chloride precipitation on cellulose fibres//Mater. Sci. Eng. C. - 2019. - Vol. 95. - P. 134-142.

11. Lan Y., Qian X., Zhao C., Zhang Z., Chen X., Li Z. High performance visible light driven photocatalysts silver halides and graphitic carbon nitride (X=Cl, Br, I) nanocomposites//J. Colloid. Interface Sci. - 2013. - Vol. 395. - P. 75-80.

12. Ong W.-J., Putri L.K., Tan L.-L., Chai S.-P., Yong S.-T. Heterostructured AgX/g-C_3N_4 (X=Cl and Br) nanocomposites via a sonication-assisted deposition-precipitation approach: Emerging role of halide ions in the synergistic photocatalytic reduction of carbon dioxide//Appl. Catal. B: Environ. - 2016. - Vol. 180. - P. 530-543.

13. Thakur P., Raizada P., Singh P., Kumar A., Khan A.A.P., Asiri A.M. Exploring recent advances in silver halides and graphitic carbon nitride-based photocatalyst for energy and environmental applications//Arab. J. Chem. - 2020. - Vol. 13, No. 11. - P. 8271-8300.

14. Guan D.-L., Niu C.-G., Wen X.-J., Guo H., Deng C.-H., Zeng G.-M. Enhanced Escherichia coli inactivation and oxytetracycline hydrochloride degradation by a Z-scheme silver iodide decorated bismuth vanadate nanocomposite under visible light irradiation//J. Colloid. Interface Sci. - 2018. - Vol. 512. - P. 272-281.

15. Guo B., Zhao C., Zhou L., Yu Z., Liu X., Zhao Z., Yuan H. Constructing a novel multi-hierarchical TiO2/g-C3N4/Ag-AgBr photocatalyst with dual Z-scheme heterojunction utilizing Ag as the charge transfer mediator//J. Alloys Compd. - 2022. - Vol. 900. - P. 163514.

16. Guo J.-F., Ma B., Yin A., Fan K., Dai W.-L. Highly stable and efficient Ag/AgCl@TiO2 photocatalyst: Preparation, characterization, and application in the treatment of aqueous hazardous pollutants: Nanotechnologies for the Treatment of Water, Air and Soil//J. Hazard. Mater. - 2012. - Vols. 211-212. - P. 77-82.

17. Azimzadehirani M., Elahifard M., Haghighi S., Gholami M. Highly efficient hydroxyapatite/TiO2 composites covered by silver halides as E. colidisinfectant under visible light and dark media//Photochem. Photobiol. Sci. - 2013. - Vol. 12, No. 10. - P. 1787-1794.

18. Zhong S., Jiang W., Han M., Liu G., Zhang N., Lu Y. Graphene supported silver@silver chloride & ferroferric oxide hybrid, a magnetically separable photocatalyst with high performance under visible light irradiation//Appl. Surf. Sci. - 2015. - Vol. 347. - P. 242-249.

19. Dai Y.-D., Lyu R.-J., Wu T., Huang C.-C., Lin Y.-W. Influences of silver halides AgX (X = Cl, Br, and I) on magnesium bismuth oxide photocatalyst in methylene blue degradation under visible light irradiation//J. Photochem. Photobiol. A. - 2020. - Vol. 397. - P. 112585.

20. Hu C., Lan Y., Qu J., Hu X., Wang A. Ag/AgBr/TiO_2 Visible Light Photocatalyst for Destruction of Azodyes and Bacteria//J. Phys. Chem. B. - 2006. - Vol. 110, No. 9. - P. 4066-4072.

21. Zhu H., Chen M., Yue J., Liang L., Jiang X. Experimental and theoretical studies on the role of silver in gold nanorods growth//J. Nanopart. Res. - 2017. - Vol. 19, No. 5. - P. 183.

22. Wan X., Wang T., Dong Y., He D. Development and application of TiO_2 nanoparticles coupled with silver halide//J. Nanomater. - 2014. - Vol. 2014. - P. 192:192.

23. Modan E.M., Plăiașu A.G. Advantages and Disadvantages of Chemical Methods in the Elaboration of Nanomaterials//Ann. Dunarea Jos. - 2020. - Vol. 43, No. 1. - P. 53-60.

24. Xu H., W. Zeiger B., S. Suslick K. Sonochemical synthesis of nanomaterials//Chem. Soc. Rev. - 2013. - Vol. 42, No. 7. - P. 2555-2567.

25. Chen D., Yoo S.H., Huang Q., Ali G., Cho S.O. Sonochemical Synthesis of Ag/AgCl Nanocubes and Their Efficient Visible-Light-Driven Photocatalytic Performance//Chem. Eur. J. - 2012. - Vol. 18, No. 17. - P. 5192-5200.

26. Choi J., Reddy D.A., Kim T.K. Enhanced photocatalytic activity and anti-photocorrosion of AgI nanostructures by coupling with graphene-analogue boron nitride nanosheets//Ceram. Int. - 2015. - Vol. 41, No. 10. - P. 13793-13803.

27. Shi H., Chen J., Li G., Nie X., Zhao H., Wong P.-K., An T. Synthesis and Characterization of Novel Plasmonic Ag/AgX-CNTs (X = Cl, Br, I) Nanocomposite Photocatalysts and Synergetic Degradation of Organic Pollutant under Visible Light//ACS Appl. Mater. Interfaces. - 2013. - Vol. 5, No. 15. - P. 6959-6967.

28. Shaker-Agjekandy S., Habibi-Yangjeh A. Ultrasonic-assisted preparation of novel ternary ZnO/AgI/Ag_2CrO_4 nanocomposites as visible-light-driven photocatalysts with excellent activity//Mater. Sci. Semicond. Process. - 2016. - Vol. 44. - P. 48-56.

29. Li L., Yang X., Xie C., Wang Y., Wei L., Yang J. Synthesis and photocatalytic mechanism of visible-light-driven Ag/AgBr/(I/S) composites for organic dyes degradation//Opt. Mater. - 2022. - Vol. 123. - P. 111947.

30. Ndolomingo M.J., Bingwa N., Meijboom R. Review of supported metal nanoparticles: synthesis methodologies, advantages and application as catalysts//J. Mater. Sci. - 2020. - Vol. 55, No. 15. - P. 6195-6241.

31. Louis C. Catalyst preparations / Catherin Louis. - 1st Edition. - Boca Raton: CRC Press, 2016. – 488 p.

32. Bang J.H., Suslick K.S. Applications of Ultrasound to the Synthesis of Nanostructured Materials//Adv. Mater. - 2010. - Vol. 22, No. 10. - P. 1039-1059.

33. Li J., Wu Q., Wu J. Synthesis of Nanoparticles via Solvothermal and Hydrothermal Methods//Handbook of Nanoparticles – Springer, Cham. - 2016. – P. 295-328.

34. Tian B., Zhang J. Morphology-Controlled Synthesis and Applications of Silver Halide Photocatalytic Materials//Catal. Surv. Asia. - 2012. - Vol. 16, No. 4. - P. 210-230.

35. Wang L., Shi Y., Wang T., Zhang L. Silver chloride enwrapped silver grafted on nitrogen-doped reduced graphene oxide as a highly efficient visible-light-driven photocatalyst//J. Colloid. Interface Sci. - 2017. - Vol. 505. - P. 421-429.

36. Mahmoodi N.M., Taghizadeh A., Taghizadeh M., Abdi J. In situ deposition of Ag/AgCl on the surface of magnetic metal-organic framework nanocomposite and its application for the

visible-light photocatalytic degradation of Rhodamine dye//J. Hazard. Mater. - 2019. - Vol. 378. - P. 120741.

37. Akhundi A., Habibi-Yangjeh A. Ternary g-C_3N_4/ZnO/AgCl nanocomposites: Synergistic collaboration on visible-light-driven activity in photodegradation of an organic pollutant: Graphene and C3N4-based Photocatalysts//Appl. Surf. Sci. - 2015. - Vol. 358. - P. 261-269.

38. Yang Q., Hu M., Guo J., Ge Z., Feng J. Synthesis and enhanced photocatalytic performance of Ag/AgCl/TiO_2 nanocomposites prepared by ion exchange method//J. Materiomics. - 2018. - Vol. 4, No. 4. - P. 402-411.

39. Urakaev F.Kh., Burkitbaev M.M., Tatykaev B.B., Uralbekov B.M. Mechanochemical synthesis of colloidal silver chloride particles in the NH4Cl–AgNO3–NH4NO3 system//Colloid J., 2015, Vol. 77, No. 5, P. 641-651.

40. Tatykaev B.B., Burkitbayev M.M., Uralbekov B.M., Urakaev F.Kh. Mechanochemical Synthesis of Silver Chloride Nanoparticles by a Dilution Method in the System NH_4 Cl-$AgNO_3$ -NH_4 NO_3// Acta Phys. Pol. A. - 2014. - Vol. 126, No. 4. - P. 1044-1048.

41. Urakaev F.Kh., Tatykaev B.B., Burkitbayev M.M., Bakhadur A.M., Uralbekov B.M. Mechanochemical synthesis of colloidal silver bromide particles in the NaBr–$AgNO_3$–$NaNO_3$ system//Colloid J. - 2016. - Vol. 78, No. 4. - P. 525-532.

42. Urakaev F.Kh., Khan N.V., Shalabaev Zh.S., Tatykaev B.B., Nadirov R.K., Burkitbaev M.M. Synthesis and Photocatalytic Properties of Silver Chloride/Silver Composite Colloidal Particles//Colloid J. - 2020. - Vol. 82, No. 1. - P. 76-80.

43. Zuffa C., Cappuccino C., Marchini M., Contini L., Farinella F., Maini L. AgX-based hybrid coordination polymers: mechanochemical synthesis, structure and luminescence property characterization //Faraday Discuss. – 2023. – Vol. 241. – P. 448-465.

44. Friščić T., Mottillo C., Titi H.M. Mechanochemistry for Synthesis//Angewandte Chemie. - 2020. - Vol. 132, No. 3. - P. 1030-1041.

45. Lukin S., Stolar T., Lončarić I., Milanović I., Biliškov N., di Michiel M., Friščić T., Halasz I. Mechanochemical Metathesis between $AgNO_3$ and NaX (X = Cl, Br, I) and Ag_2XNO_3 Double-Salt Formation//Inorg. Chem. - 2020. - Vol. 59, No. 17. - P. 12200-12208.

46. Xu C., De S., M. Balu A., Ojeda M., Luque R. Mechanochemical synthesis of advanced nanomaterials for catalytic applications//Chem. Comm. - 2015. - Vol. 51, No. 31. - P. 6698-6713.

47. A. Bowmaker G., Chaichit N., Pakawatchai C., W. Skelton B., H. White A. Solvent - assisted mechanochemical synthesis of metal complexes//Dalton Trans. - 2008. - Vol. 0, No. 22. - P. 2926-2928.

48. Vanitha M., Keerthi, Vadivel S., Balasubramanian N. Visible light photocatalysis of Methylene blue by graphene-based ZnO and Ag/AgCl nanocomposites//Desalin. Water Treat. - 2015. - Vol. 54, No. 10. - P. 2748-2756.

49. Tang Y., Jiang Z., Deng J., Gong D., Lai Y., Tay H.T., Joo I.T.K., Lau T.H., Dong Z., Chen Z. Synthesis of Nanostructured Silver/Silver Halides on Titanate Surfaces and Their Visible-Light Photocatalytic Performance//ACS Appl. Mater. Interfaces. - 2012. - Vol. 4, No. 1. - P. 438-446.

50. Adhikari R., Gyawali G., Sekino T., Wohn Lee S. Microwave assisted hydrothermal synthesis of Ag/AgCl/WO_3 photocatalyst and its photocatalytic activity under simulated solar light//J. Solid State Chem. - 2013. - Vol. 197. - P. 560-565.

51. Zarghami Z., Ebadi M., Motevalli K., Aliabadi M. Self-assembly of nanoparticles to prepare of dendritic AgCl–Ag_2S nanocomposites through a simple one-pot hydrothermal approach and its photocatalytic activity//J. Mater. Sci. Mater. - 2016. - Vol. 27, No. 2. - P. 1087-1091.

52. Tsai C.-Y., Liu C.-W., Hsi H.-C., Lin K.-S., Lin Y.-W., Lai L.-C., Weng T.-N. Preparation of AgCl/TNTs nanocomposites for organic dyes and inorganic heavy metal removal//Environ. Sci. Pollut. Res. - 2019. - Vol. 26, No. 21. - P. 22082-22096.

53. Liang Y., Lin S., Hu J., Liu L., McEvoy J.G., Cui W. Facile hydrothermal synthesis of nanocomposite Ag@AgCl/$K_2Ti_4O_9$ and photocatalytic degradation under visible light irradiation//J. Mol. Catal. A Chem. - 2014. - Vols. 383-384. - P. 231-238.

54. Byrappa K. Handbook of Hydrothermal Technology / Kullaiah Byrappa, Masahiro Yoshimura. - 2nd Edition. - Chennai: William Andrew, 2013. - 796 p.

55. Ho H.C., Bonnesen P.V., Nguyen N.A., Cullen D.A., Uhrig D., Goswami M., Keum J.K., Naskar A.K. Method To Synthesize Micronized Spherical Carbon Particles from Lignin//Ind. Eng. Chem. Res. - 2020. - Vol. 59, No. 1. - P. 9-17.

56. Gao J., Huang C., Lin Y., Tong P., Zhang L. In situ solvothermal synthesis of metal–organic framework coated fiber for highly sensitive solid-phase microextraction of polycyclic aromatic hydrocarbons//J. Chromatogr. A. - 2016. - Vol. 1436. - P. 1-8.

57. Żaba A., Sovinska S., Kirish T., Węgrzynowicz A., Matras-Postołek K. Photodegradation Process of Organic Dyes in the Presence of a Manganese-Doped Zinc Sulfide Nanowire Photocatalyst//Mater., 2021. - Vol. 14, No. 19. - P. 5840.

58. Ye S., Zhang D., Liu H., Zhou J. ZnO nanocrystallites/cellulose hybrid nanofibers fabricated by electrospinning and solvothermal techniques and their photocatalytic activity//J. Appl. Polym. Sci. - 2011. - Vol. 121, No. 3. - P. 1757-1764.

59. Yu D., Bai J., Liang H., Wang J., Li C. A new fabrication of AgX (X = Br, I)–TiO_2 nanoparticles immobilized on polyacrylonitrile (PAN) nanofibers with high photocatalytic activity and renewable property//RSC Adv. - 2015. - Vol. 5, No. 111. - P. 91457-91465.

60. Akbarzadeh R., Fung C.S.L., Rather R.A., Lo I.M.C. One-pot hydrothermal synthesis of g-C_3N_4/Ag/AgCl/$BiVO_4$ micro-flower composite for the visible light degradation of ibuprofen//Chem. Eng. J. - 2018, Vol. 341. - P. 248-261.

61. Yu D., Bai J., Liang H., Ma T., Li C. AgI-modified TiO_2 supported by PAN nanofibers: A heterostructured composite with enhanced visible-light catalytic activity in degrading MO//Dyes Pigm. - 2016. - Vol. 133. - P. 51-59.

62. Huang S., Xu Y., Xie M., Ma Y., Yan J., Li Y., Zhao Y., Xu H., Li H. Multifunctional C-Doped $CoFe_2O_4$ Material as Cocatalyst to Promote Reactive Oxygen Species Generation over Magnetic Recyclable C–CoFe/Ag–AgX Photocatalysts//ACS Sustainable Chem. Eng. - 2018. - Vol. 6, No. 9. - P. 11968-11978.

63. Chang J.-Q., Zhong Y., Hu C.-H., Luo J.-L., Wang P.-G. Synthesis and significantly enhanced visible light photocatalytic activity of BiOCl/AgBr heterostructured composites//Inorg. Chem. Commun. - 2018. - Vol. 96. - P. 145-152.

64. Han L., Wang P., Zhu C., Zhai Y., Dong S. Facile solvothermal synthesis of cube-like Ag@AgCl: a highly efficient visible light photocatalyst//Nanoscale. - 2011. - Vol. 3, No. 7. - P. 2931-2935.

65. Nguyen H.P., Kim T.H., Lee S.W. Visible light-Driven AgBr/AgCl@MIL-101(Fe) Composites For Removal of Organic Contaminant From Wastewater//Photochem. Photobiol. - 2020. - Vol. 96, No. 1. - P. 4-13.

66. Tóth Z.-R., Maity S.K., Gyulavári T., Bárdos E., Baia L., Kovács G., Garg S., Pap Z., Hernadi K. Solvothermal Crystallization of Ag/Ag_xO-AgCl Composites: Effect of Different Chloride Sources/Shape-Tailoring Agents//Catalysts. - 2021. - Vol. 11, No. 3. - P. 379.

67. Yan T., Zhang H., Luo Q., Ma Y., Lin H., You J. Controllable synthesis of plasmonic Ag/AgBr photocatalysts by a facile one-pot solvothermal route//Chem. Eng. J. - 2013. - Vol. 232. - P. 564-572.

68. Cao F., Wang Y., Wang J., Deng R., Zhou T., Liu H., Wu B., Zhou J., Li S., Qin G. Solvothermal Synthesis and High Visible-light-responsive Photocatalytic Activity of AgX (X = Cl, Br, I) Nanostructures//Chem. Lett. - 2018. - Vol. 47, No. 1. - P. 92-94.

69. Zhu M., Chen P., Liu M. Graphene Oxide Enwrapped Ag/AgX (X = Br, Cl) Nanocomposite as a Highly Efficient Visible-Light Plasmonic Photocatalyst//ACS Nano. - 2011. - Vol. 5, No. 6. - P. 4529-4536.

70. Xu G., Li P., Wang N., Qin X., Wang Z., Guan B., Chen P., Liu M. Sub-10-nm Ag/AgX (X = Br,Cl) Nanoparticles: Superior Visible-Light-Driven Plasmonic Photocatalysts//Adv. Mater. Interfaces. - 2022. - Vol. 9, No. 9. - P. 2102077.

71. Zhang J., Liu X., Suo X., Li P., Liu B., Shi H. Facile synthesis of Ag/AgCl/TiO2 plasmonic photocatalyst with efficiently antibacterial activity//Mater. Lett. - 2017. - Vol. 198. - P. 164-167.

72. Wang F., Lin P., Huang G.S., Hu Y., Chen L., Song Z. A novel heterostructured AgI/Ag3BiO3 nanocomposite with enhanced photocatalytic and stability under visible light//J. Optoelectron. Adv. Mater. - Vol. 2, No. 11. - P. 37-35.

73. Zhang C., Ai L., Li L., Jiang J. One-pot solvothermal synthesis of highly efficient, daylight active and recyclable Ag/AgBr coupled photocatalysts with synergistic dual photoexcitation//J. Alloys Compd. - 2014. - Vol. 582. - P. 576-582.

74. Baláž M. Environmental Mechanochemistry / Matej Baláž – Springer Nature, 2021. – 624 p.

75. Sopicka-Lizer M. High-Energy Ball Milling: Mechanochemical Processing of Nanopowders. High-Energy Ball Milling / Małgorzata Sopicka-Lizer – Cornwall: Elsevier, 2010. – 436 p.

76. A. Bowmaker G. Solvent-assisted mechanochemistry//Chem. Comm. - 2013. - Vol. 49, No. 4. - P. 334-348.

77. L. James S., J. Adams C., Bolm C., Braga D., Collier P., Friščić T., Grepioni F., M. Harris K.D., Hyett G., Jones W., Krebs A., Mack J., Maini L., Guy Orpen A., P. Parkin I., C. Shearouse W., W. Steed J., C. Waddell D. Mechanochemistry: opportunities for new and cleaner synthesis//Chem. Soc. Rev. - 2012. - Vol. 41, No. 1. - P. 413-447.

78. Tatykayev B., Burkitbayev M., Uralbekov B., Urakaev F. Mechanochemical Synthesis of Silver Chloride Nanoparticles by a Dilution Method in the System NH_4Cl-$AgNO_3$-NH_4NO_3//Acta Phys. Pol. - 2014. - Vol. 126. - P. 1044-1048.

79. Soleimani M., Aflatouni F., Khani A. A new and simple method for sulfur nanoparticles synthesis//Colloid J. - 2013. - Vol. 75, No. 1. - P. 112-116.

80. K. Ganguli A., Ganguly A., Vaidya S. Microemulsion-based synthesis of nanocrystalline materials//Chem. Soc. Rev. - 2010. - Vol. 39, No. 2. - P. 474-485.

81. Deshpande A.S., Khomane R.B., Vaidya B.K., Joshi R.M., Harle A.S., Kulkarni B.D. Sulfur Nanoparticles Synthesis and Characterization from H_2S Gas, Using Novel Biodegradable Iron Chelates in W/O Microemulsion//Nanoscale Res. Lett. - 2008. - Vol. 3, No. 6. - P. 221.

82. Jin H., Sun Y., Sun Z., Yang M., Gui R. Zero-dimensional sulfur nanomaterials: Synthesis, modifications and applications//Coord. Chem. Rev. - 2021. - Vol. 438. - P. 213913.

83. Guo Y., Zhao J., Yang S., Yu K., Wang Z., Zhang H. Preparation and characterization of monoclinic sulfur nanoparticles by water-in-oil microemulsions technique//Powder Technol. - 2006. - Vol. 162, No. 2. - P. 83-86.

84. Kaiser M.R., Ma Z., Wang X., Han F., Gao T., Fan X., Wang J.-Z., Liu H.K., Dou S., Wang C. Reverse Microemulsion Synthesis of Sulfur/Graphene Composite for Lithium/Sulfur Batteries//ACS Nano. - 2017. - Vol. 11, No. 9. - P. 9048-9056.

85. Qian K., Li B., Li Y., Wang C., Yang Y. Synthesis of hollow silica-sulfur composite nanospheres towards stable lithium-sulfur battery//Ionics. - 2017. - Vol. 23, No. 5. - P. 1091-1096.

86. Zaki T., Saed D., Aman D., Younis S.A., Moustafa Y.M. Synthesis and characterization of MFe2O4 sulfur nanoadsorbents//J. Sol-Gel Sci. Technol. - 2013. - Vol. 65, No. 2. - P. 269-276.

87. Zhang J., Li J.-Y., Wang W.-P., Zhang X.-H., Tan X.-H., Chu W.-G., Guo Y.-G. Microemulsion Assisted Assembly of 3D Porous S/Graphene@g-C_3N_4 Hybrid Sponge as Free-Standing Cathodes for High Energy Density Li–S Batteries//Adv. Energy Mater. - 2018. - Vol. 8, No. 14. - P. 1702839.

88. Huang J., Cao B., Zhao F., Zhang L., Qu Y., Chen Y. A mulberry-like hollow carbon cluster decorated by Al-doped ZnO particles for advanced lithium-sulfur cathode//Electrochim. Acta. - 2019. - Vol. 304. - P. 62-69.

89. Ni W. Lithium-Sulfur Battaries / Ni, Wei, Ling-Ying Shi. – Elsevier, 2022. – P. 289-314.

90. Ramimoghadam D., Bagheri S., Hamid S.B.A. Progress in electrochemical synthesis of magnetic iron oxide nanoparticles//J. Magn. Magn. Mater. - 2014. - Vol. 368. - P. 207-229.

91. Peng J., Zhao Z., Zheng M., Su B., Chen X., Chen X. Electrochemical synthesis of phosphorus and sulfur co-doped graphene quantum dots as efficient electrochemiluminescent immunomarkers for monitoring okadaic acid//Sens. Actuators B Chem. - 2020. - Vol. 304. - P. 127383.

92. Wan S., Wang L., Xue Q. Electrochemical deposition of sulfur doped DLC nanocomposite film at atmospheric pressure//Electrochem. Comm. - 2010. - Vol. 12, No. 1. - P. 61-65.

93. Li S., Ding L., Fan L. Electrochemical synthesis of sulfur-doped graphene sheets for highly efficient oxygen reduction//Sci. China Chem. - 2015. - Vol. 58, No. 3. - P. 417-424.

94. Hiep Han T., Parveen N., Ali Ansari S., Ho Shim J., Nguyet Nguyen A.T., Hwan Cho M. Electrochemically synthesized sulfur-doped graphene as a superior metal-free cathodic catalyst for oxygen reduction reaction in microbial fuel cells//RSC Adv. - 2016. - Vol. 6, No. 105. - P. 103446-103454.

95. Shimokawa K., Furuhashi T., Kawaguchi T., Park W.-Y., Wada T., Matsumoto H., Kato H., Ichitsubo T. Electrochemically synthesized liquid-sulfur/sulfide composite materials for high-rate magnesium battery cathodes//J. Mater. Chem. - 2021. - Vol. 9, No. 30. - P. 16585-16593.

96. Dopilka A., Childs A., Bobev S., Chan C.K. Solid-State Electrochemical Synthesis of Silicon Clathrates Using a Sodium-Sulfur Battery Inspired Approach//J. Electrochem. Soc. - 2021. - Vol. 168, No. 2. - P. 020516.

97. Lei F., Xu W., Yu J., Li K., Xie J., Hao P., Cui G., Tang B. Electrochemical synthesis of ammonia by nitrate reduction on indium incorporated in sulfur doped graphene//Chem. Eng. J. - 2021. - Vol. 426. - P. 131317.

98. Deng S., Liu L., Cagnetta G., Huang J., Yu G. Mechanochemically synthesized S-ZVIbm composites for the activation of persulfate in the pH-independent degradation of atrazine: Effects of sulfur dose and ball-milling conditions//J. Chem. Eng. - 2021. - Vol. 423. - P. 129789.

99. Urakaev F.Kh., Bulavchenko A.I., Uralbekov B.M., Massalimov I.A., Tatykayev B.B., Bolatov A.K., Dzharlykasimova D.N., Burkitbayev M.M. Mechanochemical synthesis of colloidal sulfur particles in the Na_2S2O_3–$H_2(C_4H_4O_4)$–Na_2SO_3 system//Colloid J. - 2016. - Vol. 78, No. 2. - P. 210-219.

100. Islamov R.A., Bishimova I., Sabitov A.N., Ilin A.I., Burkitbaev M.M. Lack of Mutagenic Activity of Sulfur Nanoparticles in Micronucleus Test on L5178Y Cell Culture//Cell tissue biol. - 2018. - Vol. 12, No. 1. - P. 27-32.

101. Baláž P., Achimovičová M., Baláž M., Chen K., Dobrozhan O., Guilmeau E., Hejtmánek J., Knížek K., Kubíčková L., Levinský P., Puchý V., Reece M.J., Varga P., Zhang R. Thermoelectric Cu–S-Based Materials Synthesized via a Scalable Mechanochemical Process//ACS Sustainable Chem. Eng. - 2021. - Vol. 9, No. 5. - P. 2003-2016.

102. Qi S., Sun J., Ma J., Sun Y., Goossens K., Li H., Jia P., Fan X., Bielawski C.W., Geng J. Covalent bonding of sulfur nanoparticles to unzipped multiwalled carbon nanotubes for high-performance lithium–sulfur batteries//Nanotechnol. - 2018. - Vol. 30, No. 2. - P. 024001.

103. Chen X., Du G., Zhang M., Kalam A., Ding S., Su Q., Xu B., Al-Sehemi A.G. Vanadium Sulfide@Sulfur Composites as High-Performance Cathode for Advanced Lithium–Sulfur Batteries//Energy Technol. - 2020. - Vol. 8, No. 3. - P. 1901163.

104. Luo Y., Li M., Hu G., Tang T., Wen J., Li X., Wang L. Enhanced photocatalytic activity of sulfur-doped graphene quantum dots decorated with TiO_2 nanocomposites//Mater. Res. Bull. - 2018. - Vol. 97. - P. 428-435.

105. Ren X., Ren X., Pang L., Zhang Y., Ma Q., Fan H., Liu S. (Frank) MoS2/sulfur and nitrogen co-doped reduced graphene oxide nanocomposite for enhanced electrocatalytic hydrogen evolution//Int. J. Hydrog. Energy. - 2016. - Vol. 41, No. 2. - P. 916-923.

106. Safardoust-Hojaghan H., Amiri O., Salavati-Niasari M., Hassanpour M., Khojasteh H., Foong L.K. Performance improvement of dye sensitized solar cells based on cadmium sulfide/S, N co doped carbon dots nanocomposites//J. Mol. Liq. - 2020. - Vol. 301. - P. 112413.

107. Xu C., Zhou H., Fu C., Huang Y., Chen L., Yang L., Kuang Y. Hydrothermal synthesis of boron-doped unzipped carbon nanotubes/sulfur composite for high-performance lithium-sulfur batteries//Electrochim. Acta. - 2017. - Vol. 232. - P. 156-163.

108. Jiang Y., Lu M., Ling X., Jiao Z., Chen L., Chen L., Hu P., Zhao B. One-step hydrothermal synthesis of three-dimensional porous graphene aerogels/sulfur nanocrystals for lithium–sulfur batteries//J. Alloys Compd. - 2015. - Vol. 645. - P. 509-516.

109. Huang Y., Lu R., Wang M., Sakamoto J., Poudeu P.F.P. Hexagonal-WO3 nanorods encapsulated in nitrogen and sulfur co-doped reduced graphene oxide as a high-performance anode material for lithium ion batteries//J. Solid State Chem. - 2020. - Vol. 282. - P. 121068.

110. Anilkumar K.M., Jinisha B., Manoj M., Pradeep V.S., Jayalekshmi S. Layered sulfur/PEDOT:PSS nano composite electrodes for lithium sulfur cell applications//Appl. Surf. Sci. - 2018. - Vol. 442. - P. 556-564.

111. Xu L., Zhou X., Xu X., Ma L., Luo J., Zhang L. Triethylenetetramine-assisted hydrothermal synthesis of sulfur-doped few-layer $MoSe_2$/nitrogenated graphene hybrids and their catalytic activity for hydrogen evolution reaction//Adv. Powder Technol. - 2016. - Vol. 27, No. 4. - P. 1560-1567.

112. Dessie Walle M., Zhang Z., You X., Zhang M., Muya Chabu J., Li Y., Liu Y.-N. Soft approach hydrothermal synthesis of a 3D sulfur/graphene/ multiwalled carbon nanotube cathode for lithium–sulfur batteries//RSC Adv. - 2016. - Vol. 6, No. 82. - P. 78994-78998.

113. Wu D., Wang T., Wang L., Jia D. Hydrothermal synthesis of nitrogen, sulfur co-doped graphene and its high performance in supercapacitor and oxygen reduction reaction//Microporous Mesoporous Mater. - 2019. - Vol. 290. - P. 109556.

114. Ma L., Xu L., Xu X., Zhou X., Zhang L. One-Pot Hydrothermal Synthesis of Sulfur-Doped SnO2 Nanoparticles and their Enhanced Photocatalytic Properties//Nano. - 2016. - Vol. 11, No. 03. - P. 1650035.

115. Cao Y., Li X., A. Aksay I., Lemmon J., Nie Z., Yang Z., Liu J. Sandwich-type functionalized graphene sheet-sulfur nanocomposite for rechargeable lithium batteries//Phys. Chem. Chem. Phys. - 2011. - Vol. 13. - No. 17. - P. 7660-7665.

116. Zhang C., Zhang Z., Wang D., Yin F., Zhang Y. Three-dimensionally ordered macro-/mesoporous carbon loading sulfur as high-performance cathodes for lithium/sulfur batteries//J. Alloys Compd. - 2017. - Vol. 714. - P. 126-132.

117. Manoj M., Jasna M., Anilkumar K.M., Abhilash A., Jinisha B., Pradeep V.S., Jayalekshmi S. Sulfur-polyaniline coated mesoporous carbon composite in combination with carbon nanotubes interlayer as a superior cathode assembly for high capacity lithium-sulfur cells//Appl. Surf. Sci. - 2018. - Vol. 458. - P. 751-761.

118. Kovačić M., Perović K., Papac J., Tomić A., Matoh L., Žener B., Brodar T., Capan I., Surca A.K., Kušić H., Štangar U.L., Lončarić Božić A. One-Pot Synthesis of Sulfur-Doped TiO2/Reduced Graphene Oxide Composite (S-TiO_2/rGO) with Improved Photocatalytic Activity for the Removal of Diclofenac from Water//Mater. - 2020. - Vol. 13, No. 7. - P. 1621.

119. Tashrifi Z., Khanaposhtani M.M., Larijani B., Mahdavi M. Dimethyl Sulfoxide: Yesterday's Solvent, Today's Reagent//Adv. Synth. Catal. - 2020. - Vol. 362, No. 1. - P. 65-86.

120. Madruga G.M., Crivellenti L.Z., . Borin-Crivellenti S., Cintra C.A., Gomes L.G., Spiller P.R. Comparative use of dimethyl sulphoxide (DMSO)in different animal species//Vet. Med. - 2017. - Vol. 62, No. 4. - P. 179-185.

121. Evenepoel N., Wen S., Tilahun Tsehaye M., Van der Bruggen B. Potential of DMSO as greener solvent for PES ultra- and nanofiltration membrane preparation//J. Appl. Polym. Sci. - 2018. - Vol. 135, No. 28. - P. 46494.

122. Waybright T.J., Britt J.R., McCloud T.G. Overcoming Problems of Compound Storage in DMSO: Solvent and Process Alternatives//J. Biomol. Screen. - 2009. - Vol. 14, No. 6. - P. 708-715.

123. Galvao J., Davis B., Tilley M., Normando E., Duchen M.R., Cordeiro M.F. Unexpected low-dose toxicity of the universal solvent DMSO//FASEB J. - 2014. - Vol. 28, No. 3. - P. 1317-1330.

124. Choi S., Sainz B., Corcoran P., Uprichard S., Jeong H. Characterization of increased drug metabolism activity in dimethyl sulfoxide (DMSO)-treated Huh7 hepatoma cells//Xenobiotica. - 2009. - Vol. 39, No. 3. - P. 205-217.

125. Hammoudeh S.M., Hammoudeh A.M., Hamoudi R. High-throughput quantification of the effect of DMSO on the viability of lung and breast cancer cells using an easy-to-use spectrophotometric trypan blue-based assay//Histochem. Cell Biol. - 2019. - Vol. 152. - No. 1. - P. 75-84.

126. Carraher C.E., Barot G., Shahi K., Roner M.R. Influence of DMSO on the inhibition of various cancer cells by water-soluble organotin polyethers//JCAMS. - 2013. - Vol. 1, No. 4. - P. 294-304.

127. Young V.L., Boswell C.B., Centeno R.F., Watson M.E. DMSO: Applications in Plastic Surgery//Aesthet. Surg. J. - 2005. - Vol. 25. - No. 2. - P. 201-209.

128. Xia Y., Chen D., Xia Z. Inhibitory effect of dimethyl sulfoxide on collagen formation//Chin. J. Med. Aesthetics Cosmet. - 2002.

129. Mares D., Tosi B., Poli F., Andreotti E., Romagnoli C. Antifungal activity of Tagetes patula extracts on some phytopathogenic fungi: ultrastructural evidence on Pythium ultimum//Microbiol. Res. - 2004. - Vol. 159, No. 3. - P. 295-304.

130. Lawhavinit O., Kongkathip N., Kongkathip B. Antimicrobial Activity of Curcuminoids from Curcuma longa L. on Pathogenic Bacteria of Shrimp and Chicken//Agric. Nat. Resour. - 2010. - Vol. 44, No. 3. - P. 364-371.

131. Keskın D., Ceyhan N., Uğur A., Aysel A.D. Antimicrobial activity and chemical constitutions of West Anatolian olive (Olea europaea L.) leaves//J. Food Agric. Environ. - 2012. - Vol. 10, No. 2. - P. 99-102.

132. Kumari R., Ashraf S., Bagri G.K., Khatik S.K., Bagri D.K., Bagdi D. Extraction and estimation of chlorophyll content of seed treated lentil crop using DMSO and acetone//J. Pharmacogn. Phytochem. - 2018. - Vol. 7, No. 3. - P. 249-250.

133. Miguel-Chávez R., Aristeo-Cortes P., Larqué-Saavedra A. The effect of dimethyl sulphoxide (DMSO) on carrot plants grown in the field//Phyton. - 2003. - Vol. 101. - P. 101-104.

134. Guilherme M.R., Aouada F.A., Fajardo A.R., Martins A.F., Paulino A.T., Davi M.F.T., Rubira A.F., Muniz E.C. Superabsorbent hydrogels based on polysaccharides for application in agriculture as soil conditioner and nutrient carrier: A review//Eur. Polym. J. - 2015. - Vol. 72. - P. 365-385.

135. Mousa O., Vuorela P., Kiviranta J., Wahab S.A., Hiltunen R., Vuorela H. Bioactivity of certain Egyptian Ficus species//J. Ethnopharmacol. - 1994. - Vol. 41, No. 1. - P. 71-76.

136. Wu X.-F., Natte K. The Applications of Dimethyl Sulfoxide as Reagent in Organic Synthesis//Adv. Synth. Catal. - 2016. - Vol. 358, No. 3. - P. 336-352.

137. Wu X.-F. Solvents as Reagents in Organic Synthesis: Reactions and Applications. Solvents as Reagents in Organic Synthesis. – John Wiley & Sons, 2018. – 552 p.

138. Bronze-Uhle E.S., Batagin-Neto A., Xavier P.H.P., Fernandes N.I., de Azevedo E.R., Graeff C.F.O. Synthesis and characterization of melanin in DMSO//J. Mol. Struct. - 2013. - Vol. 1047. - P. 102-108.

139. Matake R., Adachi Y., Matsubara H. Synthesis of vinyl ethers of alcohols using calcium carbide under superbasic catalytic conditions (KOH/DMSO)//Green Chem. - 2016. - Vol. 18, No. 9. - P. 2614-2618.

140. Iwanami K., Hinakubo Y., Oriyama T. Catalyst-free DMSO-promoted synthesis of cyanohydrin carbonates from aldehydes//Tetrahedron Lett. - 2005. - Vol. 46, No. 35. - P. 5881-5883.

141. P.V.Torchyniuk, O.I.V'yunov, A.A.Ishchenko, I.V.Kurdyukova, A.G.Belous Synthesis of Organic-Inorganic Perovskite $CH_3NH_3PbI_3$ using Dimethyl Sulfoxide (DMSO) Solvent//Eng. Sci. - 2021. - Vol. 17. - P. 156-166.

142. Zhou B., Ding D., Wang Y., Fang S., Liu Z., Tang J., Li H., Zhong H., Tian B., Shi Y. A Scalable H_2O–DMF–DMSO Solvent Synthesis of Highly Luminescent Inorganic Perovskite-Related Cesium Lead Bromides//Adv. Opt. Mater. - 2021. - Vol. 9, No. 3. - P. 2001435.

143. Sharutin V.V., Senchurin V.S., Sharutina O.K., Gushchin A.V. Synthesis and structure of platinum complexes $[Ph_4P]+[PtCl_3(DMSO)]-$ and $[Ph_4P]+[PtCl_5(DMSO)]-$//Russ. J. Inorg. Chem. - 2013. - Vol. 58, No. 1. - P. 33-37.

144. Sharutin V.V., Senchurin V.S., Sharutina O.K. Synthesis and structure of palladium complexes $[Ph_3PhCH_2P]^+[PdCl_3(DMSO)]^-DMSO$, $[Ph_4P]^+[PdCl_3(DMSO)]^-$, and $[Ph_4Sb(DMSO)]^+[PdCl_3(DMSO)]-$//Russ. J. Inorg. Chem. - 2013. - Vol. 58, No. 5. - P. 543-547.

145. Korolenko S.E., Goeva L.V., Kubasov A.S., Avdeeva V.V., Malinina E.A., Kuznetsov N.T. Synthesis, Structures, and Properties of Zinc(II) and Cadmium(II) Complexes with Boron Cluster Anions [M(solv)6][BnHn] (M = Zn(II), Cd(II); solv = DMF, DMSO; n = 10, 12)//Russ. J. Inorg. Chem. - 2020. - Vol. 65, No. 6. - P. 846-853.

146. Urbanski S.P., Stickel R.E., Wine P.H. Mechanistic and Kinetic Study of the Gas-Phase Reaction of Hydroxyl Radical with Dimethyl Sulfoxide//J. Phys. Chem. A. - 1998. - Vol. 102, No. 51. - P. 10522-10529.

147. Bardouki H., da Rosa M.B., Mihalopoulos N., Palm W.-U., Zetzsch C. Kinetics and mechanism of the oxidation of dimethylsulfoxide (DMSO) and methanesulfinate (MSI−) by OH radicals in aqueous medium//Atmos. Environ. - 2002. - Vol. 36, No. 29. - P. 4627-4634.

148. Tomer R., Biswas P. Reaction kinetics study and the estimation of thermodynamic parameters for the conversion of glucose to 5-hydroxymethylfurfural (5-HMF) in a dimethyl sulfoxide (DMSO) medium in the presence of a mesoporous TiO2 catalyst//J. Taiwan Inst. Chem. Eng. - 2022. - Vol. 136. - P. 104427.

149. Ostermeier L., Oliva R., Winter R. The multifaceted effects of DMSO and high hydrostatic pressure on the kinetic constants of hydrolysis reactions catalyzed by α-chymotrypsin//Phys. Chem. Chem. Phys. - 2020. - Vol. 22, No. 28. - P. 16325-16333.

150. Reinsberg P., Weiß A., Bawol P.P., Baltruschat H. Electrochemical Reaction Order of the Oxygen Reduction Reaction in Li^+-Containing DMSO//J. Phys. Chem. C. - 2017. - Vol. 121, No. 14. - P. 7677-7688.

151. Lin Y.-H., Hsueh H.-T., Chang C.-W., Chu H. The visible light-driven photodegradation of dimethyl sulfide on S-doped TiO2: Characterization, kinetics, and reaction pathways//Appl. Catal. B: Environ. - 2016. - Vol. 199. - P. 1-10.

152. Abellán M.N., Dillert R., Giménez J., Bahnemann D. Evaluation of two types of TiO_2-based catalysts by photodegradation of DMSO in aqueous suspension//J. Photochem. Photobiol. A. - 2009. - Vol. 202, No. 2. - P. 164-171.

153. Mbey J.A., Thomas F., Ngally Sabouang C.J., Liboum, Njopwouo D. An insight on the weakening of the interlayer bonds in a Cameroonian kaolinite through DMSO intercalation//Appl. Clay Sci. - 2013. - Vols. 83-84. - P. 327-335.

154. Patakfalvi R., Oszkó A., Dékány I. Synthesis and characterization of silver nanoparticle/kaolinite composites//Colloids and Surfaces A: Physicochemical and Engineering Aspects. - 2003. - Vol. 220, No. 1. - P. 45-54.

155. Li Y., Zhang B., Pan X. Preparation and characterization of PMMA–kaolinite intercalation composites//Compos. Sci. Technol. - 2008. - Vol. 68, No. 9. - P. 1954-1961.

156. de Macêdo Neto J.C., Botan R., Lona L.M.F., Neto J.E., Pippo W.A. Polystyrene/kaolinite nanocomposite synthesis and characterization via in situ emulsion polymerization//Polym. Bull. - 2015. - Vol. 72, No. 3. - P. 387-404.

157. Ghosh P., Siddhanta S.K., Haque S.R., Chakrabarti A. Stable polyaniline dispersions prepared in nonaqueous medium: synthesis and characterization//Synth. Met. - 2001. - Vol. 123, No. 1. - P. 83-89.

158. Lee S., Kim Y.-J., Kim D.-H., Ku B.-C., Joh H.-I. Synthesis and properties of thermally reduced graphene oxide/polyacrylonitrile composites//J. Phys. Chem. Solids. - 2012. - Vol. 73, No. 6. - P. 741-743.

159. Aslam J., Lone I.H., Radwan N., Mobin M., Zehra S., Aslam R. Development of Poly(aniline-co-o-toluidine)/TiO_2 nanocomposite coatings for low carbon steel corrosion in 3.5% NaCl solution//J. Adhes. Sci. Technol. - 2018. - Vol. 32, No. 23. - P. 2552-2568.

160. El-Samak A.A., Ponnamma D., Hassan M.K., Adham S., Karim A., Ammar A., Alser M., Shurbaji S., Eltai N.O., Al-Maadeed M.A.A. Multifunctional Oil Absorption with Macroporous Polystyrene Fibers Incorporating Silver-Doped ZnO//ACS Omega. - 2021. - Vol. 6, No. 12. - P. 8081-8093.

161. Prozorova G.F., Pozdnyakov A.S., Kuznetsova N.P., Korzhova S.A., Emel'yanov A.I., Ermakova T.G., Fadeeva T.V., Sosedova L.M. Green synthesis of water-soluble nontoxic polymeric nanocomposites containing silver nanoparticles//Int. J. Nanomed. - 2014. - Vol. 9. - P. 1883-1889.

162. Soliman T.S., Vshivkov S.A. Effect of Fe nanoparticles on the structure and optical properties of polyvinyl alcohol nanocomposite films//J. Non-Cryst. Solids. - 2019. - Vol. 519. - P. 119452.

163. Liu Z., Wu B. One pot synthesis of bismuth–bismuth oxybromide composites with enhanced visible-light photocatalytic activity//Mater. Sci. Semicond. Process. - 2015. - Vol. 31, P. 68-75.

164. Kuznetsova N.P., Ermakova T.G., Pozdnyakov A.S., Emel'yanov A.I., Prozorova G.F. Synthesis and characterization of silver polymer nanocomposites of 1-vinyl-1,2,4-triazole with acrylonitrile//Rus. Chem. Bull. - 2013. - Vol. 62, No. 11. - P. 2509-2513.

165. Liang J., Wei W., Zhong D., Yang Q., Li L., Guo L. One-Step In situ Synthesis of SnO2/Graphene Nanocomposites and Its Application As an Anode Material for Li-Ion Batteries//ACS Appl. Mater. Interfaces. - 2012. - Vol. 4, No. 1. - P. 454-459.

166. Huang X., Zhou X., Zhou L., Qian K., Wang Y., Liu Z., Yu C. A Facile One-Step Solvothermal Synthesis of SnO2/Graphene Nanocomposite and Its Application as an Anode Material for Lithium-Ion Batteries//ChemPhysChem. - 2011. - Vol. 12, No. 2. - P. 278-281.

167. Zhang X., Sun X., Chen Y., Zhang D., Ma Y. One-step solvothermal synthesis of graphene/Mn3O4 nanocomposites and their electrochemical properties for supercapacitors//Mater. Lett. - 2012. - Vol. 68. - P. 336-339.

168. Cao A., Liu Z., Chu S., Wu M., Ye Z., Cai Z., Chang Y., Wang S., Gong Q., Liu Y. A Facile One-step Method to Produce Graphene–CdS Quantum Dot Nanocomposites as Promising Optoelectronic Materials//Adv. Mater. - 2010. - Vol. 22, No. 1. - P. 103-106.

169. Zedan A.F., Sappal S., Moussa S., El-Shall M.S. Ligand-Controlled Microwave Synthesis of Cubic and Hexagonal CdSe Nanocrystals Supported on Graphene. Photoluminescence Quenching by Graphene//J. Phys. Chem. C. - 2010. - Vol. 114, No. 47. - P. 19920-19927.

170. Fan Y., Han D., Song Z., Sun Z., Dong X., Niu L. Regulations of silver halide nanostructure and composites on photocatalysis//Adv. Compos. Hybrid Mater. - 2018. - Vol. 1, No. 2. - P. 269-299.

171. Sharma M.K. Formation of Ultrafine Silver Halide Particles in Microemulsions Useful for Photographic Technology//Surface Phenomena and Fine Particles in Water-Based Coatings and Printing Technology. – Boston, MA: Springer US, 1991. – P. 247-257.

172. Cui L., Jiao T., Zhang Q., Zhou J., Peng Q. Facile Preparation of Silver Halide Nanoparticles as Visible Light Photocatalysts//Nanomater. Nanotechnol. - 2015. - Vol. 5. - P. 20.

173. Fujishima A., Honda K. Electrochemical Photolysis of Water at a Semiconductor Electrode//Nature. - 1972. - Vol. 238, No. 5358. - P. 37-38.

174. Serpone N. Is the Band Gap of Pristine TiO_2 Narrowed by Anion- and Cation-Doping of Titanium Dioxide in Second-Generation Photocatalysts?//J. Phys. Chem. B. - 2006. - Vol. 110, No. 48. - P. 24287-24293.

175. Ma X., Dai Y., Guo M., Huang B. The Role of Effective Mass of Carrier in the Photocatalytic Behavior of Silver Halide-Based Ag@AgX (X=Cl, Br, I): A Theoretical Study//ChemPhysChem. - 2012. - Vol. 13, No. 9. - P. 2304-2309.

176. Glaus S., Calzaferri G. The band structures of the silver halides AgF, AgCl, and AgBr: A comparative study//Photochem. Photobiol. Sci. - 2003. - Vol. 2, No. 4. - P. 398-401.

177. Gordienko A.B., Zhuravlev Yu.N., Poplavnoi A.S. Electronic Structure of AgCl, AgBr, and AgI//Phys. Status Solidi B. - 1991. - Vol. 168, No. 1. - P. 149-156.

178. Yu Z., Liu Y., He W., Wang Z. Evaluation of effect from Ag-AgX (X = Cl, Br, I) on photodegradation of azo dyes: Advances in photo(electro)catalysis for environmental applications and chemical synthesis//Catal. Today. - 2019. - Vol. 335. - P. 574-581.

179. Mao S., Bao R., Fang D., Yi J. Facile synthesis of Ag/AgX (X = Cl, Br) with enhanced visible-light-induced photocatalytic activity by ultrasonic spray pyrolysis method//Adv. Powder Technol. - 2018. - Vol. 29, No. 11. - P. 2670-2677.

180. Xu L., Cui Q., Tian Y., Jiao A., Zhang M., Li S., Li H., Chen M. Enhanced synergistic coupling effect of ternary Au/Ag/AgCl nanochains for promoting natural-solar-driven photocatalysis//Appl. Surf. Sci. - 2021. - Vol. 545. - P. 149054.

181. Lu J., Wang H., Dong Y., Wang F., Dong S. Plasmonic AgX nanoparticles-modified ZnO nanorod arrays and their visible-light-driven photocatalytic activity//Chinese J. Catal. - 2014. - Vol. 35, No. 7. - P. 1113-1125.

182. Phongarthit K., Amornpitoksuk P., Suwanboon S. Photocatalytic degradation of rhodamine B, reactive orange, and bisphenol A under visible light irradiation over AgX/ZnO (X=Cl, Br, I) prepared from green approach//Optik. - 2020. - Vol. 204. - P. 164224.

183. Padervand M., Salari H., Ahmadvand S., Gholami M.R. Removal of an organic pollutant from waste water by photocatalytic behavior of AgX/TiO_2 loaded on mordenite nanocrystals//Res. Chem. Intermed. - 2012. - Vol. 38, No. 8. - P. 1975-1985.

184. Midhu Francis M., Thakur A., Balapure A., Ray Dutta J., Ganesan R. Fabricating effective heterojunction in metal-organic framework-derived self-cleanable and dark/visible-light dual mode antimicrobial CuO/AgX (X = Cl, Br, or I) nanocomposites//Chem. Eng. J. - 2022. - Vol. 446. - P. 137363.

185. Li F., Yin Y., Jiang D. Fabrication of a stable visible-light photocatalyst p-CuO/n-AgBr through hole transporting//J. Mater. Sci. - 2017. - Vol. 52, No. 11. - P. 6415-6422.

186. Cao J., Luo B., Lin H., Chen S. Photocatalytic activity of novel AgBr/WO_3 composite photocatalyst under visible light irradiation for methyl orange degradation//J. Hazard. Mater. - 2011. - Vol. 190, No. 1. - P. 700-706.

187. Yao S., Xue S., Shen X. Photocatalytic Activity of Cuboid WO3 Rods Loaded with AgCl Nanoparticles Under Visible Light Irradiation//J. Nanosci. Nanotechnol., 2017, Vol. 17, No. 8, P. 5423-5431.

188. Khan A.I., O'Hare D. Intercalation chemistry of layered double hydroxides: recent developments and applications//J. Mater. Chem., 2002, Vol. 12, Intercalation chemistry of layered double hydroxides, No. 11, P. 3191-3198.

189. Shao M., Wei M., Evans D.G., Duan X. Layered Double Hydroxide Materials in Photocatalysis//Photofunctional Layered Materials : Structure and Bonding/ eds. D. Yan, M. Wei. – Cham: Springer International Publishing, 2015. – P. 105-136.

190. Abdollahizadeh Z., Haghighi M., Shabani M. Photocatalytic removal of pharmaceutical contaminants from aqueous effluents using staggered AgX(Br, I)/CoCrNO$_3$LDH plasmon nanophotocatalysts under simulated solar-light//Sep. Purif. Technol. - 2021. - Vol. 278. - P. 119574.

191. Sun J., Zhang Y., Cheng J., Fan H., Zhu J., Wang X., Ai S. Synthesis of Ag/AgCl/Zn-Cr LDHs composite with enhanced visible-light photocatalytic performance//J. Mol. Catal. A Chem. - 2014. - Vol. 382. - P. 146-153.

192. Fan H., Zhu J., Sun J., Zhang S., Ai S. Ag/AgBr/Co–Ni–NO_3 Layered Double Hydroxide Nanocomposites with Highly Adsorptive and Photocatalytic Properties//Chem. Eur. J. - 2013. - Vol. 19, No. 7. - P. 2523-2530.

193. Long M., Cai W. Advanced nanoarchitectures of silver/silver compound composites for photochemical reactions//Nanoscale. - 2014. - Vol. 6, No. 14. - P. 7730-7742.

194. Nikokavoura A., Trapalis C. Graphene and g-C_3N_4 based photocatalysts for NOx removal: A review: 2nd International Workshop on Graphene and C3N4-based Photocatalysts//Appl. Surf. Sci. - 2018. - Vol. 430. - P. 18-52.

195. Prasad C., Liu Q., Tang H., Yuvaraja G., Long J., Rammohan A., Zyryanov G.V. An overview of graphene oxide supported semiconductors based photocatalysts: Properties, synthesis and photocatalytic applications//J. Mol. Liq. - 2020. - Vol. 297. - P. 111826.

196. Zhang H., Fan X., Quan X., Chen S., Yu H. Graphene Sheets Grafted Ag@AgCl Hybrid with Enhanced Plasmonic Photocatalytic Activity under Visible Light//Environ. Sci. Technol. - 2011. - Vol. 45, No. 13. - P. 5731-5736.

197. Liu E., Chen J., Ma Y., Feng J., Jia J., Fan J., Hu X. Fabrication of 2D SnS2/g-C3N4 heterojunction with enhanced H_2 evolution during photocatalytic water splitting//J. Colloid Interface Sci. - 2018. - Vol. 524. - P. 313-324.

198. Zhu M., Chen P., Liu M. Highly efficient visible-light-driven plasmonic photocatalysts based on graphene oxide -hybridized one-dimensional Ag/AgCl heteroarchitectures//J. Mater. Chem. - 2012. - Vol. 22, No. 40. - P. 21487-21494.

199. Choudhury B.K., Gogoi S.K. Reduced graphene oxide and Ag/AgCl composite (RGO–Ag/AgCl) for photocatalytic degradation of RhB using WLED//Nano-Struct. Nano-Objects. - 2021. - Vol. 26. - P. 100704.

200. Min Y., He G., Xu Q., Chen Y. Self-assembled encapsulation of graphene oxide/Ag@AgCl as a Z-scheme photocatalytic system for pollutant removal//J. Mater. Chem. A. - 2014. - Vol. 2, No. 5. - P. 1294-1301.

201. Bai C., Bi J., Wu J., Xu Y., Wohlrab S., Han Y., Zhang X. In- situ solid-phase fabrication of Ag/AgX (X=Cl, Br, I)/g-C_3N_4 composites for enhanced visible-light hydrogen evolution//Int. J. Hydrog. Energy. - 2019. - Vol. 44, No. 39. - P. 21397-21405.

202. Vosoughi F., Habibi-Yangjeh A., Asadzadeh-Khaneghah S., Ghosh S., Maiyalagan T. Novel ternary g-C3N4 nanosheet/Ag_2MoO_4/AgI photocatalysts: Impressive photocatalysts for removal of various contaminants//J. Photochem. Photobiol. A. - 2020. - Vol. 403. - P. 112871.

203. Zhang J., Zhang Z., Zhu W., Meng X. Boosted photocatalytic degradation of Rhodamine B pollutants with Z-scheme CdS/AgBr-rGO nanocomposite//Appl. Surf. Sci., 2020, Vol. 502, P. 144275.

204. Amornpitoksuk P., Suwanboon S. Photocatalytic decolorization of methylene blue dye by Ag_3PO_4–AgX (X=Cl−, Br− and I−) under visible light//Adv. Powder Technol. - 2014. - Vol. 25, No. 3. - P. 1026-1030.

205. Cao J., Luo B., Lin H., Xu B., Chen S. Visible light photocatalytic activity enhancement and mechanism of AgBr/Ag_3PO_4 hybrids for degradation of methyl orange//J. Hazard. Mater. - 2012. - Vols. 217-218. - P. 107-115.

206. Sun L., Wang Y., Chen W. Synthesis of novel $CaCO_3$/Ag_2CO_3/AgI/Ag plasmonic photocatalyst with enhanced visible light photocatalytic activity//Sci. China Technol. Sci. - 2015. - Vol. 58, No. 11. - P. 1864-1870.

207. Xu H., Zhu J., Song Y., Zhu T., Zhao W., Song Y., Da Z., Liu C., Li H. Fabrication of AgX-loaded Ag_2CO_3 (X=Cl, I) composites and their efficient visible-light-driven photocatalytic activity//J. Alloys Compd. - 2015. - Vol. 622. - P. 347-357.

208. Lakachew Nigusie A., Ujihara M. Plasmon-enhanced hydrogen evolution reaction on a Ag-branched-nanowire/Pt nanoparticle/AgCl nanocomposite//Phys. Chem. Chem. Phys. - 2021. - Vol. 23, No. 30. - P. 16366-16375.

209. Geng Z., Chen Z., Li Z., Qi X., Yang X., Fan W., Guo Y., Zhang L., Huo M. Enhanced photocatalytic conversion and selectivity of nitrate reduction to nitrogen over AgCl/TiO_2 nanotubes//Dalton Trans. - 2018. - Vol. 47, No. 32. - P. 11104-11112.

210. Abou Asi M., He C., Su M., Xia D., Lin L., Deng H., Xiong Y., Qiu R., Li X. Photocatalytic reduction of CO_2 to hydrocarbons using AgBr/TiO_2 nanocomposites under visible light: The 6th International Conference on Environmental Catalysis (6th ICEC) Beijing, China, September 12-15, 2010//Catal. Today. - 2011. - Vol. 175, No. 1. - P. 256-263.

211. Fan G., Ning R., Yan Z., Luo J., Du B., Zhan J., Liu L., Zhang J. Double photoelectron-transfer mechanism in Ag−AgCl/WO_3/g-C_3N_4 photocatalyst with enhanced visible-light photocatalytic activity for trimethoprim degradation//J. Hazard. Mater. - 2021. - Vol. 403. - P. 123964.

212. Zheng J., Tang X., Fan C., Deng Y., Li X., Yang Q., Wang D., Duan A., Luo J., Chen Z., Zhang B. Facile synthesis of Ag@AgCl/ZnAl-LDH sesame balls nanocomposites with enhanced photocatalytic performance for the degradation of neonicotinoid pesticides//Chem. Eng. J. - 2022. - Vol. 446. - P. 136485.

213. Rather R.A., Khan M., Lo I.M.C. High charge transfer response of g-C_3N_4/Ag/AgCl/$BiVO_4$ microstructure for the selective photocatalytic reduction of CO_2 to CH_4 under alkali activation//J. Catal. - 2018. - Vol. 366. - P. 28-36.

214. Qi H.-P., Wang H.-L., Zhao D.-Y. Facile synthesis of rGO-supported AgI-TiO2 mesocrystals with enhanced visible light photocatalytic activity//Nanotechnol. - 2020. - Vol. 31, No. 37. - P. 375701.

215. Wang P., Tang Y., Dong Z., Chen Z., Lim T.-T. Ag–AgBr/TiO_2/RGO nanocomposite for visible-light photocatalytic degradation of penicillin G//J. Mater. Chem. A. - 2013. - Vol. 1, No. 15. - P. 4718-4727.

216. Kadeer K., Reheman A., Maimaitizi H., Talifu D., Tursun Y., Abulizi A. Preparation of rGO/AgCl QDs and its enhanced photoelectrocatalytic performance for the degradation of Tetracycline//J. Am. Ceram. Soc. - 2019. - Vol. 102, No. 9. - P. 5342-5352.

217. Zhang S., Li J., Wang X., Huang Y., Zeng M., Xu J. In Situ Ion Exchange Synthesis of Strongly Coupled Ag@AgCl/g-C_3N_4 Porous Nanosheets as Plasmonic Photocatalyst for Highly Efficient Visible-Light Photocatalysis//ACS Appl. Mater. Interfaces. - 2014. - Vol. 6, No. 24. - P. 22116-22125.

218. Ebadi M., Zarghami Z., Aliabadi M. Preparation and characterization of AgCl–Ag_2S nanocomposites via a simple co-precipitation route: utilizing as a photocatalyst for methyl orange degradation//J. Mater. Sci. Mater. - 2016. - Vol. 27, No. 2. - P. 1622-1628.

219. Lucheta A.R., Lambais M.R. Sulfur in agriculture//Rev. Bras. Ciênc. Solo. - 2012. - Vol. 36. - P. 1369-1379.

220. Shankar S., Jaiswal L., Rhim J.-W. New insight into sulfur nanoparticles: Synthesis and applications//Crit. Rev. Environ. Sci. Technol. - 2021. - Vol. 51, No. 20. - P. 2329-2356.

221. Canfield D.E. Biogeochemistry of Sulfur Isotopes//Rev. Mineral. Geochem. - 2001. - Vol. 43, No. 1. - P. 607-636.

222. Boyd D.A. Sulfur and Its Role In Modern Materials Science//Angew. Chem. Int. Ed. - 2016. - Vol. 55, No. 50. - P. 15486-15502.

223. Wang J., Wang G., Cheng B., Yu J., Fan J. Sulfur-doped g-C_3N_4/TiO_2 S-scheme heterojunction photocatalyst for Congo Red photodegradation//Chinese J. Catal. - 2021. - Vol. 42, No. 1. - P. 56-68.

224. Han W., Chen L., Song W., Wang S., Fan X., Li Y., Zhang F., Zhang G., Peng W. Synthesis of nitrogen and sulfur co-doped reduced graphene oxide as efficient metal-free cocatalyst for the photo-activity enhancement of CdS//Appl. Catal. B: Environ. - 2018. - Vol. 236. - P. 212-221.

225. Hu C., Hung W.-Z., Wang M.-S., Lu P.-J. Phosphorus and sulfur codoped g-C3N4 as an efficient metal-free photocatalyst//Carbon. - 2018. - Vol. 127. - P. 374-383.

226. Periyat P., Pillai S.C., McCormack D.E., Colreavy J., Hinder S.J. Improved High-Temperature Stability and Sun-Light-Driven Photocatalytic Activity of Sulfur-Doped Anatase TiO2//J. Phys. Chem. C. - 2008. - Vol. 112, No. 20. - P. 7644-7652.

227. Wang Y., Wang Y., Meng Y., Ding H., Shan Y., Zhao X., Tang X. A Highly Efficient Visible-Light-Activated Photocatalyst Based on Bismuth- and Sulfur-Codoped TiO2//J. Phys. Chem. C. - 2008. - Vol. 112, No. 17. - P. 6620-6626.

228. Zhao G., Wang A., He W., Xing Y., Xu X. 2D New Nonmetal Photocatalyst of Sulfur-Doped h-BN Nanosheeets with High Photocatalytic Activity//Adv. Mater. Interfaces. - 2019. - Vol. 6, No. 7. - P. 1900062.

229. Li W., Feng C., Dai S., Yue J., Hua F., Hou H. Fabrication of sulfur-doped g-C3N4/Au/CdS Z-scheme photocatalyst to improve the photocatalytic performance under visible light//Appl. Catal. B: Environ. - 2015. - Vols. 168-169. - P. 465-471.

230. Lu C., Zhang P., Jiang S., Wu X., Song S., Zhu M., Lou Z., Li Z., Liu F., Liu Y., Wang Y., Le Z. Photocatalytic reduction elimination of UO22+ pollutant under visible light with metal-free sulfur doped g-C_3N_4 photocatalyst//Appl. Catal. B: Environ. - 2017. - Vol. 200. - P. 378-385.

231. Kong H.J., Won D.H., Kim J., Woo S.I. Sulfur-Doped g-C3N4/BiVO4 Composite Photocatalyst for Water Oxidation under Visible Light//Chem. Mater. - 2016. - Vol. 28, No. 5. - P. 1318-1324.

232. Wang Y., Tian Y., Yan L., Su Z. DFT Study on Sulfur-Doped g-C3N4 Nanosheets as a Photocatalyst for CO_2 Reduction Reaction//J. Phys. Chem. C. - 2018. - Vol. 122, No. 14. - P. 7712-7719.

233. He Z., Wang Y., Dong X., Zheng N., Ma H., Zhang X. Indium sulfide nanotubes with sulfur vacancies as an efficient photocatalyst for nitrogen fixation//RSC Advances. - 2019. - Vol. 9, No. 38. - P. 21646-21652.

234. Lee J.H., Cho H., Park S.O., Hwang J.M., Hong Y., Sharma P., Jeon W.C., Cho Y., Yang C., Kwak S.K., Moon H.R., Jang J.-W. High performance H2O2 production achieved by sulfur-doped carbon on CdS photocatalyst via inhibiting reverse H2O2 decomposition//Appl. Catal. B: Environ., 2021, Vol. 284, P. 119690.

235. Wang C., Guo Y., Yang Y., Chu S., Zhou C., Wang Y., Zou Z. Sulfur-Doped Polyimide Photocatalyst with Enhanced Photocatalytic Activity under Visible Light Irradiation//ACS Appl. Mater. Interfaces, 2014, Vol. 6, No. 6, P. 4321-4328.

236. Chen L., Zhu D., Li J., Wang X., Zhu J., Francis P.S., Zheng Y. Sulfur and potassium co-doped graphitic carbon nitride for highly enhanced photocatalytic hydrogen evolution//Appl. Catal. B: Environ. - 2020. - Vol. 273. - P. 119050.

237. Li L., Fang W., Zhang P., Bi J., He Y., Wang J., Su W. Sulfur-doped covalent triazine-based frameworks for enhanced photocatalytic hydrogen evolution from water under visible light//J. Mater. Chem. A. - 2016. - Vol. 4, No. 32. - P. 12402-12406.

238. Niu Y., Xing M., Zhang J., Tian B. Visible light activated sulfur and iron co-doped TiO2 photocatalyst for the photocatalytic degradation of phenol: Catalysis for Low-carbon Energy Development and Environment Quality Control//Catal. Today. - 2013. - Vol. 201. - P. 159-166.

239. Wang W., Yu J.C., Xia D., Wong P.K., Li Y. Graphene and g-C3N4 Nanosheets Cowrapped Elemental α-Sulfur As a Novel Metal-Free Heterojunction Photocatalyst for Bacterial Inactivation under Visible-Light//Environ. Sci. Technol. - 2013. - Vol. 47, No. 15. - P. 8724-8732.

240. Meng Z., Zhou B., Xu J., Li Y., Hu X., Tian H. Heterostructured Nitrogen and Sulfur co-doped Black TiO2/g-C3N4 Photocatalyst with Enhanced Photocatalytic Activity//Chem. Res. Chin. Univ. - 2020. - Vol. 36, No. 6. - P. 1045-1052.

241. Ma C., Jiang M., Yang C., Yang Z., Meng W., Zhou L., Sun C., Chen W. Construction of α-Fe_2O_3/Sulfur-Doped Polyimide Direct Z-Scheme Photocatalyst with Enhanced Solar Light Photocatalytic Activity//ACS Omega. - 2022. - Vol. 7, No. 13. - P. 11371-11381.

242. Shinde S.S., Sami A., Lee J.-H. Sulfur mediated graphitic carbon nitride/S-Se-graphene as a metal-free hybrid photocatalyst for pollutant degradation and water splitting//Carbon. - 2016. - Vol. 96. - P. 929-936.

243. Ismail A.A., Faisal M., Harraz F.A., Al-Hajry A., Al-Sehemi A.G. Synthesis of mesoporous sulfur-doped Ta_2O_5 nanocomposites and their photocatalytic activities//J. Colloid Interface Sci. - 2016. - Vol. 471. - P. 145-154.

244. Marschall R., Mukherji A., Tanksale A., Sun C., Smith S.C., Wang L., Lu G.Q. (Max) Preparation of new sulfur-doped and sulfur/nitrogen co-doped $CsTaWO_6$ photocatalysts for hydrogen production from water under visible light//J. Mater. Sci. - 2011. - Vol. 21, No. 24. - P. 8871-8879.

245. Jia Y., Wu C., Lee B.W., Liu C., Kang S., Lee T., Park Y.C., Yoo R., Lee W. Magnetically separable sulfur-doped SnFe2O4/graphene nanohybrids for effective photocatalytic purification of wastewater under visible light//J. Hazard. Mater. - 2017. - Vol. 338. - P. 447-457.

246. Zhao Z., Dai H., Deng J., Liu Y., Au C.T. Effect of sulfur doping on the photocatalytic performance of $BiVO_4$ under visible light illumination//Chinese J. Catal. - 2013. - Vol. 34, No. 8. - P. 1617-1626.

247. Chang S., Sang Y., Liu H. Efficient Photocatalytic Degradation of RhB by Constructing Sn_3O_4 Nanoflakes on Sulfur-Doped $NaTaO_3$ Nanocubes//Crystals. - 2021. - Vol. 11, No. 1. - P. 59.

248. Black J.G., Black L.J. Microbiology: Principles and Explorations. Microbiology. – John Wiley & Sons, 2018. – 898 p.

249. Patel M. Defference between Gram Positive and Gram Negative bacteria: [Electronic resource]. URL: https://www.pharmaceuticalsky.com/2020/12/differences-between-gram-positive-and.html. (Access date: 10.10.2022).

250. Cavalier-Smith T. What are Fungi?//Systematics and Evolution: Part A : The Mycota/ eds. D.J. McLaughlin, E.G. McLaughlin, P.A. Lemke. – Berlin, Heidelberg: Springer, 2001. – P. 3-37.

251. Webster J., Weber R. Introduction to Fungi / John Webster, Roland Weber – New York: Cambridge University Press, 2007. – 1744 p.

252. Kavanagh K. Fungi: Biology and Applications. Fungi / Kevin Kavanagh – Maynooth: John Wiley & Sons, 2017. – 424 p.

253. Haddar A., Ayed E.B., Sila A., Putaux J.-L., Bougatef A., Boufi S. Hybrid levan–Ag/AgCl nanoparticles produced by UV-irradiation: properties, antibacterial efficiency and application in bioactive poly(vinyl alcohol) films//RSC Adv. - 2021. - Vol. 11, No. 62. - P. 38990-39003.

254. Liu Z., Guo W., Guo C., Liu S. Fabrication of AgBr nanomaterials as excellent antibacterial agents//RSC Adv. - 2015. - Vol. 5, No. 89. - P. 72872-72880.

255. Kalnina D., Gross K., Onufrijevs P., Dauksta E., Nikolajeva V., Stankeviciute Z., Kareiva A. The Antimicrobial Action of Silver Halides in Calcium Phosphate//Key Eng. Mater. - 2015. - Vol. 631. - P. 384-389.

256. Sharifi-Rad M., Pohl P. Synthesis of Biogenic Silver Nanoparticles (AgCl-NPs) Using a Pulicaria vulgaris Gaertn. Aerial Part Extract and Their Application as Antibacterial, Antifungal and Antioxidant Agents//Nanomater. - 2020. - Vol. 10, No. 4. - P. 638.

257. Taghizadeh M.T., Siyahi V., Ashassi-Sorkhabi H., Zarrini G. ZnO, AgCl and AgCl/ZnO nanocomposites incorporated chitosan in the form of hydrogel beads for photocatalytic degradation of MB, E. coli and S. aureus//Int. J. Biol. Macromol. - 2020. - Vol. 147. - P. 1018-1028.

258. Ning S., Lin H., Tong Y., Zhang X., Lin Q., Zhang Y., Long J., Wang X. Dual couples Bi metal depositing and Ag@AgI islanding on BiOI 3D architectures for synergistic bactericidal mechanism of E. coli under visible light//Appl. Catal. B: Environ. - 2017. - Vol. 204. - P. 1-10.

259. Wang S., Zhang X., Luo T., Zhu J., Su S. Preparation of native cellulose-AgCl fiber with antimicrobial activity through one-step electrospinning//J. Biomater. Sci. Polym. Ed. - 2017. - Vol. 28, No. 3. - P. 284-292.

260. Malachová K., Praus P., Rybková Z., Kozák O. Antibacterial and antifungal activities of silver, copper and zinc montmorillonites//Appl. Clay Sci. - 2011. - Vol. 53, No. 4. - P. 642-645.

261. Feizi S., Taghipour E., Ghadam P., Mohammadi P. Antifungal, antibacterial, antibiofilm and colorimetric sensing of toxic metals activities of eco friendly, economical synthesized Ag/AgCl nanoparticles using Malva Sylvestris leaf extracts//Microb. Pathog. - 2018. - Vol. 125. - P. 33-42.

262. Sidorowicz A., Margarita V., Fais G., Pantaleo A., Manca A., Concas A., Rappelli P., Fiori P.L., Cao G. Characterization of nanomaterials synthesized from Spirulina platensis extract and their potential antifungal activity//PLoS One. - 2022. - Vol. 17, No. 9. - P. e0274753.

263. Arain R.A., Khatri Z., Memon M.H., Kim I.-S. Antibacterial property and characterization of cotton fabric treated with chitosan/AgCl–TiO_2 colloid//Carbohydr. Polym. - 2013. - Vol. 96, No. 1. - P. 326-331.

264. Zhang Q.-J., Liu Y., Zhang W.-T., Huang J.-J., Li H.-H., Lu Y.-G., Zheng M., Zheng D.-L. Synthesis, Antifungal Activity, and Cytotoxicity of AgBr-NP@CTMAB Hybrid and Its Application in PMMA//Int. J. Nanomed. - 2021. -Vol. 16. - P. 3091-3103.

265. Habibi-Yangjeh A., Davari M., Manafi-Yeldagermani R., Alikhah Asl S., Enaiati S., Ebadollahi A., Feizpoor S. Antifungal activity of TiO_2/AgBr nanocomposites on some phytopathogenic fungi//Food Sci. Nutr. - 2021. - Vol. 9, No. 7. - P. 3815-3823.

266. Ghosh S., Saraswathi A., Indi S.S., Hoti S.L., Vasan H.N. Ag@AgI, Core@Shell Structure in Agarose Matrix as Hybrid: Synthesis, Characterization, and Antimicrobial Activity//Langmuir. - 2012. - Vol. 28, No. 22. - P. 8550-8561.

267. Rehan M., Khattab T.A., Barohum A., Gätjen L., Wilken R. Development of Ag/AgX (X = Cl, I) nanoparticles toward antimicrobial, UV-protected and self-cleanable viscose fibers//Carbohydr. Polym. - 2018. - Vol. 197. - P. 227-236.

268. Lee P.-C., Yang Z.-R., Kuo C.-Y., Shin C.-H., Lin C.-B. Titanium dioxide structure modified with silver chloride by 3D printing for dye degradation and bactericidal applications. - 2022.

269. Sun D., Mao J., Wei H., Zhang Q., Cheng L., Yang X., Li P. Efficient Prevention of Aspergillus flavus Spores Spread in Air Using Plasmonic Ag-AgCl/α-Fe2O3 under Visible Light Irradiation//ACS Appl. Mater. Interfaces. - 2022. - Vol. 14, No. 24. - P. 28021-28032.

270. Vijayalakshmi R.V., Kumar P.P., Selvarani S., Rajakumar P., Ravichandran K. Chalcone dendrimer stabilized core–shell nanoparticles—a comparative study on Co@TiO_2, Ag@TiO_2 and Co@AgCl nanoparticles for antibacterial and antifungal activity//Mater. Res. Express. - 2017. - Vol. 4, No. 10. - P. 105046.

271. Naik K., Kowshik M. Anti-quorum sensing activity of AgCl-TiO_2 nanoparticles with potential use as active food packaging material//J. Appl. Microbiol. - 2014. - Vol. 117, No. 4. - P. 972-983.

272. Svoboda L., Bednář J., Dvorský R., Rybková Z., Malachová K., Henych J., Matýsek D., Němečková Z. Novel synthesis of Ag@AgCl/ZnO by different radiation sources including radioactive isotope 60Co: Physicochemical and antimicrobial study//Appl. Surf. Sci. - 2020. - Vol. 529. - P. 147098.

273. Li J., Liu B., Han X., Liu B., Jiang J., Liu S., Zhang J., Shi H. Direct Z-scheme TiO2-x/AgI heterojunctions for highly efficient photocatalytic degradation of organic contaminants and inactivation of pathogens//Sep. Purif. Technol. - 2021. - Vol. 261. - P. 118306.

274. Kim Y.H., Kim G.H., Yoon K.S., Shankar S., Rhim J.-W. Comparative antibacterial and antifungal activities of sulfur nanoparticles capped with chitosan//Microb. Pathog. - 2020. - Vol. 144. - P. 104178.

275. Ezati P., Rhim J.-W., Molaei R., Priyadarshi R., Roy S., Min S., Kim Y.H., Lee S.-G., Han S. Preparation and characterization of B, S, and N-doped glucose carbon dots: Antibacterial, antifungal, and antioxidant activity//Sustain. Mater. Technol. - 2022. - Vol. 32. - P. e00397.

276. Saedi S., Shokri M., Priyadarshi R., Rhim J.-W. Carrageenan-Based Antimicrobial Films Integrated with Sulfur-Coated Iron Oxide Nanoparticles (Fe3O4@SNP)//ACS Appl. Polym. Mater. - 2021. - Vol. 3, No. 10. - P. 4913-4923.

277. Lesnichaya M., Gazizova A., Perfileva A., Nozhkina O., Graskova I., Sukhov B. Starch-capped sulphur nanoparticles synthesised from bulk powder sulphur and their anti-phytopathogenic activity against Clavibacter sepedonicus//IET Nanobiotechnol. - 2021. - Vol. 15, No. 7. - P. 585-593.

278. Xu X., Wang S., Yu X., Dawa J., Gui D., Tang R. Biosynthesis of Ag deposited phosphorus and sulfur co-doped g-C_3N_4 with enhanced photocatalytic inactivation performance under visible light//Appl. Surf. Sci. - 2020. - Vol. 501. - P. 144245.

279. Niranjan R., Zafar S., Lochab B., Priyadarshini R. Synthesis and Characterization of Sulfur and Sulfur-Selenium Nanoparticles Loaded on Reduced Graphene Oxide and Their Antibacterial Activity against Gram-Positive Pathogens//Nanomater. - 2022. - Vol. 12, No. 2. - P. 191.

280. Ezati P., Roy S., Rhim J.-W. Pectin/gelatin-based bioactive composite films reinforced with sulfur functionalized carbon dots//Colloids Surf. A Physicochem. Eng. Asp. - 2022. - Vol. 636. - P. 128123.

281. Tijani J.O., Odeh E.I., Mustapha S., Egbosiuba T.C., Daniel A.I., Abdulkareem A.S., Muya F.N. Photocatalytic, electrochemical, antibacterial and antioxidant behaviour of carbon-sulphur Co-doped zirconium (IV) oxide nanocomposite//CLCE. - 2022. - Vol. 3. - P. 100034.

282. Riahi Z., Priyadarshi R., Rhim J.-W., Lotfali E., Bagheri R., Pircheraghi G. Alginate-based multifunctional films incorporated with sulfur quantum dots for active packaging applications//Colloids Surf. B. - 2022. - Vol. 215. - P. 112519.

283. Khan N. V., Burkitbayev M. M., Urakaev F. K. Development of the synthesis technology of S@ AgCl-Ag_2S nanocomposite in aqua medium // Bulletin of the Karaganda University: Chemistry – 2019. – №. 4. – P. 72-76.

284. Khan N. V. Synthesis of the S/AgBr nano/micropowder in DMSO-water system //Chemical Bulletin of Kazakh National University. – 2022. – Vol. 104. – №. 1. – P. 4-10.

285. CLSI M07. Methods for Dilution Antimicrobial Susceptibility Tests for Bacteria That Grow Aerobically, 11th Edition. - Introduced 2018-11-01. - Wayne: Clinical and laboratiry standards institute, 2018. - 112 p.

286. CLSI M27. Reference Method for Broth Dilution Antifungal Susceptibility Testing of Yeasts, 4th Edition. - Introduced 2017-11-30. - Wayne: Clinical and laboratiry standards institute, 2017. - 46 p.

287. Peters C. A. Environmental engineering processes laboratory manual / Catherine A. Peters. - Champaign: AEESP, 2001. – P. 1-25.

288. Gamage McEvoy J., Cui W., Zhang Z. Synthesis and characterization of Ag/AgCl–activated carbon composites for enhanced visible light photocatalysis//Appl. Catal. B: Environ. - 2014. - Vol. 144. - P. 702-712.

289. Assis M., Groppo Filho F.C., Pimentel D.S., Robeldo T., Gouveia A.F., Castro T.F.D., Fukushima H.C.S., de Foggi C.C., da Costa J.P.C., Borra R.C., Andrés J., Longo E. Ag Nanoparticles/AgX (X=Cl, Br and I) Composites with Enhanced Photocatalytic Activity and Low Toxicological Effects//ChemistrySelect. - 2020. - Vol. 5, No. 15. - P. 4655-4673.

290. Khan N., Baláž M., Burkitbayev M., Tatykayev B., Shalabayev Z., Nemkayeva R., Jumagaziyeva A., Niyazbayeva A., Rakhimbek I., Beldeubayev A., Urakaev F. DMSO- mediated solvothermal synthesis of S/AgX (X = Cl, Br) microstructures and study of their photocatalytic and biological activity//Appl. Surf. Sci. - 2022. - Vol. 601. - P. 154122.

291. Khan N.V., Baláž M., Burkitbayev M.M., Tatykayev B.B., Shalabayev Z.S., Niyazbayeva A.I., Urakaev F.K. Solvothermal DMSO-mediated synthesis of the S/AgI micro-/nano-structures and its application as photocatalytic and biological agents//Int. J. Biol. Chem. - 2022. - Vol. 15, No. 1. - P. 79-89.

292. Yeşilot S., Küçükköylü S., Mutlu T., Demir E., Demir-Cakan R. Highly sulfur-rich polymeric cathode materials via inverse vulcanization of sulfur for lithium–sulfur batteries//Mater. Chem. Phys. - 2022. - Vol. 285. - P. 126168.

293. Zhang Z., Hu J., Xu Z., Huang H., Yin S., Ma Y., Wei J., Yu Q. Degradation process of Ag/AgCl chloride-sensing electrode in cement extract with low chloride concentration//Corros. Sci. - 2022. - Vol. 198. - P. 110107.

294. Lian B., Li Y., Zhao X., Zu Y., Wang Y., Zhang Y., Li Y. Preparation and Optimization of 10-Hydroxycamptothecin Nanocolloidal Particles Using Antisolvent Method Combined with High Pressure Homogenization//J. Chem. - 2017. - Vol. 2017. - P. e5752090.

295. Katsumata H., Islam Molla M.A., Islam J.B., Tateishi I., Furukawa M., Kaneco S. Dual Z-scheme heterojunction g-C_3N_4/Ag_3PO_4/AgBr photocatalyst with enhanced visible-light photocatalytic activity//Ceram. Inter.. - 2022. - Vol. 48, No. 15. - P. 21898-21905.

296. Zhang J., Wu P., Yang Z., Gao B., Zhang J., Wang P., Nie F., Liao L. Preparation and Properties of Submicrometer-Sized LLM-105 via Spray-Crystallization Method//Propellants Explos. Pyrotech. - 2014. - Vol. 39, No. 5. - P. 653-657.

297. Goldmann C., De Frutos M., Hill E.H., Constantin D., Hamon C. Symmetry Breaking in Seed-Mediated Silver Nanorod Growth Induced by Dimethyl Sulfoxide//Chem. Mater. - 2021. - Vol. 33, No. 8. - P. 2948-2956.

298. P. S., P. S. Studies on the extraction of polyphenolic compounds from pre-consumer organic solid waste//J. Ind. Eng. Chem. - 2020. - Vol. 82. - P. 130-137.

299. Pica M. Silver halide-based composite photocatalysts: an updated account//Rend. Lincei Sci. Fis. Nat. - 2019. - Vol. 30, No. 3. - P. 453-467.

300. Zhou X., Hu C., Hu X., Peng T., Qu J. Plasmon-Assisted Degradation of Toxic Pollutants with Ag−AgBr/Al2O3 under Visible-Light Irradiation//J. Phys. Chem. C. - 2010. - Vol. 114, No. 6. - P. 2746-2750.

301. Feng Z., Yu J., Sun D., Wang T. Visible-light-driven photocatalysts Ag/AgCl dispersed on mesoporous Al2O3 with enhanced photocatalytic performance//J. Colloid Interface Sci. - 2016. - Vol. 480. - P. 184-190.

302. Yu J., Dai G., Huang B. Fabrication and Characterization of Visible-Light-Driven Plasmonic Photocatalyst Ag/AgCl/TiO2 Nanotube Arrays//J. Phys. Chem. C. - 2009. - Vol. 113, No. 37. - P. 16394-16401.

303. Saedi S., Shokri M., Rhim J.-W. Antimicrobial activity of sulfur nanoparticles: Effect of preparation methods//Arab. J. Chem. - 2020. - Vol. 13, No. 8. - P. 6580-6588.

304. Catalog website of Merck: [Electronic resource]. URL: https://www.sigmaaldrich.com/KZ/en (Access date: 18.11.2022)